DISS. ETH NO. 24478

Microinjection of Liposomal Carriers into Single Cells

A thesis submitted to attain the degree of

DOCTOR OF SCIENCES of ETH ZURICH

(Dr. sc. ETH Zurich)

presented by

Peter Gerhard Tiefenböck

Apotheker
FAU Erlangen-Nuremberg

born on 06.12.1987
citizen of Germany

accepted on the recommendation of

Prof. Dr. Jean-Christophe Leroux
Prof. Dr. Cornelia Halin

2017

Si fractus illabatur orbis,

Impavidum ferient ruinae.

If the world, broken, should fall

The ruins will strike him fearless.

Horace, Carmen III, 3

Table of Contents

Summary

Cell manipulation has attracted increasing attention in recent years with the rise of new genome-editing techniques and cell-based therapies. Microinjection (MI), although a long-described technique, continues to be among the most widely used methods to introduce substances into cells. By delivering the material directly into the cell plasma, MI circumvents the endolysosomal pathway that would otherwise lead to the degradation of sensitive biomacromolecules. The present work evaluated different liposomal formulations and assessed the fundamental aspects of their MI into cells in view of potential biomedical applications, such as the addition of artificial organelles with novel properties to generate a semi-synthetic cell.

In Chapter 1, different techniques for the intracellular delivery of material are introduced with a strong focus on MI. The instrumentation setup used for MI is described, as well as its historical development. Moreover, the technique's main advantages are discussed and are illustrated with a few prominent examples of the scientific discoveries that these features have enabled over the years. Special emphasis is placed on the injection of colloids with similar characteristics to the ones used in this thesis, highlighting what has been accomplished in the field and what remains to be achieved. In this context, two potential applications of MI are discussed: the introduction of artificial organelles into cells and the development of cell-based drug delivery vehicles.

A more detailed description of MI and its use in the intracellular delivery of different kinds of colloids is given in Chapter 2. The MI of proteins, nucleic acids and nanoparticles (NP) are reviewed in this section, focusing on the aspects of MI that proved to be crucial for the application of these systems in diverse biological problems. The versatility of MI is illustrated by the impressive variety of studies performed with it, ranging from the investigation of intracellular transport, to cell cycle regulation and the elucidation of apoptosis pathways. Towards the end of this chapter, the intracellular processing of microinjected colloids is discussed from a drug delivery perspective. The role played by the structure of the cytoplasm on the diffusion of injected colloids is explained together with its influence on delivery efficacy. In addition, the impact that clearing mechanisms such as nuclease-mediated degradation or autophagic response might have on the achievement of an effective intracellular dose of a colloid is discussed.

The main experimental findings of this thesis are presented in Chapter 3, where the MI of liposomal formulations differing in their lipid composition, surface properties and size was investigated. The cytotoxicity of the injected vesicles was studied, as well as their stability (integrity) upon cytoplasmic injection and their intracellular processing with a focus on diffusion patterns and clearing mechanisms. A size-dependent agglomeration in the cytosol was observed for the injected colloids, which in turn contributed to the distinct dilution patterns detected upon cell division. As a proof of concept of the applicability of the MI of liposomes, two applications are presented. Firstly, the possibility to introduce functional artificial organelles into cells by MI was explored. For this purpose, trypsin as a model enzyme was encapsulated into liposomes, and its catalytic activity was demonstrated in the cytosol of the injected cells. Secondly, the loading of migratory dendritic cells (DC) was investigated in the context of potential cell-based therapies exploiting the cells' natural capacity to migrate towards draining lymph

nodes *via* lymphatic vessels. The effect of MI on the cells' migration speed was studied, underlying potential limitations of the approach and its applicability for cell-based drug delivery strategies in the future.

In Chapter 4, a liposomal system with controlled release was investigated in view of its subsequent MI into live cells. Thermo-sensitive liposomes were prepared following a previously described procedure involving the decomposition of ammonium bicarbonate (ABC) at a moderately elevated temperature. According to this procedure, the encapsulation of ABC would trigger cargo release upon an increase of temperature due to the generation of CO_2 bubbles and the transient cavitation of the vesicles. Unfortunately, the system could not be reproduced, casting serious doubts on the stability of the vesicles and the described mechanism of action.

Finally, Chapter 5 recapitulates the major findings of this thesis. In addition, a possible application is presented involving migratory cells modified with artificial vesicles encapsulating prodrug-converting enzymes.

The work presented in this thesis illustrates the versatility and applicability of MI as a platform for cell manipulation in combination with liposomes encapsulating biologically relevant cargo.

Zusammenfassung

Mit dem Aufkommen neuartiger Methoden zur Veränderung des Genoms und zellbasierter Therapieansätze erfuhr die Manipulation einzelner Zellen neue Aufmerksamkeit. Eine besondere Rolle spielt dabei die Mikroinjektion (MI), die trotz ihrer weit zurückliegenden Erstbeschreibung noch immer zu den weitverbreitetsten Techniken zählt, um Stoffe in Zellen zu transportieren. Durch den direkten Eintrag in das Zytoplasma umgehen die applizierten Substanzen die Aufnahme durch das endolysosomale System, das gewöhnlich zum Abbau von fragilen Biomolekülen führt. Die vorliegende Arbeit bewertete verschiedene liposomale Formulierungen in Bezug auf ihre Toxizität and Stabilität in der Zelle nach der MI. Ihre Eignung in Bezug auf mögliche biomedizinische Anwendungen wurde ebenfalls geprüft, beispielsweise durch die Zuführung künstlicher Zellorganellen mit neuartigen Eigenschaften, um semisynthetische Zellen zu erzeugen.

Im Rahmen des ersten Kapitels dieser Arbeit werden unterschiedliche Techniken zur Zellmanipulation vorgestellt, wobei der Fokus auf der MI liegt. Der instrumentelle Aufbau einer Mikroinjektionsapparatur wird erklärt und es wird eine kurze Einführung bezüglich der technischen Entwicklungsgeschichte gegeben. Die Vorteile der MI werden anhand einiger weniger repäsentativer Beispiele diskutiert, mit Bezugnahme auf wichtige Ergebnisse, die nur mittels MI gemacht werden konnten. Besonderes Augenmerk liegt auf der Injektion kolloidaler Systeme, mit ähnlichen Eigenschaften wie die in dieser Arbeit beschriebenen. Es werden Meilensteine aufgezeigt, die nur unter Zuhilfenahme der MI erzielt werden konnten aber auch bisher weisse Flecken in diesem Forschungsgebiet. In diesem Zusammenhang werden zwei potentielle Anwendungen der MI eingehend diskutiert: Die Einführung künstlicher Organellen in die Zelle und die Entwicklung Wirkstoff abgebender Systeme auf Grundlage von Zellen.

Eine erweiterte Beschreibung der MI mit Fokus auf verschiedenste kolloidale Systeme wird im zweiten Kapitel vorgestellt. Die MI von Proteinen, Nukleinsäuren und Nanopartikeln wird kritisch bewertet. Dabei liegt ein Schwerpunkt darauf, wie MI den entscheidenden Beitrag zu Beantwortung verschiedenster biologischer Fragestellungen leisten konnte. Die vielseitige Anwendbarkeit der MI wird durch eine beeindruckende Vielzahl und Diversität wissenschaftlicher Studien dargestellt. Von der Untersuchung intrazellulärer Transportwege über die Regulation des Zellzyklus bis hin zur Aufdeckung apoptotischer Prozesse erwies sich die MI als unverzichtbarer Bestandteil der Forschung. Gegen Ende dieses Kapitels wird die Prozessierung injizierter Kolloide durch die Zelle betrachtet, im Hinblick auf eine mögliche Wirkstoffzuführung. Eine bedeutende Rolle spielt dabei die physikalische Struktur des Zytoplasma, besonders auf die Diffusion injizierter Partikel. Zusätzlich werden Abbaumechanismen im Zytosol aufgezeigt, wie etwa die Degradation durch Nukleasen und die autophagosomale Aufnahme und ihr Einfluss auf eine wirksame intrazelluläre Dosis der Kolloide.

Die wichtigsten wissenschaftlichen Erkenntnisse dieser Thesis werden im Kapitel 3 präsentiert. Die MI von Liposomen wurde im Hinblick auf unterschiedliche Formulierungen, Oberflächeneigenschaften und Grössen untersucht. Parameter waren dabei die Zytotoxizität der injizierten Kolloide, die Stabilität im Zytoplasma und die intrazelluläre Prozessierung im Hinblick auf Verdünnungsverhalten im Rahmen des Zellzyklus und Abbaumechanismen. Eine grössenabhängige Agglomeration im Zytosol wurde

beobachtet, die zu unterschiedlichen Verteilungsverhältnissen im Rahmen der Zellteilung führte. Die universale Anwendbarkeit der MI von Liposomen wird mithilfe von zwei Studien aufgezeigt: Zunächst wurde die Möglichkeit untersucht, funktionelle künstliche Organelle in die Zelle mittels MI einzuführen. Trypsin wurde als Modellenzym ausgewählt und in Liposomen verpackt. Die katalytische Aktivität dieses Enzyms wurde daraufhin im Zytosol injizierter Zellen nachgewiesen. Zusätzlich wurde die Beladung migratorischer dendritischer Zellen erforscht, im Hinblick auf potentielle zellbasierte Therapien. Diese Zellen besitzen die natürliche Fähigkeit, in Richtung von afferenten Lymphknoten *via* lymphatischer Gefässe zu wandern. Der Einfluss der MI auf die Wanderungsgeschwindigkeit wurde untersucht. Dies erlaubte, mögliche Hindernisse dieses Ansatzes zu erkennen und dessen Anwendung als zell-basierte Strategie zur Arzneistoffabgabe in der Zukunft zu bewerten.

Im vierten Kapitel wurde ein liposomales System zur kontrollierten Freisetzung im Hinblick auf die Anwendbarkeit im Rahmen der MI untersucht. Thermosensitive Liposomen wurden nach einem bereits veröffentlichten Protokoll hergestellt. Der postulierte Wirkmechanismus beruhte auf dem Zerfall von Ammoniumbikarbonat (ABC) bei moderat erhöhten Temperaturen. Dem Protokoll nach, würde das Einkapseln von ABC in Liposomen zu einer Bildung von CO_2-Gasblasen bei erhöhter Temperatur führen, die zu einer vorübergehenden Porenbildung in den liposomalen Membranen und zu einer damit verbundenen Wirkstofffreigabe beitragen würden. Es gelang nicht dieses System zu reproduzieren, im Gegenteil wurden schwerwiegende Zweifel an der Stabilität der Vesikel und dem beschriebenen Wirkmechanismus geweckt.

Zuletzt werden im Kapitel 5 die wichtigsten Erkenntnisse dieser Arbeit wiederholt und mögliche Anwendungen im Hinblick auf die Verwendung migratorischer Zellen aufgezeigt. Die Modifikation dieser Zellen mit liposomal eingeschlossenen prodrug-konvertierenden Enzymen spielt dabei eine wichtige Rolle.

Die Ergebnisse, die in dieser Thesis präsentiert werden, zeigen die weitreichende Anwendbarkeit der Mikroinjektion auf. Sie kann als Plattform zur Zellmanipulation durch Liposomen mit biologisch aktiver Beladung dienen.

Chapter 1

Background and Purpose

Cell manipulation

The intracellular delivery of materials has received growing interest in the last years with the advent of new genome-editing tools like the clustered regularly interspaced short palindromic repeats (CRISPR/Cas9) system [1]. CRISPR/Cas9 allows cutting genomic DNA at selected locations and inserting new genes or removing existing ones with precision within organisms. For the successful implementation of such system, the delivery into cells should preferably be done in a way that circumvents the endolysosomal pathway, since the DNA and protein constituents are prone to degradation. The use of co-incubation to deliver these compounds to cells usually results in their uptake through endosomes, which later fuse with lysosomes where the biomacromolecules face a degrading environment consisting of low pH and proteases [2]. To evade this fate and allow the compounds of interest to reach the cytoplasm, researchers may employ fusogenic strategies [3] or trigger the disruption of the endo/lysosomal membranes [4]. Alternatively, several cell manipulation techniques have been described, where the cargo is transferred directly into the cytoplasm, like electroporation [5], cell-squeezing [6] or MI [7].

Electroporation is based on an electric field applied to cells, leading to transient permeabilization of the cellular membrane. Material in the surrounding solution can thereby diffuse into the cells through the membranes, remaining trapped in the cytoplasm after the membrane is resealed. This technique is employed in the transfection of hard-to-transfect cells such as primary DC [8]; yet, the toxicity associated with it limits its use to more sensitive cell types. This is because the electric field can lead to permanent permeabilization of the membranes, causing loss of homeostasis and subsequent cell death. Another drawback of this method is that since the loading of the cell is mediated by diffusion, the amount of material which is loaded cannot be precisely controlled [9]. A newly developed technique called nanochannel electroporation allows circumventing this problem by connecting the cell to the cargo in solution *via* a thin channel (diameter 90 nm). Delivery can be very precise, however the throughput is so far on the single-cell level [10].

Another technique for cell manipulation proposed more recently is the cell-squeezing device developed by the group of Klavs Jensen in 2012 [6, 11]. In this method, cells are deformed by squeezing them through narrow microchannels, generating transient membrane holes. The material in the surrounding solution can then diffuse into the cells, similar to electroporation. Several different cell lines were tested, *e.g.* human epithelia adenocarcinoma cells (HeLa), primary mouse T lymphocytes and primary mouse-derived DC, showing high viability overall after the process. However, the delivered amount of a 70 kDa dextran was found to be substantially lower compared to a 3 kDa dextran, suggesting that larger colloids would be delivered less efficiently by this approach.

When compared to electroporation and cell-squeezing, MI differs from them in that it does not rely on passive diffusion of the colloids through the permeabilized membrane. Instead, it dispenses the material directly inside the cells by applying a positive pressure. As discussed below, MI presents a series of unique features that make it a valuable tool to address diverse biological problems.

Microinjection – A tool for cell manipulation

Historical background and instrumentation

Although already described in 1911 [12], the use of MI only became widespread from the 1970s onwards. It was around that time that Diacumakos [13] and Graessmann [14] independently described a technique to transplant genetic material *via* a thin glass needle. Further improvements by Ansorge simplified the system in terms of an automated pressure system, and made the technique accessible to other researchers [15]. Since then, MI has proven to be an essential tool in fundamental research, enabling the transfer of a large variety of materials into cells [16].

The instrumentation needed for MI consists of a few different components (Fig. 1.1). The key part is the borosilicate injection needle, which has an inner diameter of around 500 nm and is backfilled with a solution containing the compound of interest. The injection needle is mounted onto a holder, which can be operated by a joystick and is freely maneuverable in all directions. The joystick also allows automatic injections after setting the lower limit at which the needle should pierce the cells. The material can then be easily dispensed to all cells by simply clicking on the joystick to move the needle in between cells. In a MI setup, the needle holder is in turn connected to a pump supplying a certain backpressure to the tip. The pressure is normally kept below 100 hPa to prevent clogging of the tip, whereas the pressure supplied for injections is usually up to 150 hPa. The duration of an injection can be adjusted by setting the time the injection pressure is applied, and it often ranges between 0.1-0.5 s. By controlling the time and pressure of injection, the volume introduced can be modulated to some extent. The whole MI setup is mounted on an inverted microscope to visualize the cells and allow easy access to them with the injector tip. Temperature and humidity control is also necessary to ensure cell viability, especially if injections have to be performed over several hours [7, 17].

Virtually all types of cells can be used for MI experiments, although cells that grow in adhesion on a tissue culture substrate are easier to inject than those that grow in suspension. For non-adherent cells, like *e.g.* primary human blood stem cells or lymphoblast-like Raji cells, the cell culture dishes can be pre-coated with fibronectin or poly(lysine) to ensure the attachment of the cells [18, 19].

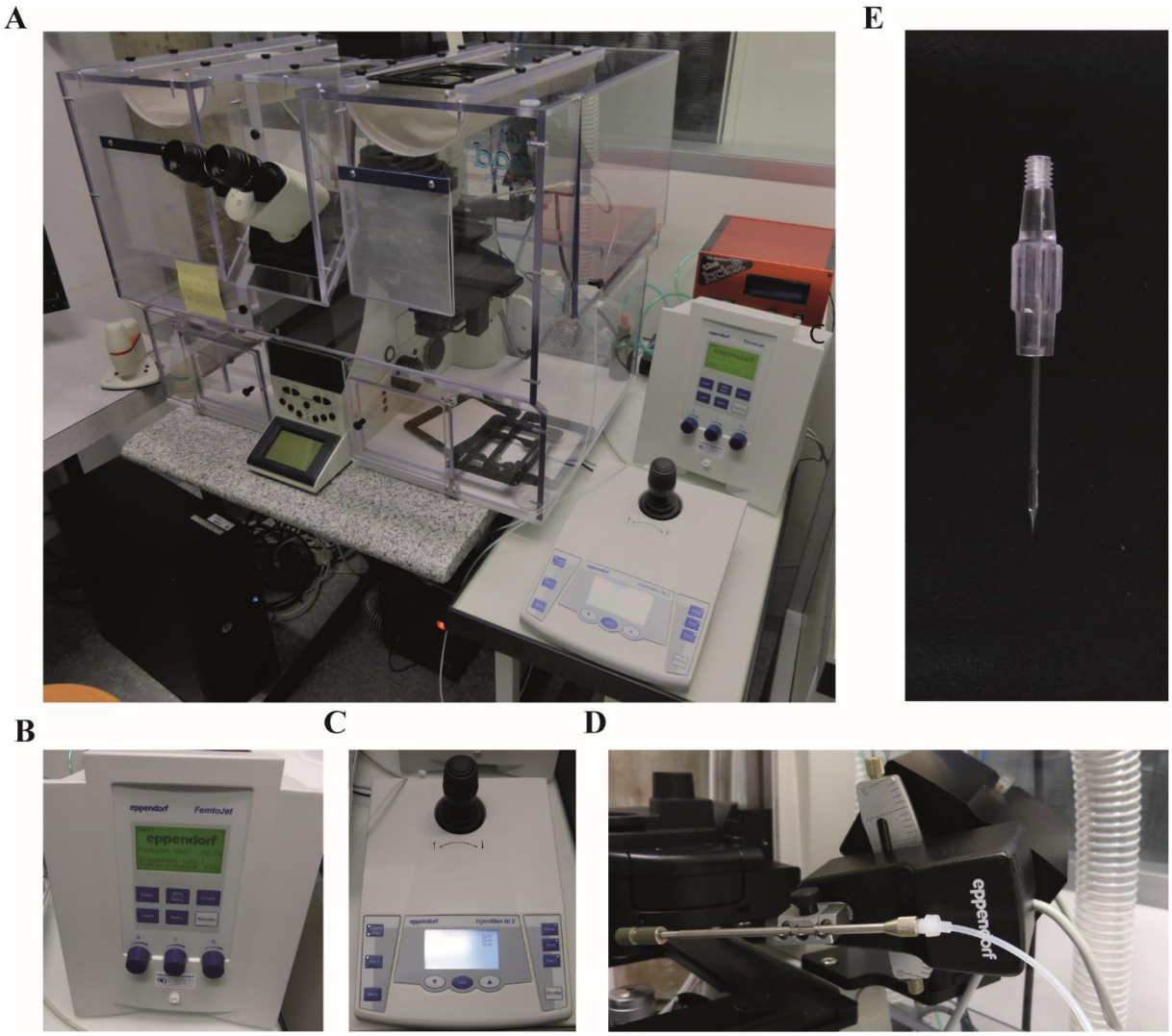

Figure 1.1 Instrumental Set-up for MI. A, Overview inverted microscope with attached MI equipment. B, pump supplying injection- and backpressure, C, joystick for needle positioning, D, robotic arm with attached needle holder, E, MI injection needle. All instruments except for the microscope were purchased from Eppendorf, Hamburg, Germany.

Advantages and achievements of Microinjection

The most visible side of MI is probably connected to its role in assisted reproduction, *i.e. in-vitro* fertilization (IVF). MI allows the delivery of genetic material into the germ cell, and has been used for years not only to enable conception in humans but also to generate transgenic animals [20, 21] . In this case, the MI setup uses two glass capillaries: one to apply a negative pressure and immobilize the oocyte, and a second one to inject the genetic material or the spermatozoids directly into the oocyte. Because oocytes have a higher volume than most cell types used for research, the inner diameter of the needles used for IVF is typically in the micrometer range, which is much larger than the ones used in the studies described hereafter.

An appealing feature of MI is that it allows controlling the amount of material injected with more precision than electroporation and cell-squeezing, where the transferred amount depends on diffusion and permeabilization/resealing of cell membranes [9]. The ability to control the injection volume is desirable not only for general reproducibility of experiments but for cases where the concentration of the material introduced determines the outcome. For instance, with the CRISPR/Cas9 system the gene-editing activity is only observed above a certain concentration threshold but if this is excessively exceeded, the induction of DNA degradation results in cytotoxicity [22]. Although the volume dispensed to individual cells varies within one MI session due to differences in the injection tip, injection pressure and/or the size of cells, it is possible to calculate an average injection volume per cell with reasonable accuracy [23]. Among the different methods that have been described for this purpose, the extrapolation of the fluorescence intensity of water-in-oil droplets is reported in this thesis. Generally, the reported values for microinjected volume are in the range of 5-20% of the cell volume, above which cells may burst due to the high intracellular pressure [24].

In addition to the injection volume, MI allows controlling the timing of injection. This proved to be crucial for studies of time-resolved processes such as the cell cycle, where a given cell is found on a different stage of its life cycle depending on the moment at which it is analyzed [25, 26]. The possibility to decide the exact time at which the material is introduced in the cells is also relevant in studies where the effect occurs immediately upon the delivery and/or is of transient nature. For this reason, MI was a valuable tool in the identification of several proteins involved in cytoskeletal organization and intracellular transport [27-29].

The site of injection can also be selected with MI, enabling on-demand cytosolic or nuclear delivery of material. Site-specific injections were instrumental in the study of transport processes between the different intracellular compartments, *e.g.* between the nucleus and the cytoplasm. Early studies reported that the injection of DNA into the nucleus increased the transfection efficiency compared to the cytoplasm [30], but that translocation of genetic material to the nucleus was somehow possible for smaller oligonucleotides (ON) injected in the cytosol [31]. Some years later, other authors proposed that the diffusion of plasmids through the nucleus was size-dependent after observing that larger plasmids remained trapped in the cytoplasm [32, 33]. It is now known that the entry of nucleic acids to the nucleus occurs *via* the nuclear pore complex (NPC) [34], which imposes a size restriction to the material that can access the nucleus. In terms of spatial precision, MI has not been surpassed by any other technique of intracellular delivery, except perhaps for atomic force microscopy (AFM)-based probes [35, 36], where the tip of the cantilever is used to pierce the cell.

Recently, MI has enabled injecting individual cells in tissue slices [37]. This advancement granted the possibility to study cellular processes of higher complexity occurring in the context of tissues, such as cell-to-cell communication, tissue homeostasis, remodeling and development. Moreover, the cells in the proximity of the injected ones can serve as negative controls, as they will have been exposed to identical conditions.

Currently, the use of MI on systems of higher complexity than *in vitro* cell cultures is limited by the technique's low throughput. Even for an experienced researcher, not more than 2'000 cells can be injected per hour, rendering the technique unsuitable for its use on animal experiments and in the development of cell-manipulating technologies with clinical translation potential (*e.g.* gene therapy, gene editing, *etc.*). Although several automated MI systems have been developed in the last years [38, 39], the injection throughput currently possible has not surpassed 100 cells/min. Microfluidic devices where floating cells are transported through microchannels towards the MI needle could potentially attenuate the throughput problem. However, the injection limit is unlikely to exceed 3600 cells/h with

current setups, because only one injection needle is employed and because every injection step still takes around 1 s including the positioning of the cells in the microchannel [40, 41].

The unique features of MI mentioned above have enabled numerous discoveries in biology and have earned it a special place in the field of drug delivery. One of the most prominent advantages of MI compared to other techniques of intracellular delivery is the possibility to bypass the endolysosomal pathway, allowing the efficient delivery of sensitive biomacromolecules like enzymes, antibodies (Ab) nucleic acids and NP [30, 42-44]. Besides resulting in degradation, their entrapment in intracellular vesicles prevents them from moving freely in the cell and finding their site of action at specific compartments like the nucleus. Membrane-destabilizing strategies are therefore required to enable the escape of the cargo introduced in the cell, such as fusogenic peptides [45] and the presence of membrane disrupting polymers [46]. However, these strategies unavoidably increase the degree of complexity of the system, making it harder to control in terms of proper characterization. Furthermore, when colloids are internalized by endosomes, they are covered with a layer of biomacromolecules (*i.e.* the protein corona) that modifies their surface properties [47]. Targeting moieties added to drug delivery systems can be shielded by the protein corona, leading to a loss of their targeting capabilities [48]. Hence, the introduction of drug delivery systems *via* MI evades the barriers imposed by the cell's endocytic system and therefore provides interesting possibilities to address fundamental aspects of the colloids' intracellular processing and activity.

Intracellular processing of injected material

Upon intracellular delivery *via* MI, the injected material encounters a sieving meshwork of cytoskeletal components (*i.e.* microtubules, actin filaments) that hinders its diffusion inside the cytosol in a size-dependent manner [32]. Larger particles are substantially blocked in diffusion and stay at the site of injection. The attachment of poly(ethylene glycol) chains (PEGylation) on the surface of particles improves the diffusion properties [49], possibly by preventing interaction with cytosolic proteins. Microinjected material can also be subject to intracellular clearance mechanisms such as those mediated by autophagosomes, which are intracellular vesicles that clear the cytoplasm from *e.g.* dysfunctional proteins by capturing them in a random process in the cytosol and later on fusing with the lysosomes to degrade them [50-54]. PEGylation has also shown beneficial effects in preventing the uptake into autophagosomes [51], probably by shielding the particles against recognition by the autophagosomes.

Microinjection of colloids

Among the variety of existing drug delivery systems, liposomes are often used as protective containers for sensitive cargo. Liposomes are spherical vesicles consisting of phospholipids, and capable of encapsulating a wide variety of materials in their lumen [55]. Their introduction into cells by MI has been explored in only a few studies for varied purposes, such as intracellular sensing and controlled release of encapsulated cargo [56, 57]. Since the composition of the liposomal membrane can be designed to resemble that of natural cell membranes, they may fuse to intracellular vesicles upon MI.

This property was exploited by Seksek *et al*. who injected liposomes containing a fluorescent sensor with which they measured the pH inside Golgi vesicles [56].

Depending on their composition, liposomes can also be made responsive to different stimuli such as temperature, pH and oxidative species [58]. The MI of stimuli-responsive liposomes into cells grants the possibility to develop novel drug delivery systems that can release their cargo in a controlled manner upon their introduction in cells. For example, thermosensitive liposomes coated with gold were injected into cells and after applying a pulse of near infrared light, the heating of the gold shell led to the disruption of the liposomes and the release of the dye they contained [59]. While encapsulating fluorescent dyes allows answering valuable questions and is suitable for proof-of-concept studies, the loading of molecules with biomedical relevance can yield much more interesting applications. Some exciting developments that would be empowered by MI include the introduction of artificial organelles containing active enzymes and of bioreactors inside of which chemical reactions could be carried out [60, 61].

Reaction in vesicles as a step towards functional artificial organelles

Artificial vesicles like liposomes or polymersomes (vesicles constituted of amphiphilic block copolymers), constitute excellent reaction containers for enzymatic and chemical reactions because they bring the substrates in close proximity and enhance the reaction rates [60]. Several examples of chemical and enzymatic reactions successfully taking place in the lumen of artificial vesicles have been reported in the literature [62-64]. Grochmal *et al*. described a liposomal reaction vessel inside of which two amino acids reacted to form a dipeptide. An activated amino acid was entrapped inside the liposome exhibiting higher resistance against hydrolysis compared to the unencapsulated form. The second hydrophobically modified amino acid was added and diffused through the liposomal membrane into the interior where the synthesis of the dipeptide took place [62]. However, a higher concentration of the second amino acid had to be provided, probably due to diffusion hindrance. The importance of diffusion of the substrate into the lumen of the liposome/polymersome cannot be understated; in order to allow reactions inside the vesicles the substrate has to be relatively lipophilic, unless pores are inserted into the vesicle's membrane for the substrate to pass [65].

Reports on the use of artificial vesicles as containers for enzymatic reactions are more common in literature than for chemical reactions, likely due to the availability of different enzyme-substrate pairs [61]. For example, a few liposome-based detoxifying systems have been described where an encapsulated enzyme degrades a toxin. Petrikovics *et al*. encapsulated phosphotriesterase in sterically-stabilized PEGylated liposomes [66], which catalyzes the hydrolysis of paraoxon, a metabolite of the insecticide parathion. Injections of the liposomes into the bloodstream of mice revealed the high potency of this detoxifying approach. Importantly, paraoxon was a suitable substrate for an enzymatic reaction inside vesicles due to its hydrophobicity.

The development of artificial organelles requires the implementation of an optical readout system that is compatible with microscopy, since it is the most often used technique for the detection of cells subjected to MI. For this reason, a substrate showing fluorescence after enzymatic cleavage is preferred.

Several systems based on enzyme-encapsulating polymersomes haven been described, which can be considered as artificial organelles [67, 68]. Tanner *et al*. developed a highly sophisticated system of artificial peroxisomes where two enzymes reacting in an enzymatic cascade were encapsulated [68]. In addition, pore proteins were added to the shell of the 200-nm polymersomes, allowing the diffusion of reactive oxygen species to the vesicle interior. Successful endosomal escape was shown for the system, which was attributed to the polymer interactions with the membranes of endocytic vesicles. While impressive, a system implying the encapsulation of two different enzymes plus the insertion of a third protein in the membrane is difficult to work with. A simpler polymersome-based system encapsulating trypsin as a model enzyme was described by Ben-Haim *et al*. [67]. The readout was achieved with a lipophilic permeable dye-peptide conjugate, which was dequenched upon cleavage by trypsin, exhibiting fluorescence. Because the system was co-incubated with cells instead of introduced *via* MI, it was taken up by lysosomes within 10 min of incubation, and although the authors claimed successful endosomal escape based on the fact that the vesicles where found in the Golgi and endoplasmic reticulum after 1 h, the mechanism of escape -if any- was not explained. These trypsin-encapsulating polymersomes served as a source of inspiration for the trypsin-loaded liposomes later described in this thesis, which were delivered to cells by MI for their further analysis.

Cell-based therapies – Modern Trojan horses

In recent years, the concept of employing cells as vehicles to deliver drugs to their sites of action and improve the therapeutic outcome has received growing interest [69-72]. By loading migratory cells with particles encapsulating drugs or enzymes, they can act as Trojan horses, hiding their toxic cargo until they reach the site of action and deliver their load [73]. In addition, some cell types, like T-cells or DC, exhibit migration towards sites of tumors or inflammation. In case of DC, this movement is directed by the presence of chemoattractants or chemotactic cytokines like CCL2, whereas the binding to inflamed tissue is mediated by cell adhesion molecules such as P- and E-selectins, present on the surface of endothelial cells [74]. These properties inspired us to use DC to study the migration upon MI (see Chapter 3).

Different kind of cargoes are possible like NP loaded with cytotoxic drugs [75], phototoxic NP [73, 76] or even enzyme-polymer complexes [77]. Cheng *et al*. showed that neural stem cells (NSC), which exhibit tumor-tropic migration, could be loaded *via* incubation with silica NP containing the cytotoxic agent doxorubicin. The drug was bound *via* a pH-sensitive bond to the NP, which upon co-incubation with tumor cells, wandered towards these and induced their death [75]. However, the time posed a limiting factor since NSC were also susceptible to doxorubicin. Ninety-six hours after cell loading most of the NSC were found dead, indicating that the cells could only be used during a limited window of time to target tumors. In such approaches, the choice of vesicle encapsulating the drug may help prevent the premature death of the cellular Trojan horses [78]. For example, Batrakova *et al*. encapsulated catalase within poly(ethyleneimine) (PEI)/PEG copolymer assemblies to target oxidative stress [77]. These so-called nanozymes were phagocytosed by macrophages, which were shown to cross the blood-brain barrier, allowing brain delivery of drugs. The nanozymes retained their activity inside the carrying macrophages, and were released into the brain tissue over 4-5 days. However, the release from the macrophages was not explained, although it is a crucial step since many reactive oxygen species (ROS) are poorly membrane-permeable and can only react with the enzyme when it is outside of the cells. In a

very different approach published by Huang *et al*., particle uptake by the carrier cells was not required because the particles were directly bound to the cell surface. Liposomes encapsulating SN-38, the active metabolite of the topoisomerase inhibitor irinotecan, were bound to the cell surface of T cells *via* thioether bonds [79]. Upon reinfusion into the body, the T cells carrying particles on their surface migrated towards lymphomas, reducing tumor burden and enhancing animal survival. In this study, the problem of incubation and later release from the cell was circumvented. However, it is possible that the drug was released at all times during the cell migration, leading to a high systematic exposure.

Based on these past studies, a number of considerations have emerged in order to harness the benefits of using migratory cells as carriers for enzymes. Firstly, measures need to be put in place to preserve enzymatic activity following endocytic uptake, requiring a protective container. Secondly, depending on the application, a mechanism to ensure the release of the enzyme back into the surrounding medium might be necessary to enable enzymatic activity. Taken together, cell-based therapies have the potential to change cancer treatment in the upcoming years. However, important obstacles remain to be addressed, such as the cell-loading step and the prevention of carrier cell toxicity. MI can improve the loading of the carrier cells bypassing the endolysosomal pathway, and could therefore play a central role in this emerging field.

The scope of this thesis

In this context, the aim of this work was to investigate the fundamental aspects of the introduction of liposomes into cells by MI (Fig. 1.2), exploring the factors that will enable future applications of MI in artificial organelles, reactors and cell-based therapies.

In Chapter 2, the use of MI is reviewed in terms of the delivery of different colloids and in the context of the scientific discoveries it has enabled over the years. Besides the injection of proteins, Ab and NP, the introduction of DNA and RNA complexes is also reviewed, explaining the insights it has provided on topics like cytosolic trafficking and intracellular processing. The unique features of MI are described in detail, for instance the circumvention of the endolysosomal pathway and the possibility to define the precise timing and subcellular localization of the injection. Examples of studies in which these features were found to be useful are also provided.

Chapter 3 deals with the main scope of this thesis, the injection of liposomes encapsulating biologically active cargo directly into the cytosol of cells. First, the cytotoxicity and intracellular stability of the injected liposomes were investigated using formulations with different lipid compositions and PEGylation states. The liposomes' intracellular processing upon MI was studied by analyzing their potential capture by degrading compartments like autophagosomes and lysosomes. Special focus was placed on the aggregation patterns with which the colloids distributed in the cytosol after MI, and on the linearity (or non-linearity) with which they were diluted upon cell division. Subsequently, the injection of enzyme-encapsulating vesicles was investigated and finally, the injection of liposomes into migratory cells was explored, underlining the potential of MI in the development of artificial organelles and cell-based therapies.

In Chapter 4, the possibility of injecting a thermo-responsive liposomal system to trigger intracellular cargo release through an external stimulus was explored. The liposomal system selected for this purpose

had been proposed by Sung and coworkers in 2012 [80], and was found to be dysfunctional due to several technical flaws. A systematic study of the reasons underlying its irreproducibility was thereby carried out.

Finally, Chapter 5 summarizes the findings of this thesis and provides an outlook on how the findings regarding artificial organelles and cell-based therapies can be employed in the future.

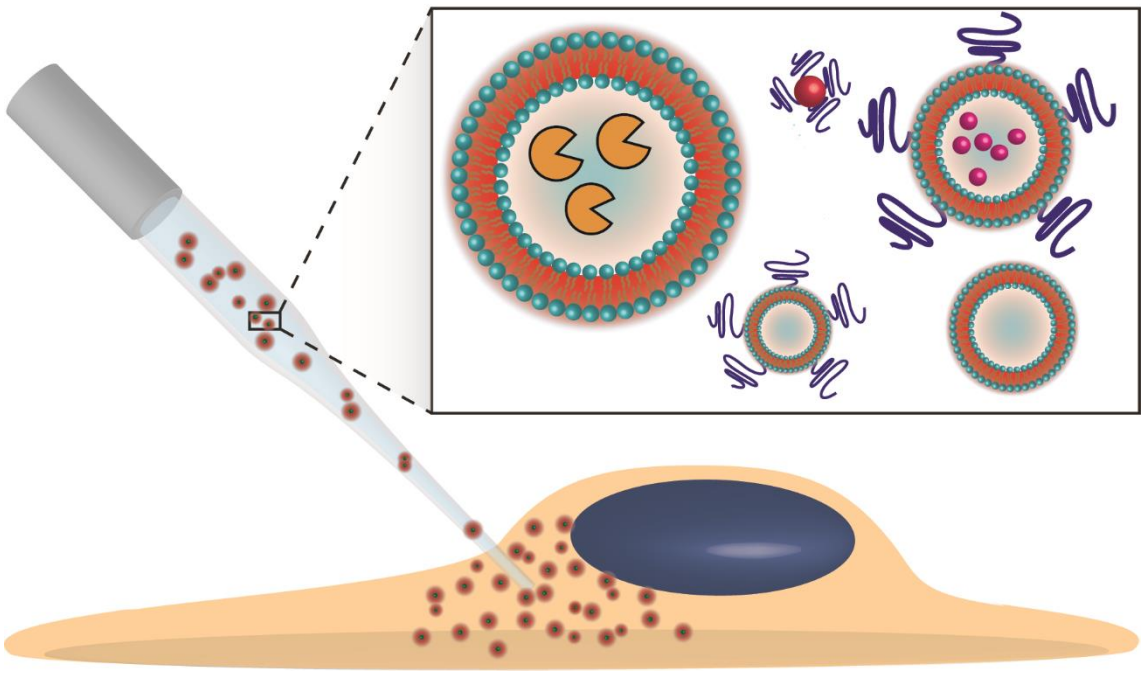

Figure 1.2 Graphical representation of the main aim of this thesis, the introduction of liposomal carriers into cells.

Chapter 2

Delivering Colloids into Cells:

What can we expect from microinjection?

Peter Tiefenboeck, Jong Ah Kim, Jean-Christophe Leroux

Swiss Federal Institute of Technology Zurich (ETHZ), Department of Chemistry and Applied Biosciences, Institute of Pharmaceutical Sciences, Vladimir-Prelog Weg 1-5/10, 8093 Zurich, Switzerland.

Introduction

As pointed out in Chapter 1, cell manipulation and intracellular delivery is crucial for the elucidation of intracellular processes, the development of gene-editing approaches and more recently, *ex-vivo* cell-based therapies [1]. While co-incubating cells with non-membrane permeable materials (*e.g.* colloids) to trigger their uptake *via* endocytosis is an often adopted approach, it is not suitable for those that are degradation-prone or have cytosolic activity, which is the case for many biomacromolecules with therapeutic potential. This is because the endolysosomal pathway eventually leads the internalized material to the lumen of endosomes and lysosomes, where the harsh environment of low pH and degradative proteases threatens the material's stability and impairs its biological activity [70]. Besides challenging their activity through destabilization, the endolysosomal vesicles can prevent the trapped cargo from reaching their targets in other intracellular compartments of the cell, requiring the implementation of membrane-destabilizing strategies to escape [45, 81-85].

Several techniques have been developed to overcome the hurdles imposed by the endocytic delivery of materials, all of which present strengths and weaknesses that should be considered in view of the material and biological system of interest [1]. Among the most exploited ones are electroporation [9], cell-squeezing [6], nanoneedles [86] and MI [16], as discussed in the former chapter. MI, the oldest of these techniques [12] employs a very thin glass needle which is filled with an isotonic injection solution. For simplicity, injections are generally done on cells adhered to substrates like coverslips or petri dishes, and although injections on cells in suspensions are also possible, they are more cumbersome and may require additional cell-holding devices [21].

Since only one cell can be injected at a time by the tip, the throughput of MI is rather limited and even when performed by an experienced technician, it is generally around 1'000-2'000 injected cells per hour. While this may be sufficient to study numerous cell processes at the single-cell level, automated MI systems will need to be developed to enable biomedical applications such as cell-based therapies. Although several automated MI devices were introduced in the last years [38, 39, 41], the speed of injection currently possible remains below 100 cells/min. More recently developed microfluidic devices may have the potential to substantially increase the number of cells injected per unit of time, bringing hope for cell-based therapies [6, 40]. Nevertheless, glass needle-mediated MI continues to be the most widespread approach due to its simplicity and versatility. From small molecules like fluorescent dyes [87], to larger nanocarriers (NP) like liposomes and DNA/polycation complexes [57, 88], a variety of cargoes has been efficiently injected into cells *via* MI, leading to versatile applications and numerous discoveries in diverse fields.

Unlike other techniques for intracellular delivery, MI allows to decide the exact time and site in which the material is introduced. The ability to inject protein inhibitors at specific stages of the cell cycle has yielded important mechanistic insights into the regulation of cell cycle progression. By selecting the subcellular compartment in which the material is delivered, for instance the nucleus instead of the cytoplasm, MI enabled seminal studies on the transport of nucleic acids in and out of the nucleus [89]. Moreover, MI can provide a way to study cellular processes in the context of complex tissues, as illustrated by reports of *ex vivo* injections in tissue slices [37], and in cells that are otherwise difficult to transfect, such as human blood stem cells [18] and mesenchymal stem cells [90]. MI has also enabled pioneering studies on the introduction of enzymes into giant vesicles inside of which the catalytic activity could be studied, representing a first step towards the development of artificial cells [91, 92]. Other fundamental studies performed with MI included the investigation of the viscosity and other

physical properties of the cytoplasm, where the diffusion of particles of different sizes inspired models to describe the cytosol [32].

In this review, we provide an overview of the different kinds of colloids that have been administered into cells by MI (namely, proteins, nucleic acids and nanocarriers, Fig. 2.1), and emphasize the specific features of MI that have enabled important breakthroughs in biology and that are likely to have an impact on further developments concerning artificial organelles and cell-based therapies. Finally, the intracellular processing and clearance of injected material is discussed in view of the implications for drug delivery, explaining the different possible outcomes depending on the type of colloid introduced and of cytoplasmic parameters (*i.e.* viscosity and cytoskeletal elements).

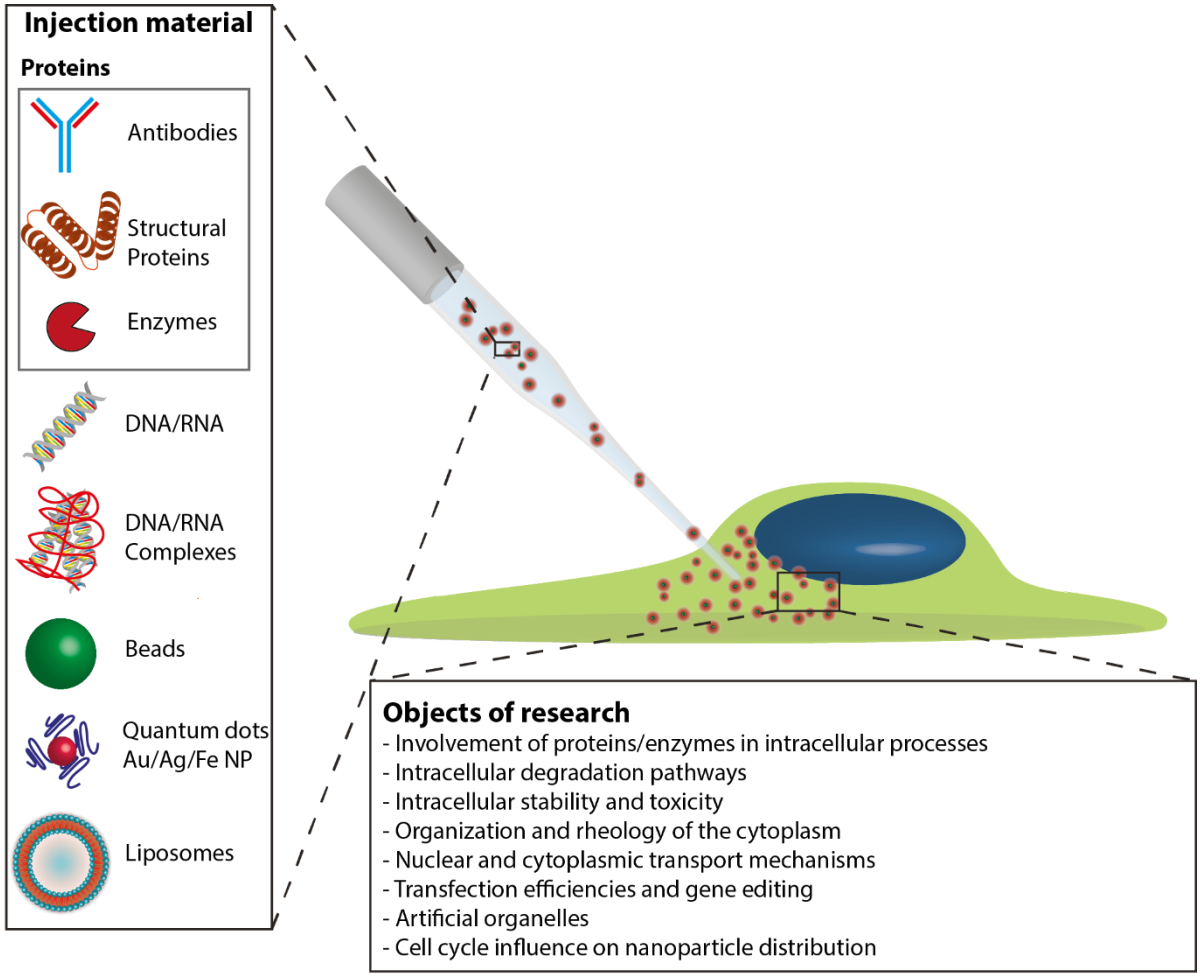

Figure 2.1. Schematic overview of injected colloids and objects of research.

Determination of Injection Volume

Knowing the amount of material injected into one cell is important for most experimental setups to generate reproducible data. Generally, the injected amount should be below 20% of the cell's volume to prevent it from bursting [24]. Several methods for the quantification of the injection volume have been proposed and while all of them present limitations, the volume quantifications reported in the literature appear rather comparable when the differences in the cell types used are considered. For instance, fibroblasts have an average cell volume of 3000 fL [93] allowing injections in the range of 10-20 fL [94], whereas oocytes that are much larger (100-300 pL on average [95]) can take up to 1-3 pL [96]. In both cases the injection volumes account for less than 5% of the total cell volume.

Capecchi *et al*. determined the injection volume in fibroblasts using radioactive tracers (^{3}H-(2'-deoxythymidine-5'-triphosphate) (^{3}H-dTTP)) and measuring the total radioactivity of all injected cells (approximately 5'000 cells) *via* scintillation counting. With this method, they found that the average injection volume per cell accounted for 1-2% of the total cell volume [30]. Despite being an accurate quantification method, it implies complications inherent to working with radioactive material. A simpler approach to estimate the average amount dispensed per cell is to fill the injection needle with a known volume of material and inject cells until the needle is emptied [97]. However, this procedure has a large margin of error due to the loss of injection material that happens during the cleaning steps needed to unclog the tip during injections, and due to the holding pressure that is applied to the needle to prevent the clogging in the first place. Another method described early on but still often used for simplicity is measuring the difference in the meniscus position inside the injection needle before and after injection, and calculating the volume dispensed based on the inner diameter of the tip [94, 96].

A major drawback of the above-mentioned techniques is that they provide only an average estimation of injected sample amount, potentially overlooking the variability among the values for single cells. An alternative to overcome this issue is to correlate the fluorescence of every injected cell with a standard curve. In order to allow a correlation between volume and fluorescence intensity, a dye previously dissolved in an aqueous buffer is injected into oil to generate spherical droplets. The fluorescence intensity of these droplets is then quantified, together with size determination and volume calculation to give a ratio of fluorescence intensity to volume [23, 24]. Applying this method, Minaschek *et al*. revealed the high variability in injected volume in 3T3 fibroblasts, which ranged from 4 fL to 2'446 fL for different capillaries [23]. Other reported values using the same quantification technique indicated 420 fL for HFF cells [98] and 1.5-30 fL for human fibroblasts [99].

Taken together, the injected volume reported in the literature ranges from a few fL to 1 pL, and among all the described techniques to quantify injection volume, the most common one remains the correlation with the standard curve of fluorescence intensity of dye-in-oil droplets.

Microinjection of Proteins

The introduction of proteins such as Ab into cells *via* MI has been a powerful tool to answer numerous biological questions through gain- or loss-of-function experiments. Proteins exhibiting a specific

biological function can be injected in specific compartments of the cells to study the resulting changes or be introduced to block intracellular processes (*e.g.* Ab) and inform of the downstream consequences.

The recruitment of surface proteins to intracellular organelles where they exert their biological function has been studied *via* MI. Using fluorescently labelled proteins, MI-based studies identified the role of individual components of large multiprotein complexes, such as those forming the endosomal sorting complexes required for transport (ESCRT complexes). The different ESCRT complexes (named ESCRT-0 to –III) are involved in membrane remodeling and the removal of damaged proteins from the cell surface. One of the components of the ESCRT-0 complex, the protein Hepatocyte growth factor regulated tyrosine kinase substrate (Hrs), accumulates in the endosomes and recognizes ubiquitylated cargo during the endosomal sorting process. By injecting a fluorescent version of Hrs, Kojima *et al.* found that the protein was targeted to the endosomes independently of its binding to other components of the complex, which ensured an equilibrium between endolysosomal and cytoplasmic distribution of the ESCRT-0 complex [100].

In another set of studies empowered by MI, the transport mechanisms that a protein might be subject to in the cytosol were investigated, together with the factors determining its entry or exclusion from specific subcellular compartments. Three proteins (calmodulin, nucleoplasmin and lysozyme) were studied independently from each other in regard of the circumstances of their nuclear entry. Calmodulin is a protein with diverse biological functions that acts by binding calcium intracellularly and transducing signals to other effector proteins, for which it shuttles in between the different subcellular compartments. Using MI, its import into the nucleus was found to be unaffected by adenosine triphosphate (ATP) depletion, whereas it could be arrested by low temperatures and by wheat germ agglutinin which blocks the NPC [101]. This suggested that the import of calmodulin into the nucleus does not occur *via* passive diffusion nor active import. The authors postulated a so-called facilitated import, where calmodulin is likely to bind to other proteins mediating the translocation. In the case of nucleoplasmin, a molecular chaperone involved in chromatin organization and transcriptional regulation, its uptake into the nucleus was blocked upon exposure to low temperatures and depletion of ATP, suggesting that the uptake mechanism was energy-dependent [102]. Binding to the nuclear envelope, however was not affected by these triggers. These findings helped to distinguish between two different processes in nuclear uptake. The rapid binding to the nuclear envelope occurs as a first step followed by a slower energy-dependent translocation through the NPC. In contrast, the translocation of smaller proteins like lysozyme (14.4 kDa) could not be inhibited neither by low temperatures nor ATP depletion, which is line with their nowadays well-established entry mechanism by diffusion [103]. Besides investigating the mechanism of nuclear import, MI has allowed studying the intracellular transport of injected proteins within the cytosol. The enzyme horseradish peroxidase (HRP) was injected into neurons and the distance travelled by it from the site of injection was calculated by fixing the cells at different time points and adding in the medium the substrate diaminobenzidine to detect the enzyme's localization. The transport mechanism was later on found to be mediated by microtubules [42, 104]. MI enabled in these studies the unhindered introduction of the proteins into the cytosol, which would have otherwise been trapped in endosomes, preventing their diffusion and/or active transport.

The organization of actin and tubulin and their involvement in cellular transport processes was elucidated injecting fluorescently labelled filaments of the two proteins into cells, and subsequently analyzing their colocalisation with other labelled cytosolic proteins. The filaments were added into the preexisting network and showed similar behavior to the native proteins in that they participated in the growing of microtubules and were responsive to cytoplasmic messengers like calcium [105-108]. Based on the observations, the microinjected actin was divided into two classes in terms of mobility: immobile actin which locates in stress fibers, focal contacts and filaments, and mobile actin found in the

interfibrillary space [106]. Other studies also addressed the changes in actin organization after injecting different cytoskeletal reorganization-triggering protein-like members of the rho family. They revealed that rho was strongly implicated in the organization of the cytoskeletal network affecting cell shape [29], and in the formation of stress fibers and focal adhesion [109]. Some of these investigations were performed before green fluorescent protein (GFP)-labeling became available, when MI of pre-labelled proteins was the only method to observe them in living cells. Nevertheless, MI still plays an important role even in the current post-GFP era, since the bulky GFP label may interact with preexisting fiber hindering the insertion of the labelled actin.

The study of apoptosis was also empowered by MI, in particular in the elucidation of the early onset of the apoptotic cascade. Since many of the proteins involved in this cascade are strongly toxic for the cells (*e.g*. caspases [110]), the study of their interactions would not have been possible with transfection techniques because the transfected cells would not withstand the expression. The involvement of cytochrome c in apoptosis, which was shown to be caspase-dependent, was discovered *via* injections of cytochrome c (or triggers for the release of cytochrome c) into cells [111-115].

Besides answering fundamental questions, MI has also been used to obtain proof of concept for applied studies. A peptide-estradiol conjugate called Protac (proteolysis of targeting chimeric molecule) was shown to bind estrogen receptors (EsR) upon MI and to connect them with an ubiquitin ligase, targeting them for degradation. The conjugate was proposed as a potential therapeutic approach in which cancer-promoting proteins would be targeted intracellularly for ubiquitylation and subsequent degradation. Given the conjugate's poor membrane permeability, the use of MI proved to be key to introduce it into cells and obtain proof of concept [116].

The MI of Ab directly into the cytosol is a useful approach to study intracellular changes upon blockade of one specific protein. The instant inhibition allows observing changes with precise control over time, which is not possible for example when the protein is knocked down. Moreover, knockdown of housekeeping genes can be incompatible with cell viability, making it impossible to detect a reaction cascade following the inhibition. In addition, the injection into specific locations of the cell, like the nucleus or the cytoplasm, allows the compartment-specific blockade of proteins not achievable with other techniques. This feature can be very useful for proteins that carry out different functions depending on their localization. Furthermore, Ab can also be used as coinjection markers to identify the successfully injected cells, either by direct coupling of a fluorophore [18] or after detection with a secondary Ab [117, 118].

The possibility to inject Ab in different subcellular compartments at discrete times of a cell's life cycle has provided the means to identify the role of specific proteins in complex biological processes such as cell proliferation, signaling and cell cycle regulation [25, 26, 119]. The injection of an Ab against cyclin A unveiled the protein's role in regulating cell cycle progression from one phase to another. When injected in G1 phase, the anti-cyclin Ab inhibited DNA synthesis and delayed entry into S phase, whereas when injected in G2 phase the entry into M phase was completely inhibited [25, 26]. In another pioneering study, Dixon *et al*. blocked the interaction between histones and lamin, a filament protein present in the nucleus, by nuclear injection of Ab against the lamin A/C histone-binding site, thus inhibiting mitotic entry and showing that this protein-protein interaction was responsible for the spatial genome organization [120].

MI of Ab into the cytosol has also led to important insights in the investigation of cell morphology, intracellular organization and transport. MI of anti-myosin Ab revealed that myosin was not only relevant in the determination of cell shape but also in the cellular motility, which was increased upon

myosin blockage [27]. Moreover, the injection of Ab against kinesin, a microtubule-dependent motor protein responsible for organelle transport, allowed establishing the protein's involvement in the centrifugal movement of granules [121], the organization of intermediate filaments [122] and the control of cell shape [123].

The translocation mechanisms of virus proteins to the cell surface their infection of host cells were investigated by injecting Ab specific against viral proteins and transport vesicle-associated proteins. Kreis *et al.* studied the translocation of the vesicular stomatitis virus glycoprotein (VSV-G) from the Golgi complex to the cell membrane, a viral component serving as a model for the intracellular transport of membrane proteins [124]. Shielding of the VSV-G's cytoplasmic domain with injected Ab blocked the glycoprotein's transport to the cell surface. Additionally, protein's transport was also blocked upon injection of Ab against the vesicle-associated coat protein (COP) β-COP, which is associated with the Golgi complex in the budding of new vesicles and transport to cellular membranes [28]. Based on their observations, the authors were able to show the involvement of β-COP in intracellular transport processes of viral proteins from the ER/Golgi to the cell surface *via* COP-coated vesicles. In this particular case, MI was more appropriate than other techniques since the rapid onset of the effects within 30 min after manipulation would not have been possible to observe with incubation methods, which demand longer times to introduce biomolecules into the cell and would lead to the entrapments of the Ab in endolysosomal vesicles. Moreover, a complete knockdown of *e.g.* β-COP would have greatly complicated the study of this particular function given its involvement in many other processes.

Taken together, MI of proteins and Ab allowed the elucidation of several intracellular pathways involved in the translocation of proteins to specific compartments. Besides that, studies on cell deformation and apoptotic processes could solely be performed by MI, since the effects were anticipated to happen soon after the introduction of the triggering biomacromolecule.

Microinjection of DNA/RNA

By delivering genetic material directly into cells without inducing its entrapment inside endolysosomal vesicles, MI enabled fundamental breakthroughs on the transport of DNA and RNA in the intracellular compartment. In 1980, Capecchi and collaborators discovered that the introduction of DNA into the nucleus led to a transfection efficiency of 50-100%, whereas cytoplasmic injections were not followed by subsequent gene expression [30]. This suggested that the DNA did not translocate from the cytoplasm to the nucleus, and that this step was a prerequisite for subsequent translation. MI was at the time of this discovery the only technique enabling such study, given the unique possibility to introduce material in specific subcellular compartments. Further MI-based studies showed that ON and their analogues preferentially ended up in the nucleus after MI [31], which indicated that the size of the DNA/RNA molecules introduced in cells was a limiting factor in the translocation to the nucleus and subsequent expression. Later on, Dowty *et al*. reported that the process took place *via* the NPC, which limited the entry of moieties above a certain size threshold [34]. Occlusion of the NPC with wheat germ agglutinin and ATP-depletion blocked the entry of several injected ON into the nucleus [125], suggesting the translocation process through the NPC was energy-dependent [125, 126].

While chemical- and viral-mediated transfections are nowadays the most common techniques for cell genome manipulation, MI played an important role in the early days when lipid-based transfection

reagents were not yet commonplace. Before the invention of lipid-mediated gene transfection in 1987 [127], only a few methods were available to transfect cells with nucleic acids, such as those based on calcium phosphate particles [128], viruses [129] and electroporation [5]. Pioneering work on the MI of genetic material performed by Graessmann [14] and Diacumakos [13] in the 1970's paved the way for subsequent studies of functional genomics. For instance, MI of the DNA of the Epstein-Barr virus (EBV) revealed the existence of a cellular barrier against the viral entry, but only in certain cell types in which the infection would not occur unless assisted by MI [19]. Three decades later, the underlying mechanism was unraveled and EBV was found to enter *via* CD21, which is expressed on B lymphocytes but not on fibroblasts [130].

Although nowadays MI has been replaced to some extent by more efficient transfection techniques, it remains in use for its precision, ability to modify difficult-to-transfect cells (*i.e.* neurons, blood stem cells and mesenchymal stem cells) [18, 90], and the possibility to treat single cells in tissue slices, among other features. The study of morphological plasticity in the hindbrain was possible after the delivery of a plasmid encoding for fluorescent actin into neurons was achieved in brain tissue slices by MI [131]. In addition, MI enabled the study of the mechanisms of differentiation and proliferation of neural stem cells in brain slices of mouse embryos. Taverna *et al*. injected RNA pools isolated from transgenic neural stem cells into the cytosol of apical progenitor cells in organotypic brain tissue slices, and found that these extracts -but not those of adult mouse brains- were able to shift the balance of the progenitor cells from differentiation towards proliferation (Fig. 2.2) [37, 132]. Given its precision in manipulating individual cells, MI also offers the possibility to leave neighboring cells untreated [133], providing an internal negative control for such studies on tissue slices. Moreover, if an experiment requires several different DNA constructs and/or peptides to be introduced simultaneously into the cell, MI is certainly an advantageous approach compared to lipid-based transfection techniques requiring extensive optimization. The combinatorial flexibility of MI was illustrated in a study of neuronal transport processes, where neurons were simultaneously injected with several plasmids, peptides and Ab [133].

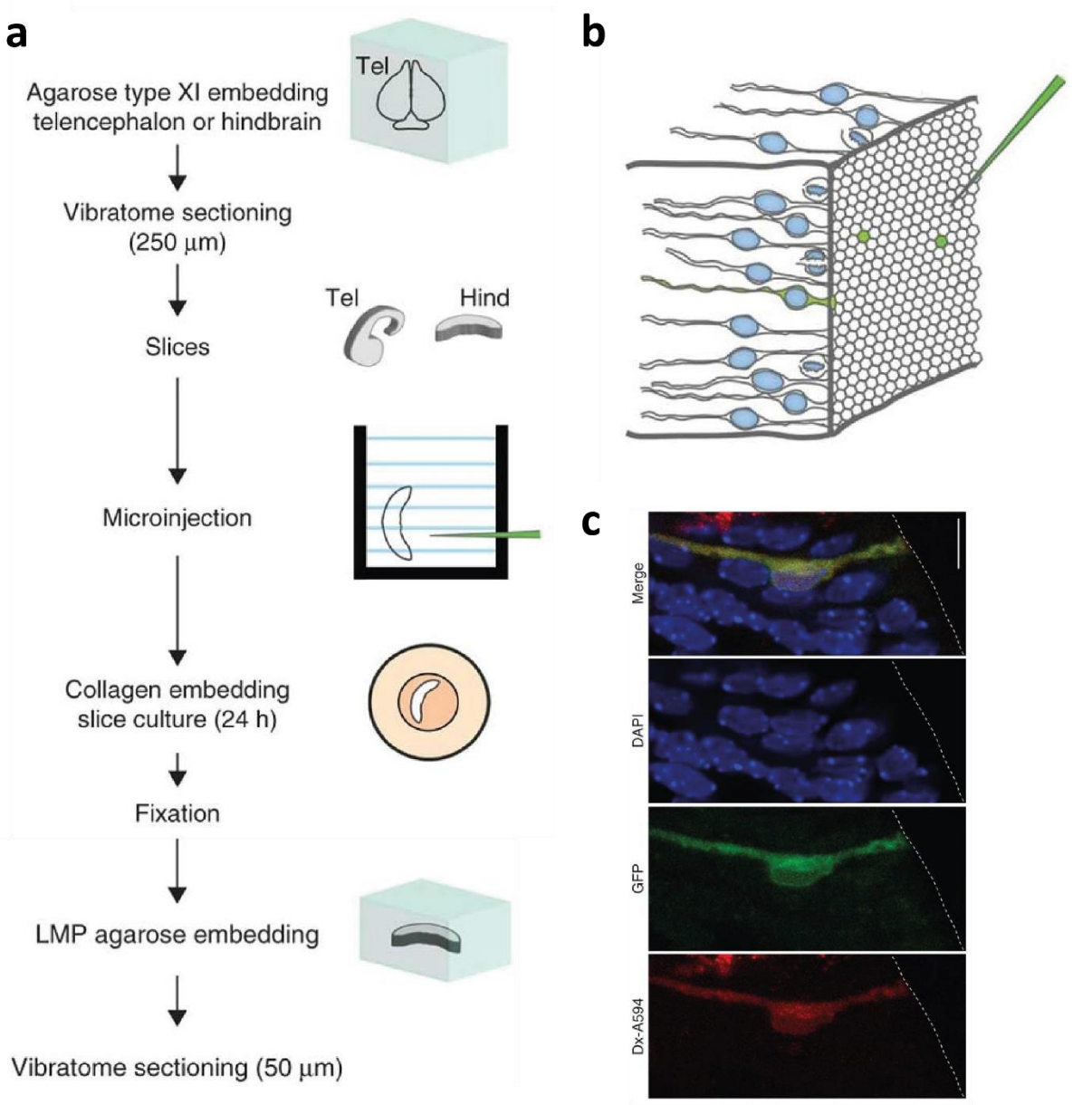

Figure 2.2. Microinjection of individual neurons in cultured brain tissue slices. A) Scheme of the procedure followed to obtain tissue slices from embryonic mouse brain and perform MI of single cells. B) Cartoon depicting a brain tissue slice on which single cells were injected with a fluorescent injection marker (green); nuclei indicated in blue. C) Tissue slice where an apical progenitor cell expressed the reporter protein GFP after being injected with injection marker and RNA extract from transgenic neural stem cells. Injection marker (Dx-A594, red), GFP (green), nuclei (DAPI, blue). The tissue slice was incubated for further 30 h after MI, followed by fixation, staining and imaging. Scale bar 10 µm. Adapted from Taverna *et al*. with permission [37].

An interesting field connected to the MI of DNA/RNA is the injection of hybridized constructs. Using a Foerster resonance energy transfer (FRET)-based approach, it was shown that injected ON could remain hybridized inside the cell with a half-life only 15 min before FRET was lost due to degradation [134]. This indicated that the hybridization state of nucleic acids can serve as a measure for intracellular stability of ON, which determines the longevity and effect strength. Besides FRET, fluorescence *in situ*

hybridization (FISH) has also been employed to study the half-life of injected DNA, which was shown to be around 1-2h in common cell lines [135]. The quick degradation of the injected DNA was attributed to binding of the strands to intracellular transport proteins and to the presence of cytosolic nucleases that break double strands and trigger their degradation [88, 134, 135].

The complexation of DNA with positively charged lipids or polymers (to form lipoplexes or polyplexes, respectively) is known to promote transfection efficacy by protecting the DNA and minimizing its degradation [88]. Before the underlying mechanisms were understood, the possibility to inject these complexes in different compartments of the cells provided important insights into the process of transfection itself, specifically the release of DNA from the complexes. Early studies showed that cytoplasmic injections of DNA complexed with PEI or polylysine (PLL) had higher transfection efficiency compared to uncomplexed DNA [136-138]. Moreover, the injections of PLL-complexed DNA revealed that high nitrogen to phosphate (N/P) ratios decreased the transfection efficiency. It is nowadays known that an excessively strong binding of the DNA to the complexing polymer can override the benefits of complexation in terms of stability, because it decreases the amount of DNA dissociated and therefore lowers transfection efficacy [139, 140]. As shown by Zabner *et al*., similar concepts apply as well for lipoplexes, where a low lipid-to-DNA ratio was found to be necessary to allow expression [141].

Microinjection of Nanocarriers

Although most nanocarriers are easily internalized by cells upon co-incubation, they do so at the expenses of being covered with a layer of proteins that modifies their surface properties [47]. One of the consequences of the protein corona is that NP carrying targeting moieties can lose their targeting capabilities after being in contact with biological medium [48]. In addition, nanocarrier internalization *via* endocytosis normally leads to entrapment in endocytic vesicles and potentially also degradation in the lysosomal compartment, demanding the implementation of membrane-destabilizing strategies to achieve an effective intracellular dose of the material [142]. MI provides a portal of entry for colloids into cells that not only effectively overcomes the endolosysomal barrier but also preserves their surface properties [143]. Table 2.1 shows different kinds of NP and vesicles that have been injected into cells and presents them according to size, surface properties and object of research.

Table 1, NP injected into cells, sorted by type and size.

Type	Diameter (nm)	Further specification	PEGylation	Object of research	Year	Ref.
Quantum dots	10		+	Intracellular mobility	2017	[144]
	10-15		+	Imaging/stability	2002	[145]
	12.5		+	Labeling	2010	[146]

	13.3	Sulfobetaine labeled	+/-	Stability/targeting	2012	[147]
	13-18		+	Intracellular localization	2013	[44]
	15-50	YFP/b-PE-conjugate	+/-	Intracellular localization	2008	[148]
	25-28	NLS signal	+	Labeling	2004	[149]
Gold NP	1.2-2.7		+	Intracellular distribution, stability	2016	[150]
	15	Nucleoplasmin coated	-	Intracellular mobility	1988	[102]
	22-36	Nucleoplasmin coated	-	Intracellular mobility	2002	[151]
Ag NP/Fe_3O_4 NP	7.8-21.5	Citrate and TMAOH capped	-	Toxicity	2011	[152]
Liposomes	50-100		+	Intracellular dye sensitivity	2008	[57]
	70		-	Intracellular fusion	1995	[56]
	75-137		+	Artificial organelles	2017	[153]
	100	Gold coated	+	Intracellular release	2000	[59]
DNA/RNA Complexes	72.9-102	Protamine-condensed	-	Intracellular transport, transfection	2015	[140]
	165	Poly(ethylenimine) condensed	-	Autophagosomal capture	2014	[53]
	250	Cationic lipid condensed	-	Dissociation	2005	[154]
Poly(styrene) NP	40-100		-	Autophagosomal capture	2014	[53]
	100		+	Mobility in cytoplasm	2008	[49]
	100-200		-	Mobility in cytoplasm	2002	[155]
	100-500		+	Mobility in cytoplasm	2014	[156]
	122		+/-	Intracellular localization	2014	[52]

	210	+/-	Intracellular mobility/rheology	2005	[157]
Silica NP	12	+	Autophagosomal capture	2014	[51]
Polysaccharide NP	3.2-24.8	-	Intracellular mobility	1987	[158]

Abbreviations: YFP yellow fluorescent protein, b-PE b-phycoerythrin NLS nuclear localization sequence, TMAOH tetramethylammonium hydroxide.

Semiconductor nanocrystals (quantum dots, QD) overcome the fluorescence bleaching problem of small molecule-based dyes [159], but their biocompatibility has proven to be an obstacle for biological applications. Dubertret *et al*. have successfully exploited their favorable *in vivo* imaging properties by encapsulating individual QD in phospholipid micelles to achieve a stable suspension and colloidal stability, and injecting them into *Xenopus* embryos. In their study, the authors demonstrated the particles' coating prohibited aggregation for at least 4 days, which ultimately allowed them to harvest the QD's high stability and persistent staining capabilities in this first proof-of-concept study [145]. The toxicity of these particles was low, which could attributed to the ZnS shell of the particles [160]. In comparative studies of injected *versus* incubated QD, the former were shown to remain in the cytoplasm for 24 h without any cellular processing, whereas the QD taken up *via* endocytosis were unable to escape the endosomal vesicles and did not reach the cytoplasm [44]. Similar results were reported for QD labelled with a cell-penetrating peptide consisting of a C-terminal 8 arginine repeat-block, which despite enhancing the uptake during co-incubation, confined the particles to the endolysosomes and failed to deliver them to the cytosol as efficiently as MI [148]. The intracellular fate of injected QD was studied as well in *Xenopus* embryos, where the surface chemistry of the particles was found to be a determining factor. While QD with sulfobetaine capping did not aggregate inside the embryos, PEGylated phospholipid micelle-encapsulated QD clustered one week after MI [147]. Actin has been proposed to play a role in the diffusion of QD inside the cell since disruption of the actin network enhanced the QD intracellular diffusion [144].

The use of targeted QD for intracellular staining in combination with MI has yielded interesting developments. By attaching a nuclear localization sequence (NLS) or a mitochondrial localization sequence (MLS) to the QD, specific staining of the nucleus or the mitochondria could be achieved [149]. Furthermore, the attachment of 5'000 molecular weight (MW) PEG-chains on the surface of QD lead to a 28-nm particle that was excluded from the nucleus, indicating a size limitation to go through the nuclear pores [149]. Building up on this knowledge, streptavidin-coated QD were used as modular imaging probes in combination with biotinylated hapten molecules. Upon their injection, the QD bound to the hapten conjugates by streptavidin-biotin interactions, which in turn bound to specific proteins expressed with fused hapten-binding tags in genetically modified cells [161]. With this approach, multiple proteins could be tracked in living cells at the single-particle level during much longer trajectories than previously possible.

MI-based studies have also combined electron microscopic analysis with gold nanoparticles (Au NP) to study subcellular structures. The attachment of the protein chaperone nucleoplasmin on the surface of Au NP led them to localize at the nuclear membrane, likely at pore-associated fibrils [102], enabling the study of uptake processes into the nucleus and revealing that binding to the nuclear envelope was a prerequisite for nuclear entry. Using NLS-labelled Au NP, nuclear accumulation was found to only be

possible for sizes below 39 nm [151]. This finding prompted the development of bulky Au NP-conjugated hybridization-sensitive probes, which given the size restrictions of the NPC did not translocate to the nucleus and were thus able to hybridize with cytoplasmic mRNA. Similarly as with QD, the PEGylation of Au nanoclusters prevented their aggregation and promoted their stability inside the cell [150].

Besides metallic NP, several reports have described the injection of liposomes, which are often used as protective containers for sensitive cargo. Seksek *et al*. delivered by MI 1,2-dioleoyl-*sn*-glycero-3-phosphocholine (DOPC) liposomes encapsulating a pH-dependent fluorescent sensor, which upon their ATP-mediated fusion with Golgi vesicles, enabled the measurement of the pH of the Golgi vesicles [56]. The process was described as energy- and size-dependent, since only liposomes in the size range of 60-70 nm could be fused, whereas smaller or larger liposomes were not capable of fusion. The authors suggested that the used liposomes were close in size and lipid composition of naturally occurring vesicles, which also show fusion. The proposed mechanism and site-specificity is seemingly very elusive, since no further explanations were given regarding onset of fusion or physical-chemical actions leading to this event. Chen *et al*. also investigated intracellular sensors using fluorophores, liposomes and MI. They evaluated several dyes upon injection for their sensing capacity of the intracellular environment by comparing their fluorescence when encapsulated inside liposomes (where they would not be exposed to the intracellular environment) or when attached to the liposomes' external surface [57]. Moreover, liposomes with controlled release strategies have also been studied in combination with MI for the development of novel drug delivery systems. For instance, intracellular controlled release was tested by injecting thermosensitive liposomes coated with gold and applying near infrared light to the injected cells. The heating of the gold shell led to the disruption of the liposomal bilayer and the release of the encapsulated cargo [59]. As further explained in Chapter 3, we studied the fundamental aspects of injecting liposomes into cells, and found that they were well tolerated by cells, and could remain stable in the cytosol for up to two days. The intracellular stability depended on the liposomes' composition and PEGylation state. This prompted us to investigate liposomes encapsulating a model enzyme, which we were able to show preserved its catalytic activity upon injection in the cytosol. Even if only a study model, systems such as these enzyme-encapsulating liposomes allow to answer fundamental questions that accelerate the development of functional artificial organelles and cell-based therapies. Although numerous fundamental questions have and will likely continue to be answered with similar systems, the most exciting outcomes of injecting NP might arise from systems encapsulating biologically active cargo, mimicking artificial organelles and giving yield to cell-based therapies.

Intracellular processing of injected colloids

Following their introduction *via* MI, colloids encounter the intracellular environment and subcellular structures present in the cytosol. Intracellular transport mechanisms may move them between different areas of the cytosol, relocating them from their initial injection site. They may also be captured by organelles and potentially be destabilized by the degradative conditions contained in their lumen. In addition, the injected material may be affected by the cell's own life cycle stages. The intracellular processing of injected particles can therefore be analyzed in light of different phenomena, such as the diffusion pattern in the cytosol, the degradation processes in the cell's organelles and the dilution of the injected load upon cell division.

Almost 30 years ago, Luby-Phelps *et al*. conducted foundational studies to describe the structure of the cytoplasm using dextrans of different sizes (3 - 58 nm) and polysaccharide (Ficoll) beads of up to 25 nm [32, 158, 162-166]. Using a microscopy technique called fluorescence recovery after photobleaching (FRAP), they could show that the diffusion coefficient in the cytoplasm decreased with the size of injected dextrans [162]. Moreover, they found that the injected material was excluded from several subcellular structures, such as mitochondria and endocytic vesicles, indicating that these hydrophilic compounds were unable to overcome intracellular membranes. In these early studies, the effective viscosity that particles larger than 3 nm encountered in the intracellular milieu was calculated to be 3-4 times higher than that of water [158]. However, the cytoskeletal network was likely the major contributor to this calculation, since the actual viscosity of the cytoplasmic fluid alone was later found to be comparable to that of water [164]. The cytoplasm was therefore described as a molecular sieve, where the intermediate filaments acted as a network of fibers contributing to the sieving mechanism. This would explain why particles cannot cross the cytoplasm freely, since depending on their size they are held back by the network of fibers [32, 166].

The described model may provide explanations for several findings concerning the injection of nucleic acids [33]. Transfection efficiency, for instance, could be understood in light of the diffusion of the injected DNA construct through the cytosol, which is in turn determined by the site of injection (proximity to the nucleus) and the construct's own size (larger DNA constructs diffuse slower) [34, 167]. Generally, it is perceived that smaller fragments of DNA or RNA are easier and/or faster to transfect [168]. This is partly due to the fragments' microtubule-mediated shuttling towards the nucleus [169, 170] and probably also due to their ease of translocation into the nucleus. It is now known that the NPC imposes the size cut-off for nuclear translocation around 39 nm [151]. Compared to cytosolic injections, material injected directly into the nucleus encounters a higher viscosity, as shown by the slower diffusion of nucleic acids upon intranuclear injections [167]. The higher viscosity as seen in the difference in diffusion was proposed to be connected to the binding of the injected material to nuclear components, such as positively charged histones [167].

The behavior observed with injected NP could also be understood in light of the sieving meshwork model of the cytoplasm. After being injected into the cytoplasm, 13-18 nm QD remained dispersed in the cytosol with a higher concentration at the injection site, and did not agglomerate over time nor were captured by intracellular organelles like endocytic or autophagosomal vesicles [44]. In fact, their intracellular distribution remained unchanged for 24 h after injection. This could be attributed to their small size, which would allow them to pass through the meshes of the cytoplasmic sieve. PEGylation was shown to enhance the free diffusion of the particles [49], and together with bovine serum albumin (BSA), it blocked the absorption to actin filaments [157]. As a result, functionalized particles diffused faster compared to unmodified ones. Interestingly, other particles have been reported to behave differently to the QD as further discussed in Chapter 3. Although a systematic study would be required to clarify the underlying reasons, the injection of liposomes of different sizes suggested the agglomeration in the cytosol would be size-dependent. Whereas small unilamellar vesicles (SUV) of around 80 nm showed some degree of agglomeration in the injected cells, large unilamellar vesicles (LUV) of around 130 nm underwent strong agglomeration within the first 8 h after MI and displayed a highly polarized intracellular distribution. The agglomeration of the liposomes was found to be reversible, as an injection of buffer into the cells easily disrupted the clusters of particles. It is possible that larger particles would establish stronger interactions with the cytoplasmic meshwork and would therefore localize to areas of lower intracellular remodeling.

Depending on the nature of the colloids injected, they can be cleared from the cytoplasm by endogenous cellular mechanisms. Nucleic acids are degraded in the cytoplasm by Ca^{2+}-sensitive nucleases [88]. For

other injected colloids of larger size, the clearance from the cytoplasm can take place through an autophagy-mediated response. Although autophagy is a relatively young field and numerous mechanistic questions remained to be answered, it is currently believed that the sequestration of intracellular material *via* autophagosomes is initiated in a stochastic manner with the formation of autophagosomal membranes around seemingly random cytosolic domains. Subsequently, the autophagosomes fuse with the lysosomes, leading to the cargo's degradation by lysosomal proteases and low pH [54]. In the early days of MI, proteins were described to undergo autophagy-mediated clearance [50]. BSA, lactoglobulin, ovalbumin, catalase and apoferritin were observed in perinuclear vesicles after MI, which were identified as autophagosomes. Their capture in autophagosomes was described to be size-dependent, with the larger ones being taken up faster than smaller ones [50]. Besides proteins, some NP have also been described to be taken up by autophagosomes upon MI. Polystyrene particles of 100 nm diameter and PEI/DNA complexes were reported to accumulate in the perinuclear region after injection [52], which was later on confirmed to be due to their uptake into autophagosomes and lysosomes using electron microscopy and gold labels [53]. Interestingly, liposomes of sizes comparable to the polystyrene particles did not colocalize with lysosomal nor autophagosomal markers 24 h and 48 h after injection, neither in their PEGylated nor unPEGylated forms as described in Chapter 3. It is possible that their composition largely based on natural lipids prevented their recognition by the autophagosomal system. From a drug delivery perspective, the capture of injected material by autophagosomes constitutes an obstacle, as not only this can lead to the degradation of the material but also prevent it from reaching its subcellular target. In order to overcome the rapid uptake of injected colloids by autophagosomes, surface PEGylation has been explored, showing a shielding effect and preventing the capture of PEGylated proteins like light chain ferritin (LCF) and silica NP [51]. This could be due to the hydrophilicity of the PEG chains, which prevents the attachment of cellular proteins and the recognition by such clearing mechanisms [171]. Hence, depending on the composition of the colloid injected and on its surface modifications, autophagy may impose a hurdle for drug delivery purposes.

If the colloids are not eliminated by clearing mechanisms, they will eventually be affected by the cell's life cycle. Cell division influences the fate of microinjected material in different ways due to the breakdown of the nuclear membrane during mitosis and/or the distribution of the cell's cytoplasm among daughter cells [89]. For nucleic acids, DNA injected into the cytoplasm showed higher transfection efficiency when the cells underwent division soon after the injection [89]. This was attributed to the breakdown of the nuclear membrane during mitosis, which allowed the DNA to access the nucleus more easily and undergo translation. Upon intranuclear MI and subsequent cell division, the injected DNA was excluded from the nucleus of the daughter cells, remaining in their cytosol and ultimately decreasing the transfection efficiency [89]. Indeed, for large colloids introduced into the nucleus *via* MI, their size can be an obstacle since after cell division they would be prevented from re-entering the nucleus through the nuclear membrane. During cytokinesis, the cytoplasm of the parent cell and the organelles contained in it are distributed between the two nascent daughter cells. In this context, it would be expected that the material injected in the cytosol would also be redistributed upon cell division. Interestingly, it was observed for injected colloids that their dilution pattern was dependent on the particles' size as described later in Chapter 3. SUV in the range of 80 nm were on average distributed evenly between the daughter cells after cytoplasmic MI, comparably to what was observed with injected QD and endocytosed low molecular size probes [172]. However, LUV of around 130 nm were segregated unevenly during cell division, resulting in some daughter cells with a large load of injected colloids and others with virtually none. This could be connected to the agglomeration behavior observed for LUV upon injection in the cytoplasm (see section "Microinjection of nanocarriers"), which already before the cell underwent cell division would have generated a polarized distribution in the cytoplasm. The uneven dilution pattern

observed upon cell division with larger colloids injected in the cytosol can have biomedical implications. Since dividing cells would inherit uneven portions of the injected colloids (*e.g.* drug- or enzyme-loaded LUV), they would also receive a different dosing of the encapsulated cargo, potentially leading to effects that are highly variable and/or difficult to predict. In contrast to the size-dependent dilution pattern observed when colloids are delivered *via* MI, those internalized by endocytosis are subjected to different dilution processes, since in such case it is particle-loaded endocytic vesicles instead of particles alone that get diluted upon cell division. Vesicular organelles can fuse together into larger vesicles, may be exocytosed from the cells or undergo other biological processing [44, 173-175].

The intracellular processing to which injected colloids are subjected can depend on characteristics such as size, surface composition and nature of the colloids. The diffusion within the cytoplasm and the patterns with which injected colloids are distributed upon cell division appear to be size-dependent. In addition, the colloids' nature and/or surface modifications seem to determine whether they are rapidly degraded by nucleases or cleared by autophagosomes. Overall, the intracellular processing of injected colloids requires careful consideration for drug delivery applications, as their characteristics may hamper the activity they were initially designed for and could also difficult their persistence in dividing cell populations.

Conclusion

MI has proven to be a powerful tool for cell manipulation, enabling seminal studies in the pre-transfection years and empowering diverse fields of research thereafter as well. MI bypasses the plasma membrane and the endolysosomal pathway, and allows for efficient delivery of membrane-impermeable and degradation-sensitive molecules into cells, sparing the need for complex fusogenic strategies. Virtually any kind of colloids can be delivered by MI, including, proteins, nucleic acids and nano-sized particles. In addition, because the exact timing and site of injection in the cells can be precisely controlled, MI has had a pivotal role in the elucidation of numerous biological processes. Early studies on the regulation of the cell cycle, the apoptosis cascade and the organization of the cytoskeleton were possible due to the injection of Abs and proteins that selectively inhibited intracellular pathways, revealing through the downstream effects the underlying intermolecular interactions ruling these biological processes. Moreover, the translocation of nucleic acids from the cytoplasm to the nucleus during transfection was only unraveled upon MI-based studies, where the protecting effect against nucleases of DNA complexes were revealed and the stability and dissociation of the complexes could be better described. The MI of NP has also unfolded the excellent intracellular targeting and imaging potential of QD, and has facilitated the introduction of artificial vesicles for their application as controlled release systems. Future fundamental discoveries and breakthroughs in applied science with MI-based studies will depend on the resolution of the throughput limitations of current MI platforms, and on further understanding the intracellular processing of each type of microinjected colloid in view of their cytosolic diffusion and cellular clearing mechanisms.

Chapter 3

Microinjection for the *ex vivo* modification of cells with functional artificial organelles

Peter Tiefenboeck, Jong Ah Kim, Ferdinand Trunk, Tamara Eicher, Erica Russo, Alvaro Teijeira, Cornelia Halin, Jean-Christophe Leroux

Swiss Federal Institute of Technology Zurich (ETHZ), Department of Chemistry and Applied Biosciences, Institute of Pharmaceutical Sciences, Vladimir-Prelog Weg 1-5/10, 8093 Zurich, Switzerland.

This chapter was adapted from the accepted manuscript

P. Tiefenboeck, J. A. Kim, F. Trunk, T. Eicher, E. Russo, A. Teijeira, C. Halin, J.-C. Leroux, Microinjection for the *ex Vivo* Modification of Cells with Artificial Organelles, ACS Nano, 2017, 11 (8), pp 7758-7769, DOI: 10.1021/acsnano.7b01404

.

Introduction

As described in Chapter 1, cell-based therapies have great potential in treating malignant or inflammatory diseases. They propose to exploit migratory cells as vehicles to transport therapeutic agents and deliver them at sites of inflammation or malignant growth to which they get recruited [176]. Most often macrophages, lymphocytes and DC are used, but recently also microorganisms have been proposed [177]. Regardless of the carrier cell used, the transported cargo needs to be first encapsulated into a nanocarrier (*e.g.* NP, vesicle) to preserve its stability [178] and to protect the cell itself from the drug's effects [70]. *Ex vivo*-manipulated macrophages and lymphocytes have been used to deliver nanocarriers loaded with chemotherapeutics [179, 180] antiretroviral drugs [181], proteins or enzymes [182] and imaging contrast agents [183]. In the context of cancer immunotherapy, DC have been endowed *ex vivo* with encapsulated adjuvants and cancer antigens to develop cell-based vaccines [184, 185]. Magnetotactic bacteria that migrate towards hypoxic regions have been used in mice to deliver liposomes bearing an antitumour drug [186].

Besides boosting the drugs' efficacy by increasing the dose achieved on-site, carrier cells can minimize side effects associated to systemic exposure [187]. Furthermore, transporting degradation-prone cargo (e.g. therapeutic proteins, nucleic acids) inside cellular vehicles can increase their half-life and preserve their function [70]. As explained before, the method with which the nanocarriers are introduced into the recipient cells has a deep effect on the cargo's stability. Their co-incubation is an extensively used approach, relying on the cell's endocytic mechanisms to internalize the nanocarriers [188]. Although convenient, controlling the amount of nanocarrier internalized can be challenging since it depends on the cells' often heterogeneous endocytic activity. Indeed some cell types that are clinically relevant for cell-based therapies have limited endocytic capacity (e.g. immune cells, stem cells). In addition, unless effective membrane-destabilizing strategies are applied [189, 190], the endocytosed material can be degraded downstream in the endolysosomal compartment, suppressing its biological activity [70, 191]. Alternative membrane-disrupting techniques have thus been developed to deliver intracellularly various kinds of nanocarriers to virtually any cell type [11, 149], like *e.g.* MI among others (as discussed in Chapter 1).

Due to its low cytotoxicity and high transfection efficiency, MI is used *in vitro* on cell lines and primary cells, and *ex vivo* on organotypic tissue slices to administer biomolecules, drugs, intracellular sensors and NP [37, 192, 193]. In this context, this chapter explores MI to endow live cells with exogenous artificial organelles encapsulating conditions that are incompatible with cell viability (e.g. a degradative enzyme or extreme pH values). The introduction of artificial organelles has been previously explored [67, 77, 194], yet in most cases the delivery to cells depended on a co-incubation step followed by uptake *via* the endolysosomal pathway, which often hampered the material's activity and/or compromised its stability. MI would be beneficial for numerous emerging systems in need of alternative delivery strategies [195]; for instance, Tanner *et al*. have developed artificial multi-enzyme-containing peroxisomes that react to redox stress, and Choi *et al.* have proposed an ATP-synthesizing hybrid proteopolymersome [68, 196]. Our work addresses the fundamental aspects of using MI to deliver lipidic vesicles in a way that evades their subcellular processing and enables their persistence in the cytoplasm for several cell division cycles. The possibility of dispensing nanocarriers containing diverse biologically active cargo as well as extreme chemical environments into cellular vehicles brings exciting prospects for the progress of cell-based therapies and drug delivery.

Materials and Methods

Experimental design

Live cells (either HeLa cultures or primary murine DC) were microinjected with liposomal formulations containing different cargoes (phosphate buffered saline (PBS) pH 7.4, with or without active trypsin enzyme, and citrate buffer pH 2) whose intracellular fate was studied over a period of 2 days following the injections. The liposomes' subcellular localization and distribution upon cell division was investigated, as well as their ability to retain the encapsulated cargo and preserve its catalytic activity in the cells' cytosol. The liposomes' impact on the injected cells was evaluated in terms of cytotoxicity and impairment of migratory properties. Experiments were carried out in triplicates unless otherwise stated.

Liposomes preparation

Liposomes were prepared by the lipid-film rehydration method [197]. The lipids used were 1,2-dipalmitoyl-sn-glycero-3-phosphocholine (DPPC), DOPC, 1,2-distearoyl-sn-glycero-3-phosphoethanolamine-N-[methoxy(polyethylene glycol)-2000] (ammonium salt) (DSPE-PEG_{2000}) (Lipoid, Ludwigshafen, Germany), stearylamine (SA) and cholesterol (CHOL) (Fluka, Buchs, Switzerland). At 37 °C, DPPC liposomes are in the gel-crystalline state whereas in DOPC vesicles, the lipids are assembled in a liquid crystalline phase [198]. The formulations (mol%) tested were DPPC:CHOL (55:45), DPPC:CHOL:DSPE-PEG (50:45:5), DOPC:CHOL (55:45), DOPC:CHOL:DSPE-PEG (50:45:5) and DPPC:CHOL:SA (40:50:10). Briefly, lipids (5 mM) dissolved in chloroform (Sigma-Aldrich, Buchs, Switzerland) were dried in small vials and kept in a desiccator overnight. The dried lipid film was rehydrated with PBS pH 7.4 (KH_2PO_4 1.54 mM, $Na_2HPO_4x7H_20$ 2.7 mM, NaCl 155.2 mM) and the resulting mixture was vortexed. After undergoing seven freeze-thaw cycles, the formed LUV were extruded ten times through two stacked 100-nm polycarbonate membranes (Sterlitech, Kent, WA). SUV were prepared by subsequent extrusion (20x) through two stacked 50-nm membranes. In order to fluorescently label the liposomes, 0.1% of the far-red lipophilic carbocyanine dye 1,1'-dioctadecyl-3,3,3',3'-tetramethylindodicarbocyanine, 4-chlorobenzenesulfonate salt (DiD; Thermo Fisher Scientific, Waltham, MA) was added to the lipid solution in chloroform. The size of the liposomes was determined by dynamic light scattering (DLS) (DelsaNano®; Beckman Coulter, Indianapolis, IN) (Table A3.1).

For the stability test, the formulations were prepared as described above except for the hydration buffer, which was changed to a phosphate buffer pH 7.4 containing 25 mM 8-hydroxypyrene-1,3,6-trisulfonic acid, trisodium salt (HPTS) and 70 mM p-xylene-bis-pyridinium bromide (DPX) (Thermo Fisher Scientific) and was adjusted to 300 mOsm. After liposome extrusion, unencapsulated dye was removed with a MidiTrap G-25 column (GE Healthcare, Little Chalfont, UK). The fluorescence of HPTS remained quenched and undetectable under the microscope as long as the liposomal membrane was intact and the cargo did not leak out. The addition of the detergent Triton X-100 in the proximity of

the injected cells induced the permeabilization of the liposomes and the leakage of the dye, which was quickly followed by its dequenching and a consequent increase in fluorescence. The detergent-induced dequenching was interpreted as an indication that the liposomes were intact inside the cell at a specific time point and the stability of the injected liposomes was thus measured as the percentage of "dequenchable" cells among the total of successfully injected cells indicated by the coinjection marker.

For the trypsin-encapsulating liposomes, DOPC:CHOL (90:10) dried lipid films (10 mM) labelled with DiD 0.05 mol% were hydrated with a 1 mg/mL solution of trypsin derived from porcine pancreas (Sigma-Aldrich) previously dissolved in PBS, and were kept in the fridge overnight. On the following day, the mixture underwent the aforementioned liposome preparation procedure. Unencapsulated enzyme was removed using a sepharose CL-4B (Sigma-Aldrich) gel column (20 cm x 0.7 cm), followed by the determination of the enzyme encapsulation efficiency (see Table A3.2).

Cell culture and microinjection

HeLa cells (CCL-2; ATCC, Manassas, VA) were grown as a monolayer in Dulbecco's modified eagle medium (DMEM) with GlutaMax™ supplemented with 10% fetal bovine serum (FBS) and 1% penicillin-streptomycin at 37 °C and 5% CO_2. All tissue culture reagents were purchased from Thermo Fisher Scientific unless otherwise stated. Cells were seeded at a density of 20'000 cells/mL (approximately 20% confluency) in 35-mm glass-bottom petri dishes (Cellvis, Mountain View, CA) previously marked in their bottoms with scratched gridded patterns. On the following day, an injection pressure of 80-120 hPa was applied for 0.2-0.5 s to inject the cells with an average volume of 793 fL (Fig. A3.1). MI were performed using Femtotips II attached to a Femtojet Microinjector and an InjectMan NI 2 (Vaudaux-Eppendorf, Schönenbuch, Switzerland), which were coupled to a Leica DMI6000B epifluorescence microscope (Leica Microsystems, Wetzlar, Germany). To identify the successfully injected cells, coinjection markers were added to the liposomes suspension, either dextran-tetramethylrhodamine (TRITC) (Sigma-Aldrich) or dextran-Cy5 (Thermo Fisher Scientific).

Quantification of the injected volume

The injection volume was determined based on previously described methods [23]. Cy5-dextran 0.1 mg/mL was injected in a petri dish containing high viscosity silicon oil (10'000 cSt at 25 °C, Sigma-Aldrich, Buchs, Switzerland) using Femtotips II attached to a Femtojet Microinjector and an InjectMan NI 2 (Vaudaux-Eppendorf, Schönenbuch, Switzerland). The diameter and the fluorescence intensity of the resulting spherical Cy5-dextran droplet was measured with a Leica DMI6000B epifluorescence microscope (Leica Microsystems, Wetzlar, Germany). The volume of the droplet was then calculated using the diameter measured, and finally a ratio between fluorescence intensity and volume was obtained using equation 1.

$$Ratio = \frac{Integrated\ Intensity}{volume} \qquad \text{Eq. 1}$$

Following the same procedure, HeLa cells were injected with the same concentration of Cy5-dextran and imaged with the same microscope settings as the droplets in oil. Using the Leica analysis software, the injected cells' borders were manually drawn and the fluorescence intensity inside of these regions was quantified. By applying the aforementioned fluorescence-to-volume ratio, the volume injected into cells was calculated.

Calculation of injected liposomes per cell.

The calculation of the number of liposomes per injection was performed assuming that the vesicles were fully unilamellar and spherical. The area per lipid was considered to be 0.63 nm^2 for DPPC, 0.675 nm^2 for DOPC and 0.33 nm^2 for CHOL [199, 200]. Since DSPE-PEG only accounts for a minor fraction of the total lipid amount, the calculations were performed considering a liposome composition of 55% phospholipid (PL) and 45% CHOL, and are therefore only shown for the unPEGylated formulations. The adjusted area per lipid was 0.495 nm^2 for DPPC LUV and SUV, and 0.519 nm^2 for DOPC LUV (Eq. 2).

$$Adjusted\ area\ per\ lipid =$$

$$((mol\%\ (PL)) \times (area\ per\ lipid\ (PL) + (mol\%\ (Chol)) \times (area\ per\ lipid\ (Chol))$$

Eq. 2

Assuming a bilayer thickness of 3.75 nm for spherical liposomes [201] and considering the mean diameters measured by DLS (130 nm for LUV and 80 nm for SUV), the total surface area was calculated as 100'236 nm^2 for LUV and 36'619 nm^2 for SUV (Eq. 3).

$$Total\ surface\ area\ liposome =$$

$$4 \times \pi \times \left(\frac{size}{2}\right)^2 + 4 \times \pi \times \left(\frac{size}{2} - bilayer\ thickness\right)^2 \qquad \text{Eq. 3}$$

By dividing the total surface area of a single vesicle over the adjusted area per lipid, the number of lipids per vesicle was calculated as 202'498 for DPPC LUV, 79'978 for DPPC SUV, and 193'059 for DOPC LUV (Eq. 4).

$$Number\ phospholipids\ per\ vesicle = \frac{Total\ surface\ area}{Adjusted\ area\ per\ lipid} \qquad \text{Eq. 4}$$

The number of vesicles per injection was then obtained by multiplying the injection volume (793 fL, see Fig. A3.1) by the concentration of vesicles in the suspension, which was in turn calculated using the Avogadro's number (6.022×10^{23}) according to Eq. 5.

$$Number\ vesicles\ per\ mL = \left(\frac{Avogadro's\ constant \times mol\ (lipids)\ per\ mL}{Number\ phospholipids\ per\ vesicle}\right) \qquad \text{Eq. 5}$$

Thus, assuming a lipid concentration of 5 mM, the number of vesicles per injection follows as 11'791 for DPPC LUV, 32'276 for DPPC SUV, and 12'368 for DOPC LUV.

Cytotoxicity assay

Upon injection with the different liposomal formulations and coinjection marker, the cells were imaged at different time points by epifluorescence microscopy in the presence of 10 µg/mL propidium iodide (PI) to detect the cells with compromised membrane integrity. As a positive control for cell death, DiD-labelled liposomes containing 10 mol% SA were injected. Cell viability was calculated for each injected formulation as the percentage of PI-positive cells among the total of injected cells.

Liposomal stability inside injected cells

Using the HPTS/DPX-encapsulating LUV described above, the integrity of the LUV was tested inside the injected cells. The release and subsequent dequenching of the encapsulated HPTS dye was induced at specific time points (4, 24 and 48 h after initial injection) by adding the detergent Triton X-100 (Sigma-Aldrich) at 1% (w/v) to the cell's surrounding medium. The increase in fluorescence intensity following the dye's dequenching was used as an indication of the stability of the LUV inside the cell at a given time point.

Intracellular localization and tracking during cell division

To stain the lysosomes, HeLa cells were transfected for 16 h with lysosomal associated membrane protein (LAMP-1) GFP CellLight constructs (Thermo Fisher Scientific). After washing, the cells were injected with the DiD-labelled liposomal formulations and analyzed by confocal microscopy after 24 h and 48 h using a Visitron spinning disk confocal system (Puchheim, Germany). To visualize the autophagosomes, HeLa cells stably expressing light chain 3 (LC3)-GFP were used [202]. The cell line was originally established by Professor Felix Randow at Cambridge University but were in this case obtained from Katrien Remaut in Ghent University. Image analysis and quantification of colocalization were performed using FIJI software.

To study the evolution of injected liposomes over a cell's lifecycle, injected cells (generation P) were imaged as they underwent two rounds of cell division (generations F1 and F2). To this end, HeLa cells were seeded the day before the experiment at a density of 10'000 cells/mL (approximately 5-10% confluency) and after injecting them with coinjection marker and liposomes (LUV or SUV) or QD, they were imaged using a Leica DMI6000B epifluorescence microscope for up to 48 h. For the QD, the 2 µM stock solution of Qtracker 655 Vascular Labels (Thermo Fisher Scientific) was diluted to 1 µM with PBS prior to injection into cells. Images were analyzed using Leica LAS AF software.

Agglomeration and resuspension analysis

LUV, SUV and QD were injected into cells and followed *via* time-resolved microscopy for 12 h. Analysis was performed on images taken after 0 h and 8 h using FIJI software. Briefly, a region of interest (ROI) defining the area of the injected cell was set and the percentage of area occupied by the fluorescent particles was calculated at the 2 time points. For this purpose, a fluorescence intensity threshold was set to identify pixels positive for fluorescence. For the resuspension analysis, cells containing aggregates of injected colloids were injected again with PBS to disrupt the aggregates. Image analysis was performed as explained above.

Positive control lysosomes

HeLa cells were seeded one day prior to experiments in 8-well chambers (LabTek, Thermo Fisher Scientific, Waltham, MA) at a density of 10'000 cells per well. Cells were subsequently incubated with Lysotracker Green for 16 h, after which they were incubated with DPPC LUV (200 µM in OptiMEM (Thermo Fisher Scientific, Waltham, MA) for 4 h. Images were taken with a Visitron spinning disk confocal microscope 24 h later. Image analysis was performed with FIJI.

Positive control autophagosomes

HeLa cells were seeded one day prior to experiments in 8-well chambers (LabTek, Thermo Fisher Scientific, Waltham, MA) at a density of 10'000 cells per well. Cells were incubated for 4 h with N-(2,3-Dioleoyloxy-1-propyl)trimethylammonium methyl sulfate liposomes (DOTAP, 100 µM in OptiMEM) according to the work of Roberts *et al*. [203]. Images were taken with a Visitron spinning disk confocal microscope 2 h later. Image analysis was performed with FIJI.

Purification of trypsin-encapsulating liposomes.

Following extrusion, 300 µL of the trypsin-encapsulating liposomes (DOPC:CHOL 90:10 mol%) were transferred to a self-packed sepharose CL-4B gel column (0.7 cm x 20 cm) to remove the unencapsulated enzyme. PBS was added to the column and eluting fractions of 200 µL each were collected. The fractions' UV absorbance was measured on a 96-well quartz glass plate (Hellma Analytics, Müllheim, Germany) at 280 nm and 340 nm using a Tecan plate reader (Männedorf, Switzerland). While liposomes absorbed both at 280 nm and 340 nm, the fractions containing trypsin absorbed only at 280 nm. In order to determine whether the enzyme was still active after liposome preparation and purification, the fractions' enzyme content was calculated based on enzymatic activity measurements. For the trypsin activity measurements, 40 µL of 100 µM Rhodamine 110, bis-(Cbz-L-isoleucyl-L-prolyl-L-arginin amide), dihydrochloride (BZiPAR) substrate (Thermo Fisher, Waltham, MA) was mixed with 10 µL of a range of known amounts of trypsin (10-500 ng/mL) in a 96-well plate and after incubating for 5 min in darkness at room temperature, the mix was diluted with 200 µL of 10 mM 4-(2-hydroxyethyl)-1-piperazineethanesulfonic acid (HEPES) buffer pH 7.5 containing 15% (v/v) ethanol. The fluorescence intensity was then recorded with a plate reader (Tecan) at 492 nm excitation and 523 nm emission over 20 min, and the values obtained were plotted as a function of time. The slopes of the resulting curves were used for the calibration of the enzyme concentration.

Determination of trypsin encapsulation efficiency.

The elution fractions obtained during the purification process which contained trypsin (fractions 10-13, elution volume 1900-2700 µL) were used to determine the trypsin encapsulation efficiency. The fractions were diluted 1:100 (v/v) with PBS and upon incubation with 1.0% (w/v) Triton X-100 (final concentration) for 10 min at 65 °C to induce complete cargo release from the liposomes, the enzyme activity was quantified using the BZiPAR substrate dequenching assay. The encapsulation efficiency was then calculated dividing the encapsulated amount in ng over the amount of trypsin used during the encapsulation procedure (300 µg). The procedure was performed in three independent experiments and by averaging their results an encapsulation efficiency percentage of 3.41 ± 0.53 was obtained (mean ± SD).

Calculation of enzymes per liposome.

The calculation of the number of active enzymes per liposome was performed according to Sugawara *et al*. [65] assuming that the vesicles were spherical. The area per lipid was considered to be 0.675 nm^2 for DOPC and 0.33 nm^2 for CHOL [199, 200]. Since the composition of the trypsin liposomes was 90% DOPC and 10% CHOL, the adjusted area per lipid was 0.64 nm^2 (Eq. 2). Assuming a bilayer thickness of 3.75 nm for spherical liposomes [201] and a mean size of 130 nm as measured by DLS, their total surface area was 100'236 nm^2 (Eq. 3). By dividing the total surface area of a single vesicle over the adjusted area per lipid, the number of lipids per vesicle was calculated as 156'717 (Eq. 4). The lipid-to-protein ratio was then calculated by dividing the number of encapsulated trypsin molecules over the number of lipids in the formulation. Since the LUV encapsulated 3.41% of trypsin, the concentration was 1.46 nM (hydration volume 1 mL, trypsin concentration in the hydration buffer 1 mg/mL, $MW_{Trypsin}$ = 23,300 g/mol). In addition, since the lipids were used at a concentration of 10 mM, the lipid-to-protein ratio was 6832 (Eq. 6).

$$Lipid - to - protein\ ratio = \frac{n\ (lipid)}{n\ (protein)} \qquad \text{Eq. 6}$$

Finally, by dividing the number of lipids per vesicle over the lipid-to-protein ratio, the number of proteins per liposome was calculated as 23 (Eq. 7).

$$Number\ proteins\ per\ liposome = \frac{Number\ phospholipids\ per\ vesicle}{lipid-to-protein\ ratio} \qquad \text{Eq. 7}$$

Digestion of residual surface-bound trypsin enzyme in trypsin-encapsulating liposomes.

Trypsin-encapsulating liposomes were incubated for 15 min with 5 mg/mL pepsin (Sigma-Aldrich) in a 10 mM glycine-HCl buffer adjusted to pH 2.5 to degrade potential surface-bound trypsin. After stopping the digestion by increasing the pH to 8 with 1 M NaOH, the pepsin was separated from the liposomes with a CL-4B gel column (0.7 cm x 20 cm) using 300 µL of the reaction mixture. In order to verify the absence of trypsin on the liposome's surface, trypsin activity measurements were made in the purified pepsin-digested liposomes and in equivalent liposomes not undergoing the pepsin treatment. The measurements were also done before and after treatment with 1.0% (w/v) Triton X-100 (final concentration) for 10 min at 65 °C.

Validation of the enzymatic activity assay used to evaluate liposome-encapsulated trypsin.

The protease substrate BZiPAR 20 µM (previously dissolved in PBS) was injected with the Femtojet microinjector into a petri dish containing high viscosity silicon oil (10'000 cSt at 25 °C, Sigma-Aldrich) with an injection pressure of around 700 hPa. This resulted in a spherical droplet of BZiPAR suspended in the oil. Subsequently, DiD-labelled trypsin-encapsulating liposomes were injected into the BZiPAR-containing droplet or in its proximity directly in the oil, in an area where the substrate was not present. The fluorescence intensity of the petri dish was then recorded for 15 min with a Leica DMI6000B epifluorescence microscope, acquiring one image per minute in the fluorescence channels corresponding to the detection of BZiPAR's dequenching and the DiD label of the liposomes. Using the Leica analysis

tool, the fluorescence intensity was quantified as a function of time inside each of the droplets containing BZiPAR substrate alone, DiD-labelled trypsin-encapsulating liposomes alone or a combination of the two.

Enzymatic activity assay

Enzymatic activity was measured with a dequenching assay involving the fluorogenic protease substrate BZiPAR, which was validated as shown in Fig. A3.7 and A3.8. Cells were pre-incubated for 3 h with the protease inhibitor 4-(2-aminoethyl)benzenesulfonyl fluoride hydrochloride (AEBSF) (Pefabloc®, Fluka) at 1 mM to prevent unspecific cleavage of the assay's substrate, and were subsequently injected with DiD-labelled enzyme-loaded liposomes. BZiPAR was then added at 20 µM to the medium of the injected cells and was incubated for 30 min at 37 °C and 5% CO_2. Images of the live cells were obtained using a Leica DMI6000B epifluorescence microscope. The cleavage of BZiPAR by trypsin lead to its dequenching, followed by a marked increase in fluorescence intensity detected by microscopy. Images analysis was performed using FIJI software.

Preparation of transmembrane acidic pH-gradient liposomes.

DPPC-PEG transmembrane pH gradient liposomes containing 0.1 mol% DiD were prepared by hydrating the lipid films with isotonic citrate 250 mM pH 2 (or PBS pH 7.4 as control), based on a protocol from Forster et al. [204] with modifications. After 7 freeze-and-thaw cycles, the liposomes were extruded through double-stacked 100 nm pore size polycarbonate membranes. The pH gradient with pH 2 inside the liposomes and pH 7.4 externally was established exchanging the liposomes' external buffer for isotonic PBS with physiological pH *via* size exclusion chromatography (G-25 miditrap column, GE Healthcare). The prepared liposomes were then injected into HeLa cells as previously described. Four, 24 h and 48 h after injection the cells were incubated for 30 min with 200 nM bafilomycin A1 (Sigma-Aldrich) in DMEM supplemented with 10% FBS in order to inhibit the acidification of typically acidic subcellular organelles, such as endosomes and lysosomes, and prevent their interference with the detection of the acidic liposomes. Subsequently, the cells were incubated for 5 min with 200 nM bafilomycin A1 and 1 µM Lysotracker Green DND-26 (ThermoFisher Scientific), a marker of acidic compartments, which due to the pre-incubation step with bafilomycin should mainly stain the acidic liposomes. After washing with PBS, the cells were imaged in Live-cell imaging solution (ThermoFisher Scientific) containing 10% FBS using a Leica DMI6000B epifluorescence microscope (Leica Microsystems). Image analysis was carried out with FIJI software [205]. Cell viability was measured using the PI cytotoxicity assay described in the main methods of the article.

Dendritic cell migration assay

DC were generated from the bone marrow of CD11c - yellow fluorescent protein (YFP) mice as previously described [206]. All experiments were approved by the Cantonal Veterinary Office Zurich. Briefly, $5x10^6$ bone marrow cells were placed into bacterial dishes (Greiner Bio-One, St. Gallen, Switzerland) in DC-medium containing RPMI 1640, 10% FBS, 15 nM HEPES, 1 mM sodium pyruvate, 100 U/mL penicillin, 100 mg/mL streptomycin, 2 nM L-glutamin (GIBCO, Zug, Switzerland), 50 mg β-mercaptoethanol (Sigma-Aldrich). Additionally, 80 ng/mL granulocyte macrophage colony-stimulating factor (GM-CSF) was added, which was derived from the supernatant of myeloma cells (X63 Ag8.653) transfected with murine GM-CSF cDNA [207]. The medium was changed every three

days. On day 9-10, floating DC were collected and seeded on coverslips into tissue culture-treated dishes (TPP, Trasadingen, Switzerland) in medium containing 0.1 mg/mL lipopolysaccharide (Enzo Life Sciences, Lausanne, Switzerland). Immortalized mouse lymphatic endothelial cells (imLECs) were cultured at 33 °C in collagen (Advanced Biomatrix, San Diego, CA) and fibronectin (Millipore, Temecula, CA)-coated dishes (10 mg/mL each) in media containing 40% DMEM (low glucose), 40% F12-Ham, 20% FBS (GIBCO), 56 mmol/mL heparin (Sigma-Aldrich), 10 mmol/mL endothelial cell mitogen (AbD Serotec, Dusseldorf, Germany), 1x antibiotic antimycotic solution (Fluka) and 2 nM L-glutamin (Fluka). Additionally, murine interferon-gamma 1 U/mL (Peprotech, London, UK) was added to induce large T-antigen expression [208]. Cultured imLECs were seeded into collagen/fibronectin pre-coated channeled flow chamber ($3x10^4$ cells/chamber) (µ-Slide VI0.4, IBIDI, Martinsried, Germany) and cultured for 24 h at 37 °C with 5% CO_2.

Mature DC were injected with DiD-labelled DPPC-PEG LUV and/or coinjection marker (Dextran-TRITC), and were scraped off the coverslip. The DC suspension was introduced into the flow channel slide containing the imLECs. After a settling period of 30 min, DC migration was recorded for 30 min using a Leica DMI6000B microscope and a Nikon Eclipse TE2000-E microscope (Amsterdam, Netherlands). Trajectory analysis was performed using Imaris software (Bitplane, Zurich, Switzerland). Speed is represented as the migration length divided by the imaging time.

Positive controls of migration inhibition.

Mature DC as described in the methods were incubated for 30 min with 0.5 µM cytochalasin D [209] (Sigma-Aldrich) or 31.2 µM Y27632 [210] (Sigma-Aldrich) before their addition to the flow channel slide. After a settling period of 30 min, DC migration was recorded with a Leica DMI6000B microscope. Trajectory analysis was performed using Imaris software. Speed is represented as the migration length divided by the imaging time.

Statistical analysis

For experiments in which more than three independent groups were compared (Figs. 3.1 B, 3.2 C and A3.7), one-way analysis of variance (ANOVA) followed by a post-hoc test (Tukey for 3.2 C and A3.7, Dunnett for 3.1 B) was applied to determine statistical significance. P-values below 0.05 were considered as statistically significant (*p-value < 0.05, **p-value < 0.01, ***p-value < 0.001, ****p-value < 0.0001). For the statistical analysis of aggregation and resuspension (Fig. 3.5 and 3.6), Kruskal-Wallis one-way ANOVA on rank testing followed by a post hoc pairwise comparison with Dunn's test was performed. $p \leq 0.05$ was considered to be statistically significant). For the DC migration experiments (Fig. 3.10 C), non-parametric analysis (Mann-Whitney-U test) was performed. All statistical analyses were carried out employing GraphPad PRISM software.

Results and Discussion

Microinjected liposomes efficiently retain encapsulated cargo with low cytotoxicity

We investigated the potential of MI to modify cells by introducing catalytically active material into their cytoplasm, and addressed the fundamental aspects governing its interactions with the intracellular compartment. Using a glass capillary injection tip with an inner diameter of 500 nm, HeLa cells were injected with approximately 790 fL (Fig. A3.1) of a suspension of fluorescently labelled 130-nm liposomes (large unilamellar vesicles, LUV), corresponding to approximately 12'000 liposomes per cell. The liposomes consisted mainly of CHOL and DPPC (Tc=41 °C) or CHOL and DOPC Tc=-21 °C), either with or without PEG surface modification (DPPC-PEG, DPPC, DOPC-PEG and DOPC LUV, respectively) (Fig. 3.1A; Table A3.1). The zeta potential of liposomes with similar composition and degree of PEGylation has been reported to be close to neutrality [211-213]. The addition of a coinjection marker (fluorescently labelled dextran) to the liposomal suspensions enabled the identification of successfully injected cells by fluorescence microscopy.

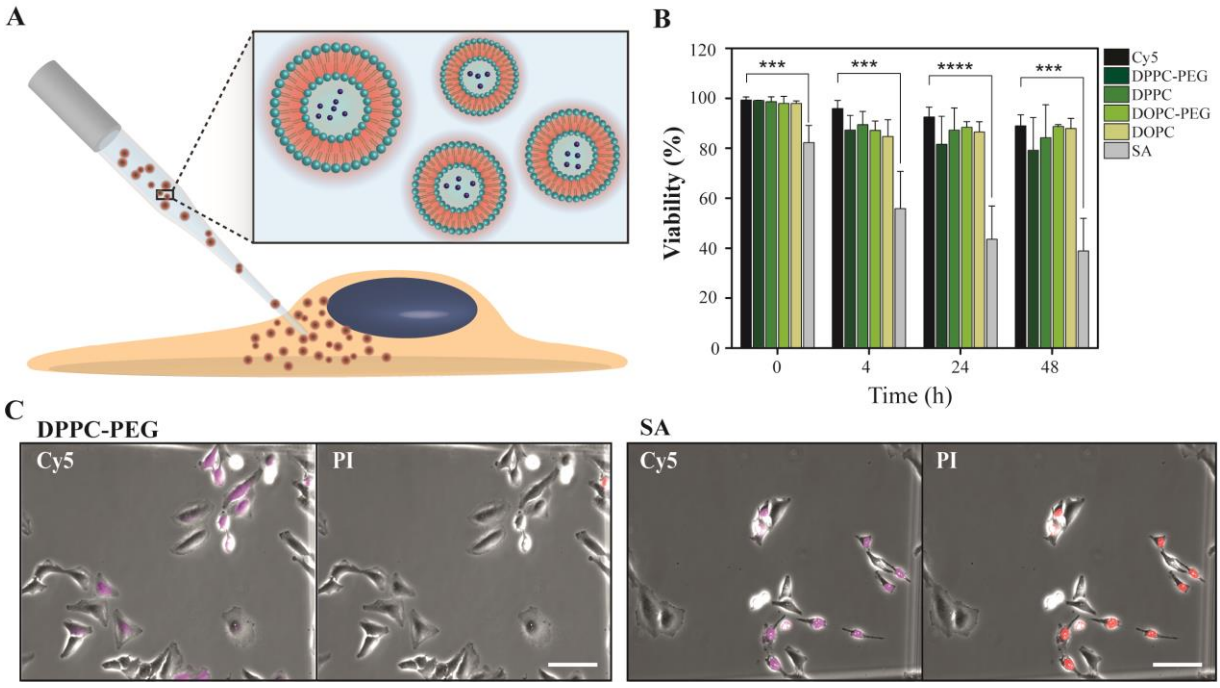

Figure 3.1 MI of liposomal formulations into cells. (A) Schematic representation of liposomes' MI into a cell. The microinjector tip pierces the cell's plasma membrane and injects the liposomes directly into the cytoplasm. Liposomes can be fluorescently labelled (red coronas) or loaded with different cargoes (blue dots in the liposomes' cores), and a co-injection marker can be included in the suspension to identify the injected cells. (B) Cell viability measured by PI exclusion 0, 4, 24 and 48 h after injection of the marker alone (Cy5), DPPC-PEG LUV, DPPC LUV, DOPC-PEG LUV, DOPC LUV and SA

LUV. Values were normalized for total injected cells at time 0 (mean + SD, n = 285-355 in 3-4 independent experiments). ***p-value < 0.001, ****p-value < 0.0001. (C) Microscopy images 4 h after injection of DPPC-PEG LUV vs. SA LUV. Injected cells are shown in magenta (Cy5) and dead PI-positive cells in red (PI). Representative images are shown, taken from a pool of 40 images obtained during 3-4 independent experiments (for DPPC-PEG or SA LUV, respectively). Scale bar 100 µm.

The MI process in itself was safe as indicated by the 99% mean cell viability of cells injected with coinjection marker alone (Fig. 3.1B). Similar observations were made for all the liposomal formulations tested, with which cell viability remained constant at around 79-89% for at least 2 days (the period of time during which the cultures were sub-confluent), indicating that the MI of liposomes was well tolerated by HeLa cells. Only the DPPC-PEG LUV induced a small decrease in cell viability down to 79% after 48 h, which was nevertheless marginal compared to the impact of the positively charged SA-loaded liposomes (SA LUV) used as toxic control (viability decreased to 84% immediately after injection and to 39% after 48 h) [214].

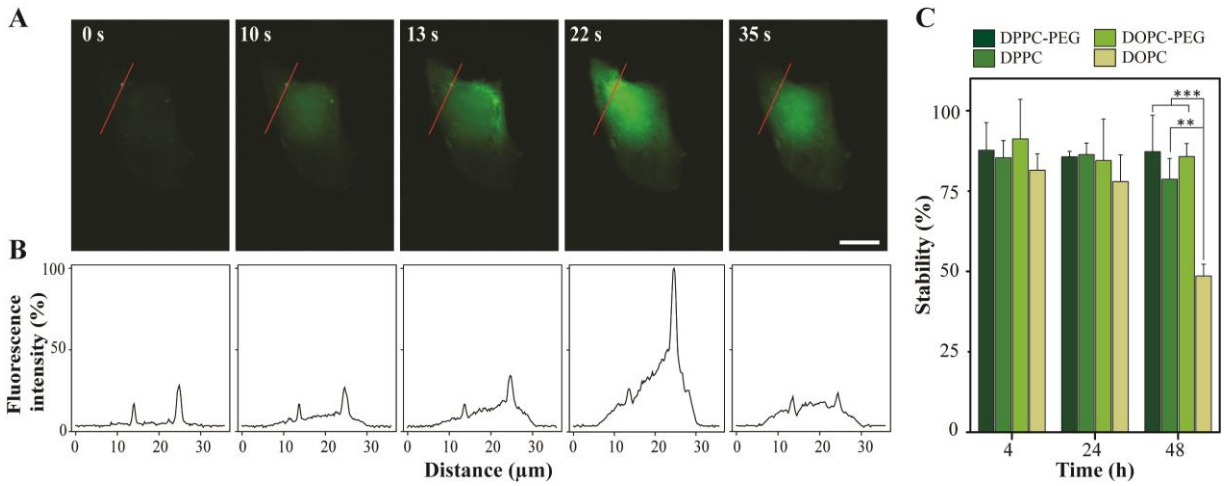

Figure 3.2 Stability of injected liposomes in cells. (A) Dequenching of HPTS/DPX-containing LUV, induced with Triton X-100 4 h after their injection into HeLa cells. The injected cells were imaged every 700 ms for 35 s from the moment of detergent addition, which was between 0 and 10 s. Images of a representative cell are shown, taken from a pool of 103 cells imaged over 3 independent experiments. Scale bar 20 µm. (A) Change in fluorescence intensity over time upon Triton X-100 addition, measured along the red line in panel a. (C) Stability of HPTS/DPX-loaded LUV injected in cells, calculated as the amount of successfully dequenched cells over the amount of total injected cells (positive for coinjection marker) (mean + SD, n = 83-161 in 3-4 independent experiments). **p-value < 0.01, ***p-value < 0.001.

High intracellular stability is overall important from a drug delivery perspective, as carrier cells need to be protected from the damaging effects of their own cytotoxic cargo. Upon their injection into cells, the LUV remained intact in the intracellular milieu and efficiently retained the encapsulated cargo (Fig. 3.2). Using a microscopy-based fluorescence dequenching assay, the different LUV formulations were found to remain stable (73-91%) for 2 days after their injection, and to successfully keep the encapsulated dye from leaking into the cells' cytoplasm. The DOPC LUV were the only ones showing

lower stability after 48 h (49%), likely due to their liquid-crystalline state at physiological temperature and the lack of steric stabilizer.

Intracellular fate of injected liposomes

Immediately after their injection, the LUV distributed evenly within the cell's cytoplasm, both in the PEGylated and unPEGylated forms. Interestingly, aggregates of liposomes seemed to coalesce in the cytosol, progressively leading to a highly polarized distribution of injected material after 11.5 h (Fig. 3.3A). The aggregation was however reversible, as observed upon injection of isosmotic PBS into the cells, which readily re-dispersed the agglomerates in the cytoplasm confirming that they did not coalesce (Fig. 3.3B). A very different intracellular distribution pattern was observed upon injection of smaller systems, namely PEGylated 18-nm QD and 78-nm SUV (DPPC-PEG and DPPC), both of which remained evenly distributed throughout the cytoplasm similarly to the coinjection marker (Fig. 3.4-3.6). Cytosolic agglomeration of injected colloids under 20 nm has been described in previous studies where PEGylation seemed to inhibit the process and determine the particles' downstream processing [51, 147]. In the results presented here however, particle size rather than PEGylation state appeared to be the factor determining the intracellular distribution of the injected material. Moreover, in such earlier reports the observed agglomeration was ascribed to the particles' recognition by the cells' autophagy machinery, which was followed by downstream degradation in the lysosomes [51]. Indeed, although MI would be expected to avoid subcellular processing (*i.e.* the endo-lysosomal route) by delivering material directly into the cytoplasmic milieu, the cells' autophagosomal system may pose an additional hurdle for efficient intracellular delivery [51, 53]. The subcellular localization of the LUV was therefore investigated microscopically, analyzing their colocalization with specific green GFP-tagged markers for the relevant subcellular compartments. The LC3 was used to label the autophagosomes [215], while the LAMP-1 was used to label the lysosomes [216]. Notably, the injected LUV did not colocalize with LC3 nor with LAMP1 at any of the tested time points (24 and 48 h after MI) (Figs. 3.3C), regardless of their PEGylation state (Figs. A3.2 and A3.3) and in contrast with the positive controls used (Fig. A3.4). These observations would suggest that the injected liposomes were not captured by autophagosomes nor lysosomes but instead remained in the cytoplasm, excluded from these subcellular compartments for at least 2 days. Hence, contrary to what has been reported for other systems, the LUV injected in the present study did not cluster as a consequence of their recognition by autophagosomes or their traffic into lysosomes, and could be visualized inside the cells where they successfully bypassed lysosomal degradation. It is likely that their agglomeration in the cytosol would instead be a result of unspecific interactions with the cell's vesicular traffic and cytoskeleton, which could push the liposomes around the cytosol until they reached regions of less shear stress and/or porosity of the cytoskeleton meshwork [162, 217].

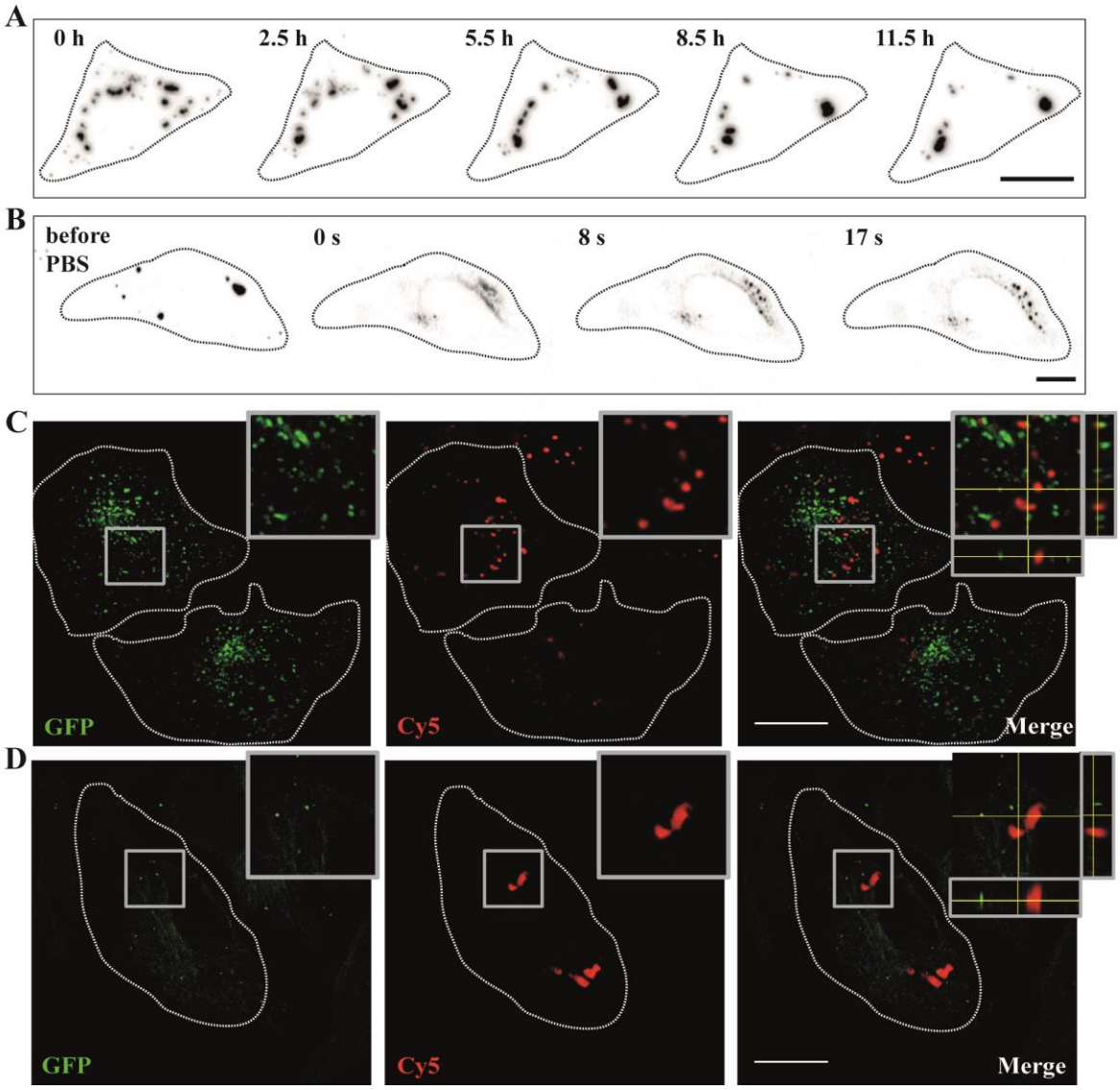

Figure 3.3 Intracellular localization and processing of injected DPPC-PEG LUV. (A) Time-lapse images showing the intracellular aggregation of DPPC-PEG LUV (black) following their injection. A representative sequence of images is shown out of 27 sequences obtained during 3 independent experiments. (B) Resuspension of aggregated DPPC-PEG LUV upon injection of PBS (time 0 s) inside the cell. A representative sequence of images is shown out of 11 obtained during 3 independent experiments. Scale bar 10 µm. (C) Lysosomal staining (GFP-LAMP1 in green) of HeLa cells 24 h after injection of DiD-labelled DPPC-PEG LUV (red). The insets show zoomed-in subcellular areas, and the inset in the Merge image shows the XZ and YZ orthogonal views of the Z-stack. Scale bar 20 µm. A representative image out of 23 images obtained during 3 independent experiments is shown. (D) Autophagosomal staining (GFP-LC3 in green) of HeLa-LC3 cells 24 h after injection of DiD-labelled DPPC-PEG LUV (red). The insets show zoomed-in subcellular areas, and the inset in the Merge image shows the XZ and YZ orthogonal views of the Z-stack. Scale bar 20 µm. A representative image out of 18 images obtained during 3 independent experiments is shown.

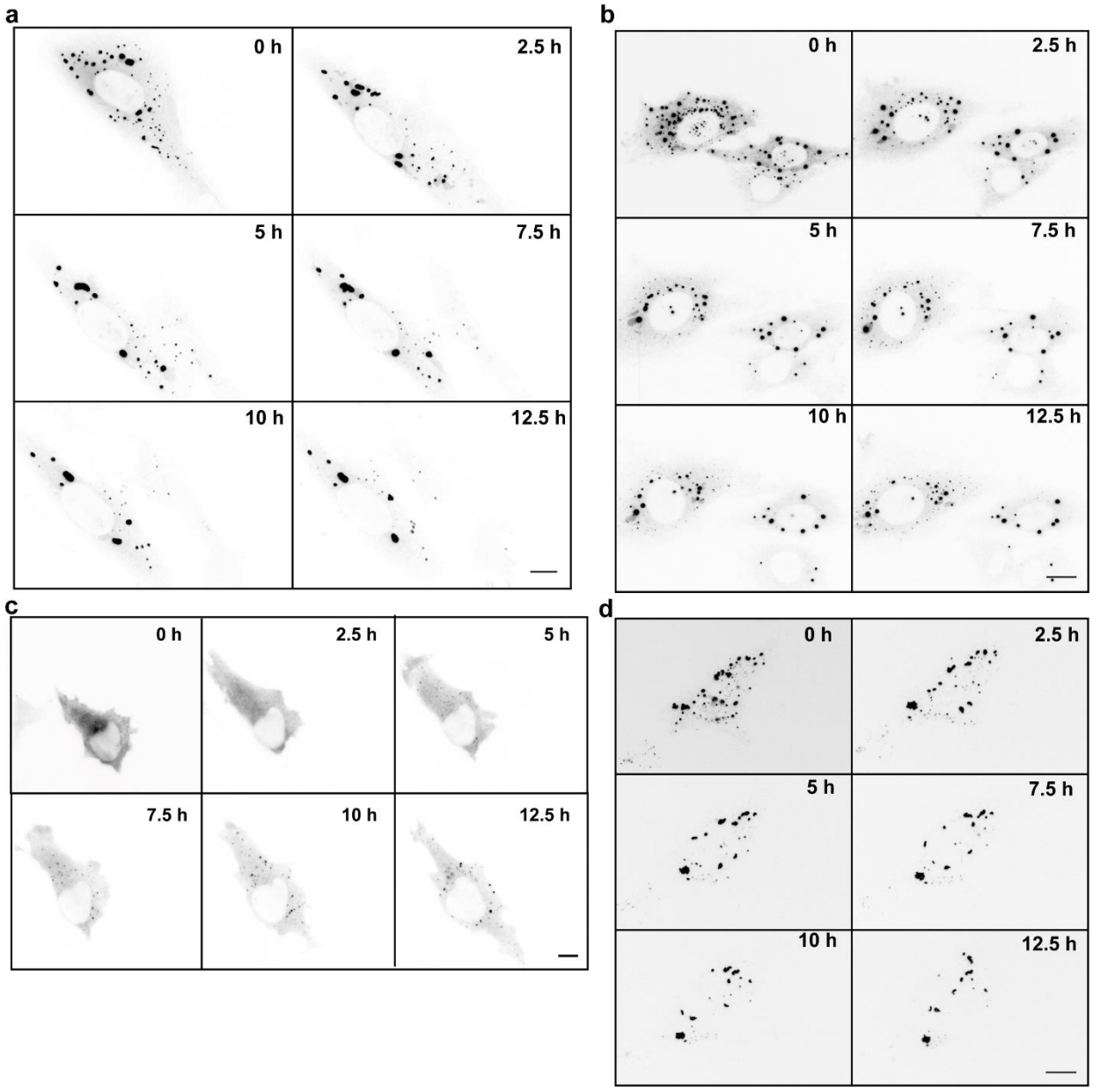

Figure 3.4 Intracellular aggregation over time of LUV, SUV and QD upon injection into cells. (a) Time-lapse images showing the intracellular distribution of DPPC-PEG SUV (black) following their injection into cells. Scale bar 20 µm. A representative sequence of images from 27 sequences acquired during 6 independent experiments is shown. (b) Time-lapse images showing the intracellular distribution of DPPC SUV (black) following their injection into cells. Scale bar 20 µm. A representative sequence of images from 14 sequences acquired during 3 independent experiments is shown. (c) Time-lapse images showing the intracellular distribution of QD (black) following their injection into cells. Scale bar 10 µm. A representative sequence of images from 9 sequences acquired during 3 independent experiments is shown. (d) Time-lapse images showing the intracellular distribution of DPPC LUV (black) following their injection into cells. Scale bar 20 µm. A representative sequence of images from 14 sequences acquired during 3 independent experiments is shown.

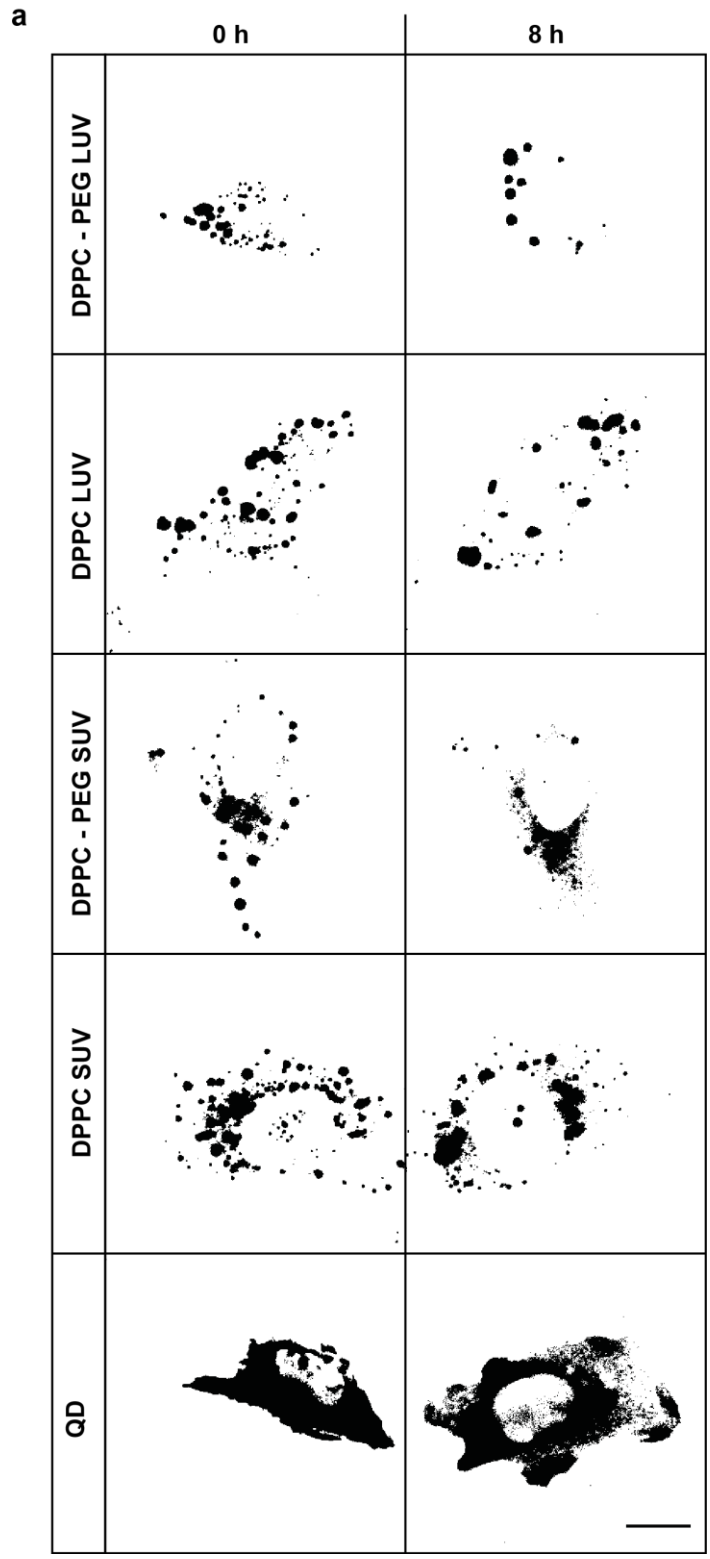

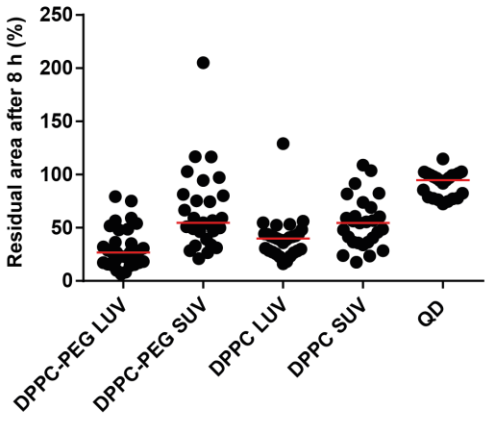

c

Comparison	p-Value
DPPC-PEG LUV *vs* DPPC-PEG SUV	**< 0.0001**
DPPC-PEG LUV *vs* DPPC LUV	**ns**
DPPC-PEG LUV *vs* DPPC SUV	**0.0025**
DPPC-PEG LUV *vs* QD	**< 0.0001**
DPPC-PEG SUV *vs* DPPC LUV	**0.0234**
DPPC-PEG SUV vs DPPC SUV	**ns**
DPPC-PEG SUV *vs* QD	**0.0211**
DPPC LUV *vs* DPPC SUV	**ns**
DPPC LUV *vs* QD	**< 0.0001**
DPPC SUV *vs* QD	**0.0015**

Figure 3.5 Analysis of the intracellular agglomeration of injected LUV, SUV and QD. (a) Time-lapse images of LUV, SUV and QD 0 and 8 h after injection, upon setting an intensity threshold for the quantification of the area occupied by the colloids inside the cell. Scale bar 20 µm. (b) Residual area occupied by the different colloids in the cell after 8 h from injection in comparison to 0 h. Between 23 and 32 cells from 3 independent experiments were analyzed in total. Red bar indicates median value. (c) Results of the statistical analysis of the data shown in (b) using Kruskal-Wallis and Dunn's Test.

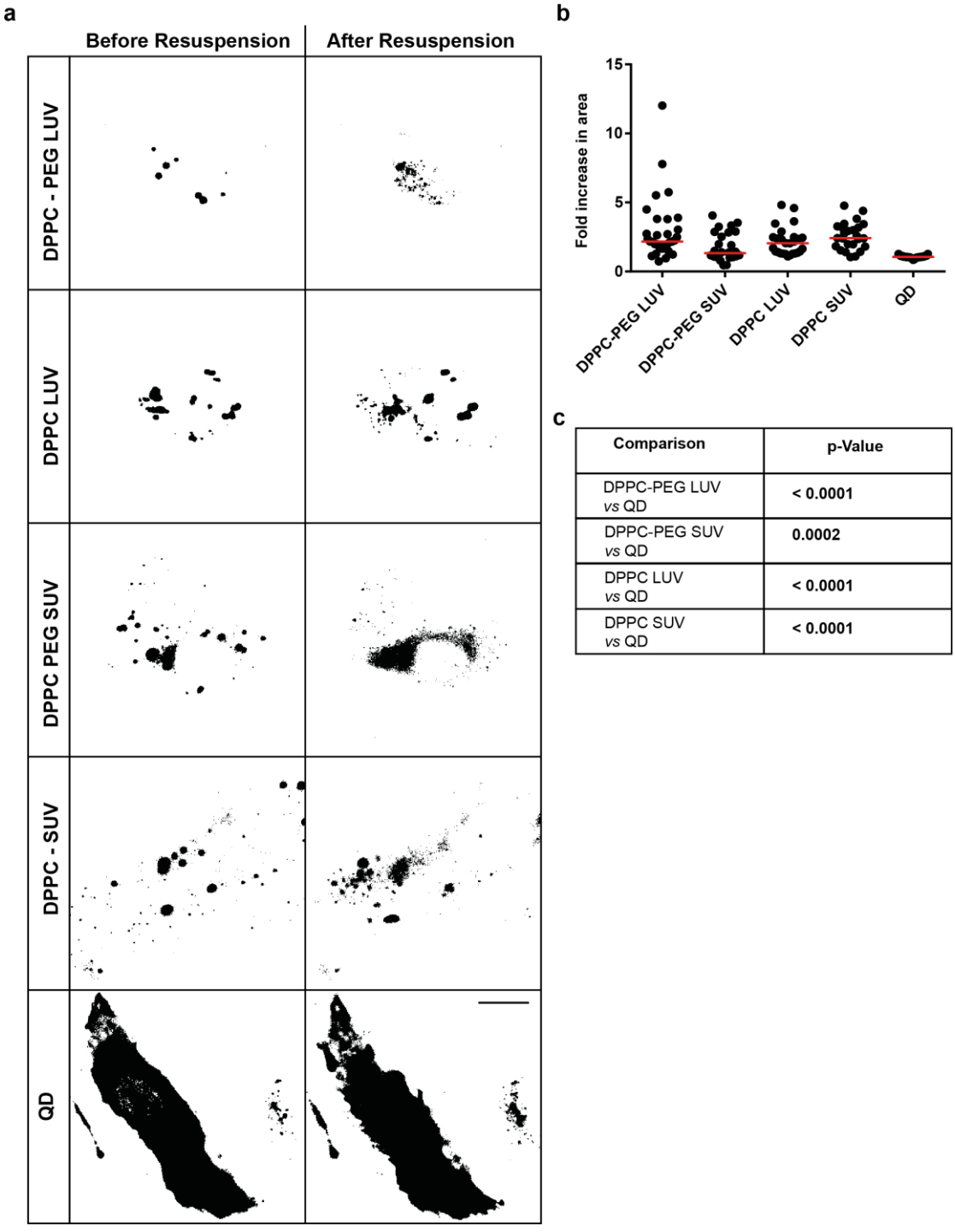

Comparison	p-Value
DPPC-PEG LUV *vs* QD	**< 0.0001**
DPPC-PEG SUV *vs* QD	**0.0002**
DPPC LUV *vs* QD	**< 0.0001**
DPPC SUV *vs* QD	**< 0.0001**

Figure 3.6 Analysis of the intracellular resuspension of aggregated LUV, SUV and QD. (a) Time-lapse images of LUV, SUV and QD before and after PBS injection to trigger resuspension of the aggregates, and upon setting an intensity threshold for the quantification of the area occupied by the colloids inside the cell. Scale bar 20 µm. (b) Fold increase in the area occupied by the colloids after injection of PBS. Between 25 and 31 cells from 3 independent experiment were analyzed in total. Red bar indicates median value. (c) Results of the statistical analysis of the data shown in (b) using Kruskal-Wallis and Dunn's Test.

Asymmetric dilution of injected colloids during cell cycle

During the 48 h that the injected liposomes stably persisted in the cytoplasm, the host cells would inexorably undergo cell division. For endocytosed NP, the intracellular dose achieved is known to distribute among daughter cells upon cell division, leading to an overall dilution of the initial dose [173, 175]. Whether the NP contained in the parent cell are inherited by the daughter cells in a symmetric or asymmetric fashion seems to depend on several factors, such as the NPs' size and physicochemical characteristics, the internalization pathway exploited and the subcellular compartment they accumulate in [173, 175]. The dilution pattern of injected LUV, SUV, QD and coinjection marker was therefore studied over two subsequent rounds of cell division by microscopy. The intracellular fluorescence of cells containing either colloids or coinjection marker was normalized to the values obtained for the parent cells that had originally received the MI. The SUV and the QD behaved similarly to the soluble coinjection marker, with which the dilution occurred in a linear fashion (Figs. 3.7A-C; Fig. A3.5). Compared to the parent generation (P), most of the cells of the first generation (F1) had approximately half of the fluorescence intensity, and those of the second generation (F2) retained half of the fluorescence of the F1 cells and less than a fourth of the P cells. The observed dilution pattern resembled that of other soluble molecules, such as the well-known dye carboxyfluorescein diacetate succinimidyl ester, which is indeed extensively used as a marker to track cell division cycles [172]. Strikingly, the LUV were diluted non-linearly upon cell divisions (Figs. 3.7D-E). The F1 generation included cells retaining up to 100% of the liposomal load of the P generation, as well as cells with virtually no liposomes at all. The uneven dilution became even more prominent in the F2 generation, where most cells retained a minor portion of the liposomes and a few cells still bore nearly 100% of the load of the P generation.

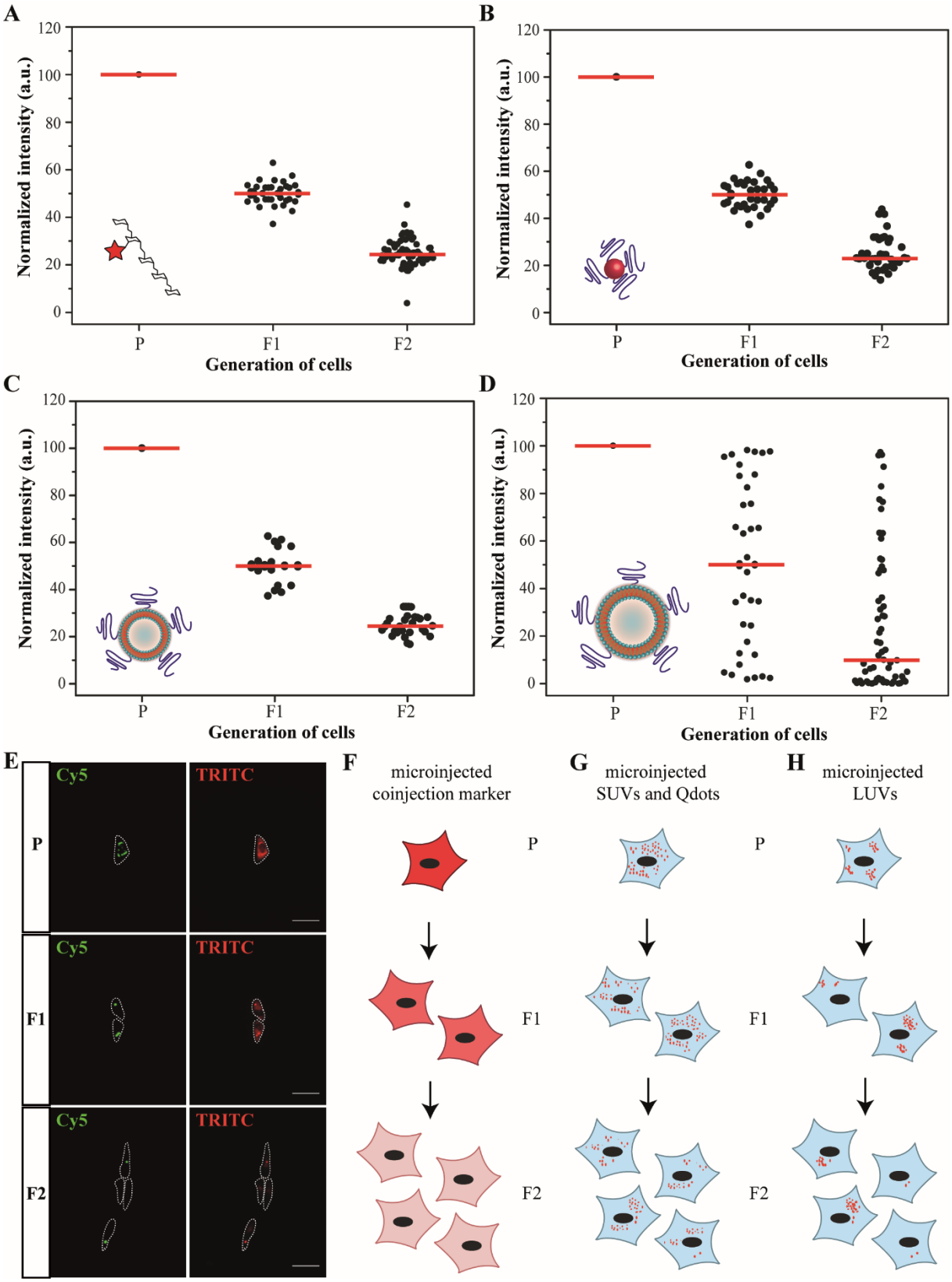

Figure 3.7 Dilution of injected material during cell division. (A-D) Analysis of the dilution during two cell divisions of the coinjection marker (A, n = 19), QD (B, n = 18), SUV (C, n = 12) and LUV (D, n = 19). The integrated intensity of individual cells was measured and normalized to 100% (generation P).

Red lines indicate median values of data pooled from 3 independent experiments. (E) Microscopy images of P, F1 and F2 generations of cells microinjected with LUV (Cy5) and coinjection marker (TRITC). Scale bar 50 μm. A representative image of 36 images obtained during 3 independent experiments is shown. (F-H) Schematic representation of the dilution upon cell division of microinjected coinjection marker (F, red), SUV and QD (G, red dots), and LUV (H, red dots). P represents parent generation; F1 and F2 describe first and second generations, respectively.

The contrasting dilution patterns observed for the smaller colloids (SUV and QD) and the LUV could be a consequence of their fundamentally distinct intracellular distributions, which could in turn be ascribed to their size differences. Whereas the smaller colloids diffused evenly throughout the intracellular milieu as would be expected for soluble molecules like the coinjection marker, the 130-nm LUV formed the aforementioned agglomerates after their injection, and hence were not equally distributed in the cytoplasm when it was divided between the daughter cells (Figs. 3.7F-H). Thus, the results suggest a link between the sizes of the colloids injected, their cytosolic distribution and their dilution upon cell division. It is worth noting that such link is not observed with particles internalized by endocytosis, since in this case it is instead particle-loaded vesicles that get diluted over cell division and therefore the dilution pattern is linked to the behaviour of the vesicular organelles, which might fuse into larger vesicles, be subject to exocytosis and other biological processes [44, 173-175]. Achieving even dosing among injected carrier cells can therefore be challenging because it is not only linked to the precision of the injection volume [98], but also to the pattern of dilution upon cell division. In only a few cell division cycles, the asymmetric dilution pattern observed with the injected LUV would result in heterogeneous loads of material among the population of carrier cells. Injecting smaller nanocarriers can lead to more even intracellular distributions, as observed with QD and SUV, presumably due to an easier diffusion across the porous cytoskeletal meshwork [162, 217]. However, small vesicular carriers are generally associated with lower loadings and would not be able to deliver as much functional material [218].

Microinjection of liposomes containing catalytically active cargo

The liposomes' innocuous persistence in the recipient cells' cytoplasm and their efficient retention of cargo over at least 2 days, suggest the potential of MI as a platform to empower cells with novel functions through the introduction of artificial organelles. Catalytically active cargo was therefore encapsulated inside DOPC LUV (Fig. A3.6; Table A3.2) and its activity was studied upon injection into the cytoplasmic milieu of cells. UnPEGylated DOPC LUV were chosen in this case in order to maximize the enzyme encapsulation efficiency [219] and stability, since in contrast to DPPC-based LUV, the preparation of DOPC ones does not require heating at enzyme-degrading temperatures. The removal of residual trypsin bound to the outer membrane of the liposomes was corroborated after an enzymatic digestion step (Fig. A3.7).Trypsin was selected as a model enzyme due to its relatively small size of 23.3 kDa and its resistance to external stress, such as the repeated freeze-thaw cycles involved in liposomes preparation. Importantly, trypsin does not need additional cofactors for its activity, a crucial feature in view of its confinement in liposomes and ultimately in the injected cells.

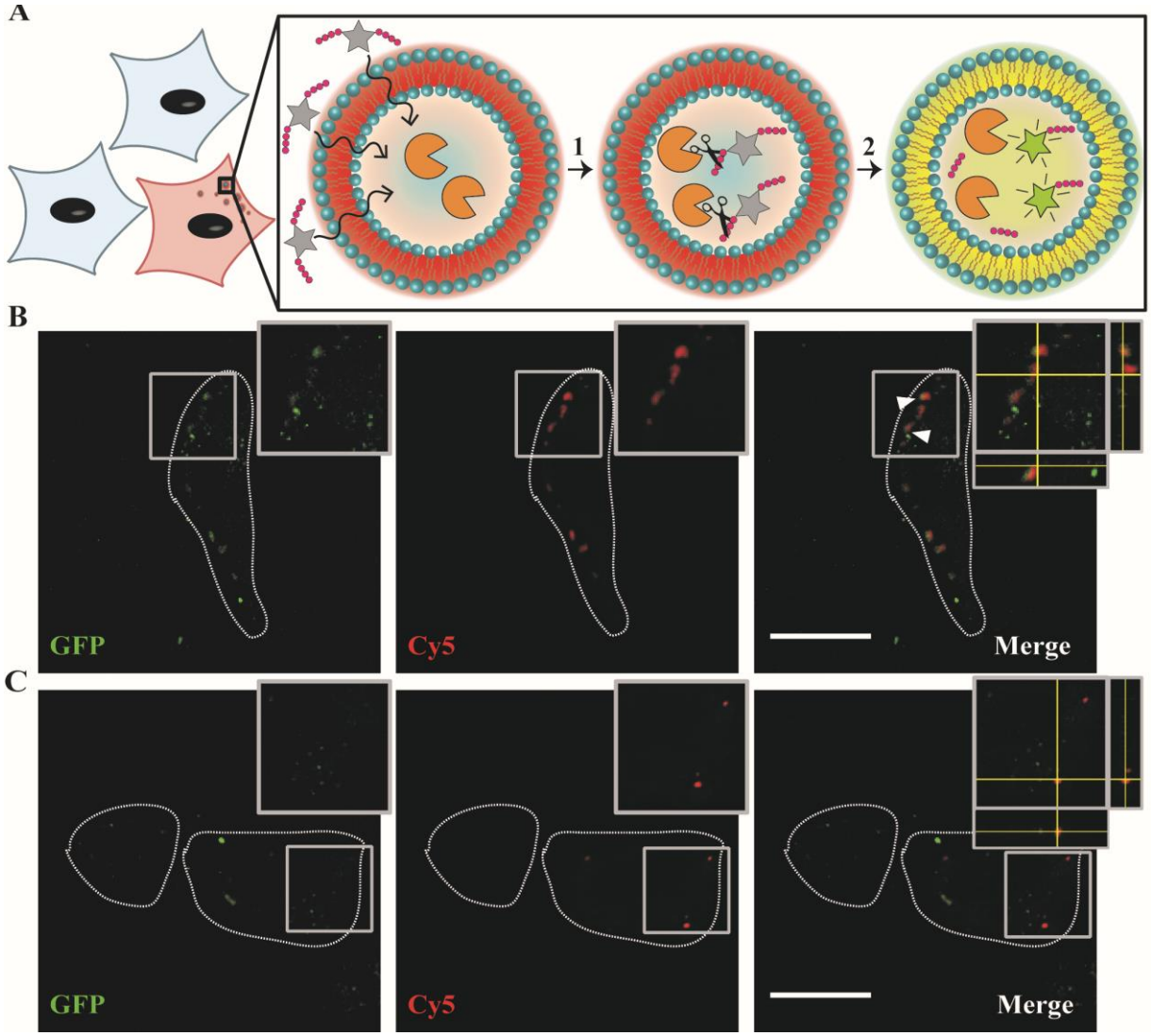

Figure 3.8 Intracellular activity of liposome-encapsulated trypsin. (A) Schematic representation of the assay used to determine the enzymatic activity inside the trypsin-loaded LUV of injected cells. The fluorogenic substrate (BZiPAR) permeates through the cell and the liposomal membrane (1), inside of which it is cleaved by the encapsulated trypsin (2) and dequenched. (B-C) Enzymatic activity in cells injected with liposomes containing trypsin (B) or PBS (C). White arrowheads indicate the overlap of processed substrate (GFP) with liposomal marker (Cy5). The insets show zoomed-in subcellular areas, and the insets in the Merge images show the XZ and YZ orthogonal views of the Z-stacks. Scale bar 20 µm. For the trypsin-containing liposomes, a representative image from 25 images obtained during 5 independent experiments is shown. For the PBS-containing LUV, a representative image from 22 images obtained during 5 experiments is shown.

The catalytic activity of the trypsin-loaded LUV was assessed upon their injection into cells with a fluorescence microscopy-based assay involving the enzymatic cleavage of the cell-permeable substrate BZiPAR. After permeating through the cell and the liposomal membranes, BZiPAR can be cleaved and dequenched by the encapsulated trypsin, leading to an increase in fluorescence (Fig. 3.8A). The assay's

validation in a cell-free environment confirmed that only when substrate and trypsin-loaded LUV were simultaneously present could a fluorescent signal be detected (Fig. A3.8). Since cells contain endogenous proteases to which BZiPAR is also sensitive, a pre-incubation step with the protease inhibitor AEBSF was included. Hence, upon pre-incubation with AEBSF, the cells were injected with trypsin-loaded LUV and imaged in the presence of BZiPAR substrate. Substrate cleavage was successfully detected in the cells injected with trypsin-loaded LUV and although not all the injected cells were positive for protease activity, there was a clear-cut difference with those injected with blank liposomes, where enzymatic activity could not be detected at all (Fig. 3.8B-C). Variable degrees of enzymatic activity in the cells injected with trypsin-loaded LUV were noted, an observation that could be attributed to the limited permeation of BZiPAR across membranes. Indeed, the enzymatic activity increased by 4-fold after inducing the rupture of the trypsin-loaded LUV and releasing the enzyme into the substrate-containing buffer (Fig. A3.7). In addition to the potentially underestimated values obtained with this assay, the relatively low encapsulation efficiency of trypsin implies a low absolute number of enzymes per liposome in the range of 23 (see calculation in Materials and Methods). In addition, the microscopy-based approach we have used to detect the enzymatic activity allows limited sampling, potentially over-representing differences between individual cells. MI itself bears the intrinsic limitation of achieving small sample sizes, as even an expertly trained operator cannot inject more than a few hundreds of cells within 1 h. In this regard, advances in automated MI setups will be of great value, as well as microfluidic platforms that allow injecting up to 20’000 cells in only 1 s [6, 38]. Finally, the range of enzymes that can be encapsulated in the nanocarriers for their subsequent injection might be restricted in view of the substrates’ capacity to permeate through cells’ and liposomes’ membranes, as shown by the significant difference in enzymatic activity between intact and detergent-permeabilized liposomes. Future efforts shall focus on developing suitable pairs of prodrugs and prodrug-converting enzymes, and on increasing the throughput of MI. Nevertheless, the semi-quantitative study showed an unequivocal response in the cytoplasm of cells injected with trypsin-loaded LUV, indicating microinjected material can preserve its biological activity inside the lumen of liposomal vesicles.

Besides biologically active cargo, microinjected liposomes could encapsulate chemical environments that are incompatible with cell viability. They could thus be exploited as bioreactors in which to perform chemical reactions in the cytoplasm of live cells. As a proof of concept, DPPC-PEG LUV encapsulating extremely acidic pH were prepared and successfully delivered intracellularly through MI. The liposomes contained 250 mM citrate buffer adjusted to pH 2. These “new organelles” which did not affect cell viability (Fig. A3.9) could be detected for at least 2 days in the cytoplasm of the injected cells and notably, their interiors remained visibly acidic upon injection (Fig. 3.9). This was indicated by the positive staining with a marker for acidic compartments in presence of an acidification inhibitor, which allowed us to distinguish the acidic liposomes from typically acidic subcellular compartments, such as endosomes and lysosomes. The introduction of vesicles containing biologically functional cargo into the intracellular compartment of cells brings exciting possibilities for cell-based therapies and emerging drug delivery strategies. Artificial properties may be added to cells by providing them with synthetic organelles encapsulating exogenous proteins or enzymes. The vesicles could also be conceived as bioreactors which carry out chemical reactions under conditions that are normally incompatible with cell viability, such as extremely acidic, alkaline, oxidizing or reducing milieu [195].

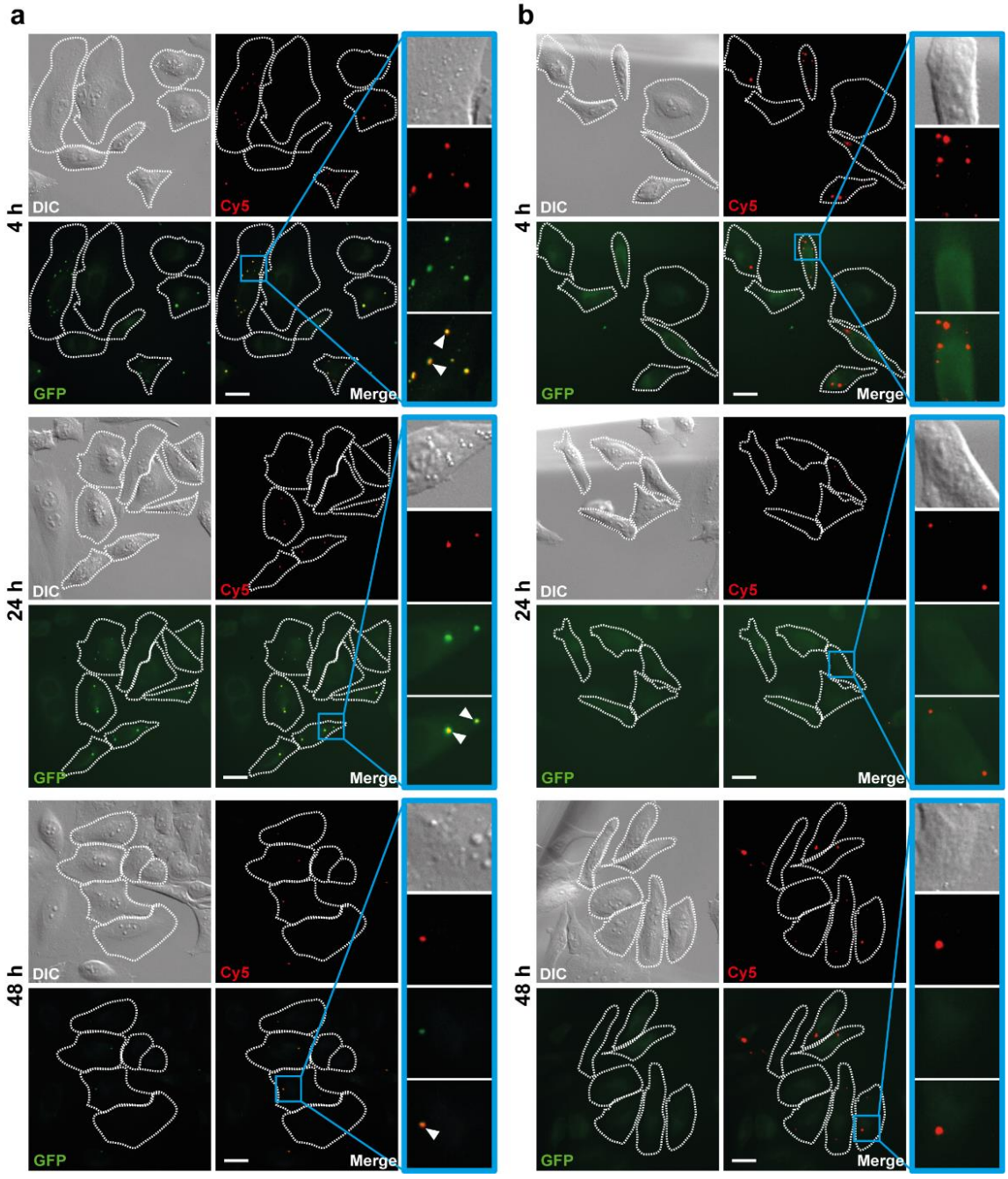

Figure 3.9 LUV encapsulating acidic buffer injected into cells. Epifluorescence microscopy images of live cells treated with bafilomycin A1 (inhibitor of organelles' acidification) and stained with Lysotracker Green DND-26 (GFP, marker for acidic compartments) 4, 24 and 48 h after being injected with DiD-stained liposomes (Cy5) with internal pH of 2 (a) or pH 7.4 (b). White arrowheads indicate colocalization between liposomes and Lysotracker stain. Scale bar 25 μm. White dotted lines show the outlines of individual cells. Representative images from 9-10 images obtained during 3 independent experiments are shown.

Injection of liposomes into migratory cells

Having established the feasibility of introducing vesicles containing biologically active material and unnatural chemical environments in HeLa cells, MI was then applied to primary DC, a migratory cell type directly relevant for cell-based therapies [184, 185]. During immune responses, DC act as antigen-presenting cells which are activated in the context of infections or vaccinations. Upon encounter of an antigen in the peripheral tissues, DC migrate to the draining lymph nodes and activate an immune response [220]. Cell-based therapies propose to exploit such site-directed migration properties to shuttle therapeutic cargo to sites of inflammation or tumour growth. The effect of liposomal MI on the migratory behaviour of DC was thus investigated using murine primary DC expressing yellow fluorescent protein (YFP). In specific, DC were generated *in vitro* from bone-marrow of CD11c-YFP mice and matured with lipopolysaccharide for 24 h according to established protocols [206, 221]. The matured DC were injected with fluorescent DPPC-PEG LUV suspensions and/or coinjection marker, and were subsequently flushed on top of a monolayer of imLECs [206]. The migration of the DC over the monolayer of imLECs was recorded *via* time-lapse microscopy (Fig. 3.10A). By tracking the DC migration paths, the migration speed could be calculated for every injected cell and compared to that of uninjected cells. The injection of liposomes and also of coinjection marker alone reduced the migration speed by almost 30% (Fig. 3.10B), suggesting the MI procedure in itself had a significant impact on the migratory capacity of DC. In fact, the decrease in speed observed with the MI was comparable to the effect of the actin inhibitor cytochalasin D, which reduces the migratory speed due to the disorganization of the intracellular actin filaments [209], as well as to the Rho-associated protein kinase (ROCK)-inhibitor Y27632, which blocks the detachment of the DC from adhesion molecules expressed by imLECs (Fig. A3.10) [210]. The injection of DPPC-PEG LUV, however, did not disrupt the DC migratory properties any further than the coinjection marker alone, suggesting that the speed impairment resulted mainly from the impact of the MI procedure itself, likely mediated by hindrance of microtubules' dynamics. The *ex vivo* modification of tissue-homing migratory cells could enable innovative therapeutic approaches. For instance, an inactive prodrug could be systemically administered and only be activated at the site of disease upon encountering the modified migratory cells, which would carry synthetic organelles loaded with the prodrug-activating enzyme.

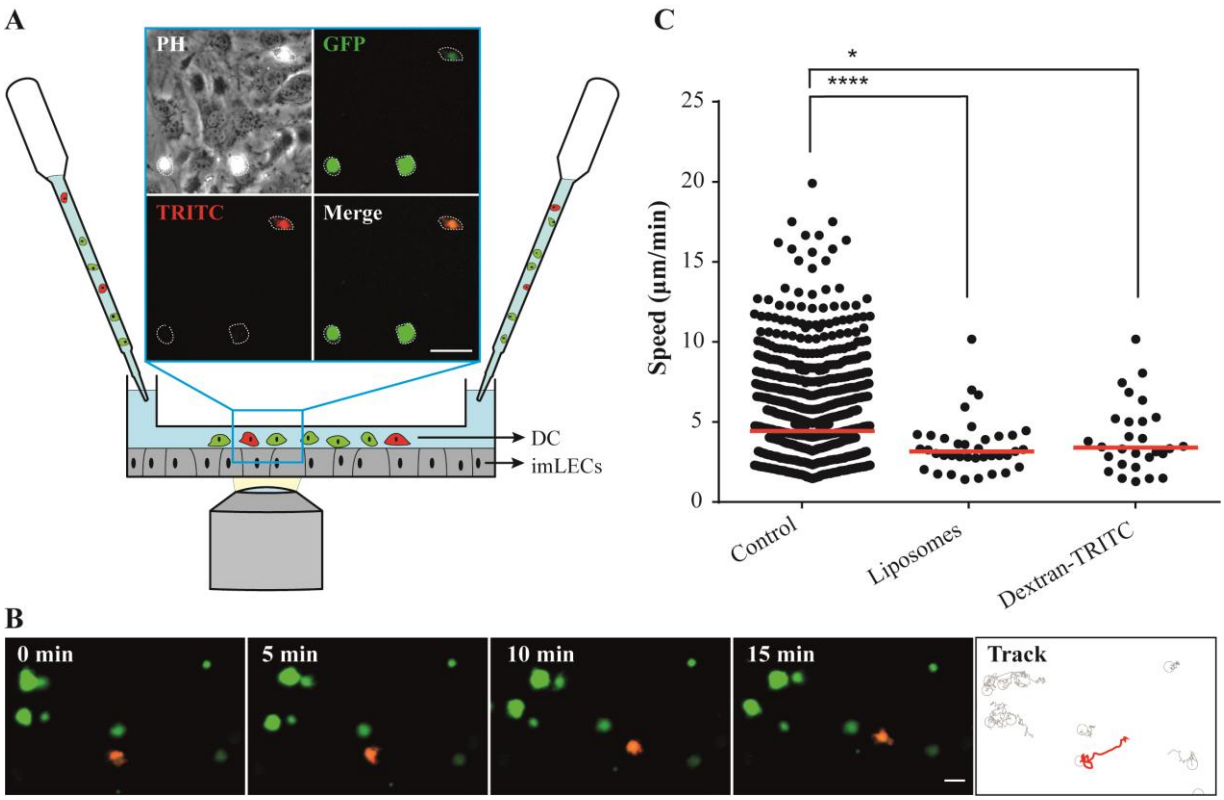

Figure 3.10 Migratory properties of injected DC. (A) Schematic representation of the channel slide assay used to evaluate the migratory properties of DC. A suspension of DC (drawn in green and visible in the GFP channel) was flushed over a monolayer of imLECs (drawn in grey and visible in the phase contrast image, PH). Injected DC containing coinjection marker were drawn in red and are visible in the TRITC channel. Scale bar 50 µm. (B) Time-lapse microscopy images of the migration of DC on top of the monolayer of imLECs. A DC simultaneously injected with coinjection marker and DPPC-PEG LUV appears in orange, while uninjected DC appear in green. The trajectory over time of the injected cell is indicated with a red line in the last panel (Track), whereas those of uninjected cells are indicated with grey lines. Scale bar 20 µm. (C) Analysis of the migratory speed of DC injected with DPPC-PEG LUV (Liposomes), coinjection marker (Dextran-TRITC) or left uninjected (Control). Each dot represents a tracked cell. The red lines indicate the median values of pooled data from 6-11 independent experiments. A Mann-Whitney-U-Test was applied, n = 28 – 37 for treated cells ($*$p-value < 0.05, $****$p-value < 0.0001).

Conclusion

In the present study, well-characterized phospholipid vesicles were introduced directly into the cell's cytoplasm and several fundamental aspects were examined. MI efficiently bypassed the bottleneck imposed by degradative subcellular organelles and did not affect cell viability. Indeed, the injected liposomes remained intact in the cells' cytoplasm for at least 2 days without fusing or undergoing further processing beyond their physical agglomeration in seemingly random corners of the cell. Notably, the encapsulated cargo was effectively retained in the liposomes' core and did not leak into the cytoplasm. Furthermore, the injection of enzyme-loaded liposomes into cells confirmed that exogenous catalytic activity can be preserved and detected in the interior of carrier cells. In view of these findings, we validated the platform on DC, one of the migratory cell types recurrently proposed for cell-based therapies and vaccines. Although the migration speed of these cells was decreased by the MI procedure, their migratory properties over an endothelial monolayer were essentially preserved upon injection of cargo. These experiments provide proof-of-concept on the applicability of MI on such therapeutically relevant systems, and will pave the way for further studies on artificial organelles as well as future developments in cell-based therapies. Based on the encouraging findings in this chapter, triggered release systems were investigated in the following chapter in order to gain control over time-specific delivery of the cargo.

Chapter 4

Investigation of a Thermosensitive Liposomal System producing CO_2

Peter Tiefenboeck, Jong Ah Kim, Ferdinand Trunk, Jean-Christophe Leroux

Swiss Federal Institute of Technology Zurich (ETHZ), Department of Chemistry and Applied Biosciences, Institute of Pharmaceutical Sciences, Vladimir-Prelog Weg 1-5/10, Zurich 8093, Switzerland

This chapter was adapted from the accepted manuscript

P. Tiefenboeck, J. A. Kim, F. Trunk, J.-C. Leroux, Comment on "A Liposomal System Capable of Generating CO2 Bubbles to Induce Transient Cavitation, Lysosomal Rupturing and Cell Necrosis", Angew. Chem. Int. Ed. 2017, 56, 11686-11689, DOI: 10.1002/anie.201703740 and 10.1002/ange.201703740

Introduction

After studying the fundamental aspects of the MI of colloids and gaining an understanding of the parameters that are relevant from a drug delivery perspective, the possibility to inject liposomes with controlled release properties was investigated. These systems have the capacity to respond to a given stimulus (*e.g*. pH, temperature, oxidative stress) that triggers the release of their encapsulated cargo [58]. Despite the advantages that MI offers in comparison to co-incubation, only a few published reports exist on the MI of controlled release systems [59, 222]. In one of these publications, the release of inositol triphosphate from gold-coated liposomes was triggered by an increase of temperature after applying a near infrared pulse of light [59]. Since the objective of our work was to deliver the liposomes by MI into the cytosol of viable cells, pH was discarded as a potential trigger for controlled release because the cytosolic pH cannot be altered without disturbing the homeostasis and risking the induction of cell death [223]. Temperature was instead deemed as a suitable trigger, since it can be easily modulated externally and the cells can withstand fluctuations of a few degrees without jeopardizing their viability.

Numerous thermo-responsive systems have been described in the literature employing different strategies. Generally, temperature-sensitive formulations include lipids or polymers, which either assist in membrane destabilization upon phase transition of the main lipid, or show phase separation and subsequent membrane disruption upon heating above the lower critical solution temperature (LCST, in case of polymers). Lysolipids such as 1-stearoyl-2-hydroxy-*sn*-glycero-3-phosphocholine (MSPC) are commonly included in these systems to assist membrane destabilization upon phase transition of the main membrane-forming lipid, *e.g.* DPPC (42 °C) [224]. However, upon contact with blood within *in vivo* experiments, the lysolipids can desorb from the liposomal membrane, leading to loss of thermoresponsiveness [225, 226]. It is possible that the MI of such liposomes into the cytoplasm would have a similar outcome; therefore, we considered testing a different thermo-responsive system.

Back in 2012, Sung and coworkers reported liposomes encapsulating ABC that would rupture and release the payload above 42 °C [80]. The release mechanism was said to be mediated by the temperature-induced decomposition of ABC, which would generate CO_2 bubbles and cause transient cavitation. The liposomes were also said to induce cell death *via* necrosis in the absence of cytotoxic drugs by disrupting the cells' lysosomal membranes. Naturally, the system's thermoresponsiveness combined with its benignity at physiological temperature but cytotoxicity at 42 °C, caught our attention. Moreover, hyperthermia is a suitable trigger to control treatments in time and space, since it can be easily modulated externally (as opposed to physiological stimuli such as pH). Follow-up publications by the authors described applications of increasing complexity where the ABC liposomes were used for localized delivery of chemotherapeutics and *in vivo* tumor targeting with aptamer-conjugated or FRET-guided versions of the vesicles [227-230]. We intended to apply the system in our laboratory but encountered insurmountable technical obstacles. Protocol clarifications kindly provided by the authors did not aid the reproduction of the work; therefore, to understand the root cause for the irreproducibility, we travelled to Sung's laboratory to work jointly. Numerous discrepancies were noted with the original protocol published by the authors, and most importantly, the purification of the liposomes was found to be ineffective. Residual ABC and calcein were highly abundant in the liposomal suspension, compromising the validity of the calcein release kinetics estimated by the authors. Indeed, when the liposomes were purified further, the release of calcein at 42 °C did no longer differ from that at 37 °C. Liposomes prepared following the methods specified by Sung and coworkers lack the thermoresponsive properties described in their 2012 paper. Essentially, in our hands neither the extent nor the rate (profile)

of cargo release from the ABC liposomes could be reproduced, and we attribute this to several reasons for which we provide evidence below.

Materials and Methods

Liposomes' preparation

Liposomes were prepared by the lipid-film rehydration method. The lipids used were DPPC, hydrogenated soybean phosphatidylcholine (HSPC), DSPE-PEG_{2000} (Lipoid, Ludwigshafen, Germany), CHOL (Fluka, Buchs, Switzerland), 1,2-di-O-octadecenyl-3-trimethylammonium-propane (chloride salt) (DOTMA) and MSPC (Avanti Polar Lipids, Alabaster, AL). The formulations used for the ABC-encapsulating liposomes and the negative control (temperature-insensitive) liposomes were HSPC:CHOL:DOTMA (57.1:38.1:4.8 mol%; 63.8 mM total lipid), whereas for the positive control (temperature-sensitive) liposomes the formulation was DPPC:DSPE-PEG_{2000}:MSPC (86.5:3.9:9.6 mol%; 5 mM total lipid). Briefly, lipids dissolved in chloroform were dried in small vials and kept in a desiccator overnight. For the negative and positive control liposomes, calcein (Sigma-Aldrich, Buchs, Switzerland) was dissolved at 200 mM in 1 M NaOH and subsequently diluted to 50 mM in PBS pH 7.4 (Na_2HPO_4 10 mM, KH_2PO_4 1.8 mM, NaCl 87 mM and KCl 2.7 mM). For the ABC-encapsulating liposomes, ABC was first dissolved at 2.7 M in milli-Q water at 4 °C and then the 50 mM calcein was dissolved in the ABC buffer. The dried lipid films were rehydrated with the corresponding solutions containing calcein. In the case of negative control and ABC liposomes, the liposomes were prepared *via* sonication in an ultrasonic bath at 40 kHz (Elma Transsonic Digital S, Singen, Germany) in order to dissolve the lipid film completely. Intervals of 5 s (sonication on and off) were applied for 15 min. The formed liposomes were then dialysed (100 kDa cut-off Float-A-Lyzer, Spectrum, Rancho Dominguez, CA) 1:2000 (v/v) against PBS pH 7.4 for 24 h at 4 °C with 3x dialysis buffer change according to the original publication [80]. Since the dialysis did not completely remove the unencapsulated calcein, the liposomes were further purified with a G-25 column (GE Healthcare, Little Chalfont, UK). The positive control liposomes underwent vortexing and 7 freeze-thaw cycles after lipid film rehydration. The final liposome suspension was extruded 10x through two stacked 200-nm polycarbonate membranes (Sterlitech, Kent, WA) and the unencapsulated dye was removed with a G-25 column. The size of the liposomes was determined after sonication using laser diffraction (Mastersizer® 2000, Malvern Instruments, Malvern, UK). For the positive control liposomes, size was determined after extrusion using DLS (DelsaNano®, Beckman Coulter, Indianapolis, IN).

Calcein release from liposomes

Cumulative release curves were recorded at excitation 490 nm and emission 520 nm with a Cary Eclipse fluorescence spectrophotometer (Agilent, Santa Clara, CA) equipped with a thermostatted multicell holder. The samples were diluted 1:100 (v/v) with PBS and measured in quartz glass fluorescence cuvettes (Hellma Analytics, Mühlheim, Germany). Values obtained were normalized to the fluorescence measured after Triton X-100 treatment (see below). For the cumulative release curves as a function of temperature, fluorescence measurements were recorded at increasing temperatures (0.1 °C/min) starting from 25 °C until 50 °C. For the cumulative release curves as a function of time, single measurements were recorded every 5 min over a period of 180 min at the constant temperatures 25 °C, 37 °C and 42 °C.

The fold increase in fluorescence intensity upon Triton X-100 treatment was measured with a plate reader (Tecan, Männedorf, Switzerland). Equal volumes of liposomes and Triton X-100 1% (m/v) (Sigma) were incubated for 10 min at 65 °C to rupture the liposomes' membrane and release the encapsulated calcein. The mixtures were then diluted in PBS 1:10 (v/v) and the fluorescence was measured. The values obtained were normalized to non-treated liposomes.

Results and Discussion

In their original publication, the authors measured the cumulative release of encapsulated calcein at different temperatures, and reported that at 42 °C about 50% of the encapsulated calcein was released after 30 min and approximately 80% by 180 min. However, in our lab the liposomes produced (average diameter 188 ± 17 nm for ABC liposomes, 206 ± 51 nm for negative control liposomes and 151 ± 4 nm for positive control liposomes) only achieved 5% release after 30 min at 42 °C, which increased to merely 17% after 180 min (Fig. 4.1A). The modest release became even more apparent when compared to a well-established temperature-sensitive system, used here as a positive control. Such formulation consisted of phospholipids (transition temperature 40 – 43 °C) and lysolipids (phospholipids lacking alkyl chains) [231], and accordingly it released nearly all cargo at 42 °C in contrast to only 15% at 37 °C (Fig. 4.1B). Temperature-insensitive liposomes hydrated with PBS instead of the ABC solution were used as negative control, and these did not release any of the encapsulated calcein at any of the temperatures tested (Fig. 4.1C). Equivalent results were obtained as well with a different encapsulated cargo of smaller molecular weight, the fluorescent dye carboxyfluorescein (CF) (Fig. A4.1).

To investigate whether the ABC liposomes produced in our laboratory would perhaps have a higher release-triggering temperature, the release of calcein was measured as a function of temperature ranging from 25 to 50 °C. Whereas the positive control liposomes exhibited a sigmoidal profile with an abrupt release within the expected temperature window leaking essentially all their cargo at 41 °C, the ABC liposomes showed a very gradual release profile that barely reached a modest 15% leakage at 42 °C (Fig. 4.2). Experiments with CF instead of calcein revealed the same results (Fig. A4.2).

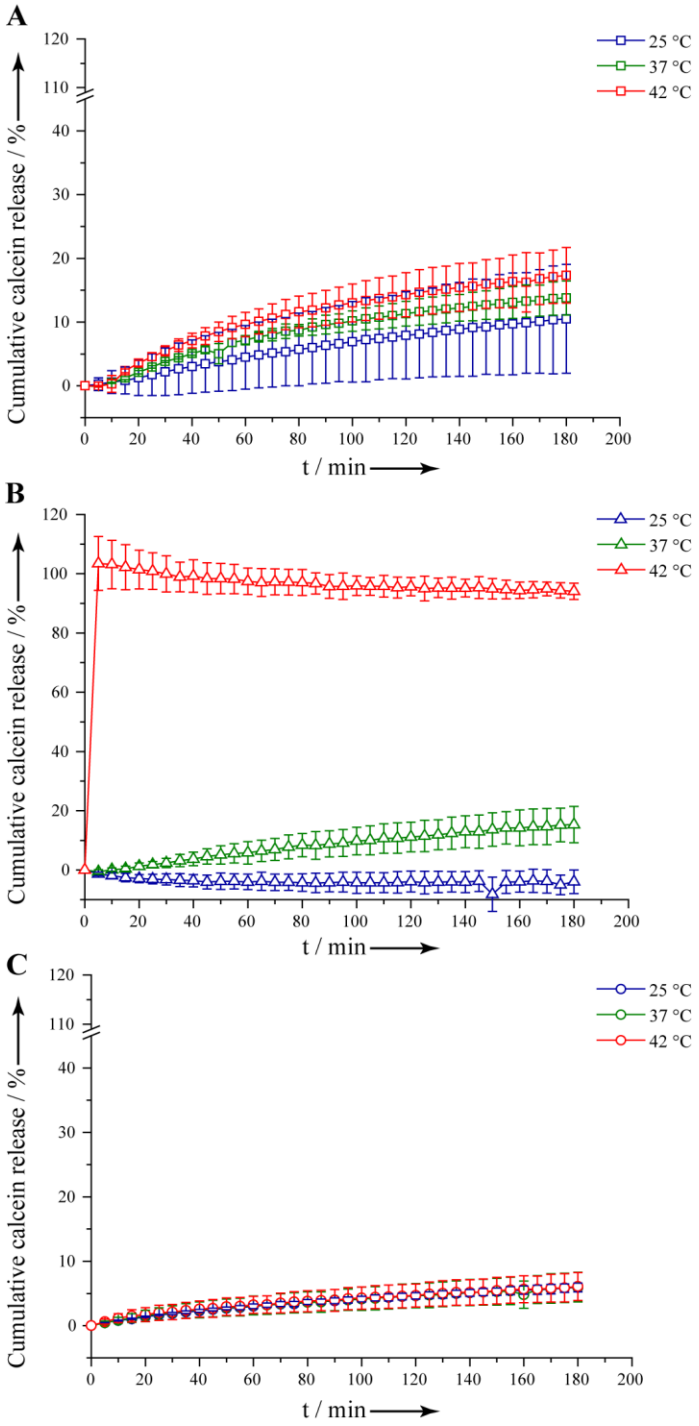

Figure 4.1. Release of encapsulated calcein as a function of time. The release of calcein from (A) ABC, (B) Positive control and (C) Negative control liposomes was measured at 25, 37 and 42 °C over a period of 180 min (mean ± SD, n = 3).

These results led us to question the sensitivity of the ABC liposomes to temperature, since in our hands they behaved similarly at 37 and 42 °C. Indeed, a freshly prepared solution of ABC generated macroscopically visible CO_2 bubbles already at 37 °C (Fig. 4.3), suggesting the encapsulation of ABC could not yield a temperature-sensitive system. Our observations are in line with a 1994-patent where an ammonium transmembrane gradient was exploited to load amphiphilic drugs into liposomes. The patent described that the mechanism relied on the acidification of the liposomes' core, which occurred upon exchange of the surrounding buffer for one without ammonia.

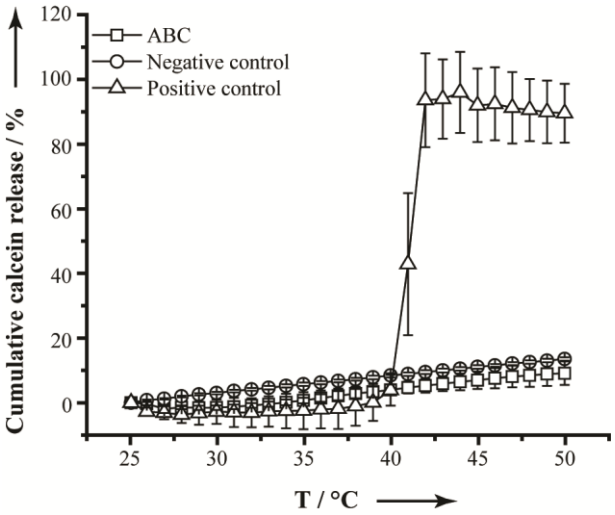

Figure 4.2. Release of encapsulated calcein as a function of temperature. Fluorescence intensity was measured as temperature was increased 0.1 °C/min. Data were normalized to the fluorescence obtained after incubating the samples with Triton X–100, which was considered as 100% release (mean ± SD, n = 3).

In order to reestablish the equilibrium upon the buffer exchange step, the encapsulated ammonia exited from the liposome core in its deprotonated form, leaving behind a proton which ultimately acidified the vesicles' lumen. Such decrease in pH in turn causes the remaining carbonate to decompose into water and CO_2, generating bubbles from the initially encapsulated ABC solution [232]. Hence, from this earlier work and also from our results it is clear that CO_2 bubbles would be generated as soon as the buffer exchange would take place during the liposomes' preparation. This would imply that the transient cavitation that Sung and coworkers reported would not be a phenomena controllable through hyperthermia, but through the timing of the buffer exchange.

Furthermore, based on the high concentration (2.7 M) at which ABC was encapsulated in the published protocol and considering its substantially higher osmolality compared to the PBS used for the buffer exchange (4460 ± 139 *vs.* 297 ± 2 mOsm/kg, as measured with a freezing point osmometer), we hypothesized that the preparation method would establish an excessively strong osmotic gradient across the liposomal membranes that would compromise their stability. The stability of the ABC liposomes was therefore studied by measuring the efficiency with which they retained the encapsulated cargo during the purification procedure. Calcein release was measured after inducing the liposomes' rupture by addition of Triton X-100. While the negative control liposomes exhibited a 5-fold increase of fluorescence (11-fold with encapsulated CF) after addition of the detergent, the ABC liposomes only increased by 3-fold (4-fold with CF). This suggests that the ABC liposomes' membrane integrity would have already been compromised before the addition of the detergent, and that part of the initially encapsulated calcein had already leaked out of the vesicles at the time of the experiment.

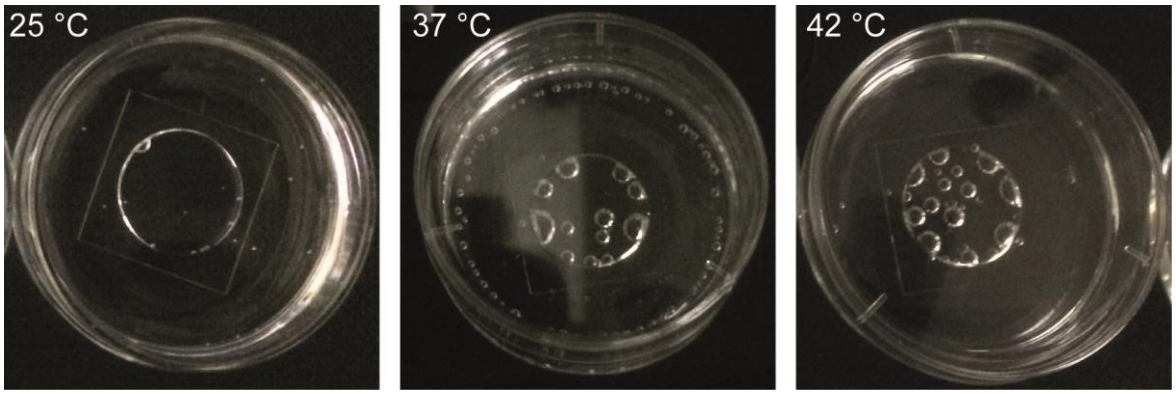

Figure 4.3. Generation of CO_2 bubbles from ABC. Freshly prepared ABC solution (2.7 M) was incubated in petri dishes for 15 min at 25 °C, 37 °C and 42 °C, after which images were acquired with a digital camera. Representative images of three independent experiments are shown.

Hence, in our hands the ABC liposomal system described by Sung and coworkers lacked the thermoresponsive properties that motivated us to work with it. More importantly, due to the strong transmembrane osmotic gradient, the authors' method yielded unstable liposomes that could not retain the encapsulated cargo.

Conclusion

The results herein presented cast serious doubts on the ABC liposomes' potential value as nanocarriers with controlled release and question the follow-up publications in which the authors applied the system [227-230]. Certainly, simple drug delivery systems controllable by hyperthermia are of great interest to the drug delivery field and would be a valuable contribution. Since our findings preclude us from further investing resources on ABC-triggered thermoresponsive release, other systems have to be considered. A possible option would be the use of polymer-modified liposomes, *e.g.* the insertion of poly(*N*-substituted acrylamides) into liposomal membranes, since these vesicles also show a good stability in biological fluids like blood [224]. In temperature-triggered release systems, the working principle is different from that of formulations with lysolipids. Upon heating above the LCST, the polymers undergo coil-to-globule transition due to changes in water-binding capacity and then phase separate. This effect leads to the destabilization of the liposomal membrane and the release of the encapsulated compound. In summary, cell manipulation with microinjected liposomes will probably increase in versatility when implementing stimuli-responsive release systems.

Chapter 5

Conclusion and Outlook

Fueled by the rise of new genome-editing technologies and cell-based therapies, the development of intracellular delivery strategies to manipulate cells has increasingly received attention in the past years. Among the existing techniques [1], MI was used during this doctoral thesis for its capacity to introduce materials in cells while circumventing the endolysosomal pathway to prevent the degradation of sensitive biomacromolecules and colloids. In addition, MI's unique features such as the possibility to inject compounds at a precise time in specific subcellular compartments, rendered it especially appropriate for the introduction of liposomal carriers explored in this thesis. The fundamental aspects concerning the liposomes' intracellular delivery and activity upon MI were explored, and their potential to endow cells with artificial organelles containing enzymatic cargo or chemical reactions was analyzed.

By injecting nanocarriers of different compositions, surface properties and size, a comparative study was carried out on several aspects of the MI of colloids into live cells. In order to test the influence of particle size, we chose different liposomal and nanocrystal systems (LUV of 130 nm, SUV of 80 nm and QD of 20 nm). Our main findings presented in Chapter 3 and summarized in figure 5.1, show that neutral charged liposomes induced marginal toxicity on the injected cells and that after their introduction in the cytosol they remained stable without releasing the encapsulated cargo. Liposomal stability inside the injected cells was found to be comparable among the different formulations tested, although small differences were observed depending on the lipid composition of the vesicles. Specifically, liposomes made of lipids with higher transition temperatures remained intact inside the cells for slightly longer time. This could be explained by the fact that lipids with higher transition temperatures build liposomal membranes exhibiting a gel-crystalline state at 37 °C, which is less permeable compared the unordered liquid-crystalline state above the transition temperature. Moreover, PEGylation was also found to have a stabilizing effect. This was an expected outcome in view of the well-known shielding properties of PEG chains.

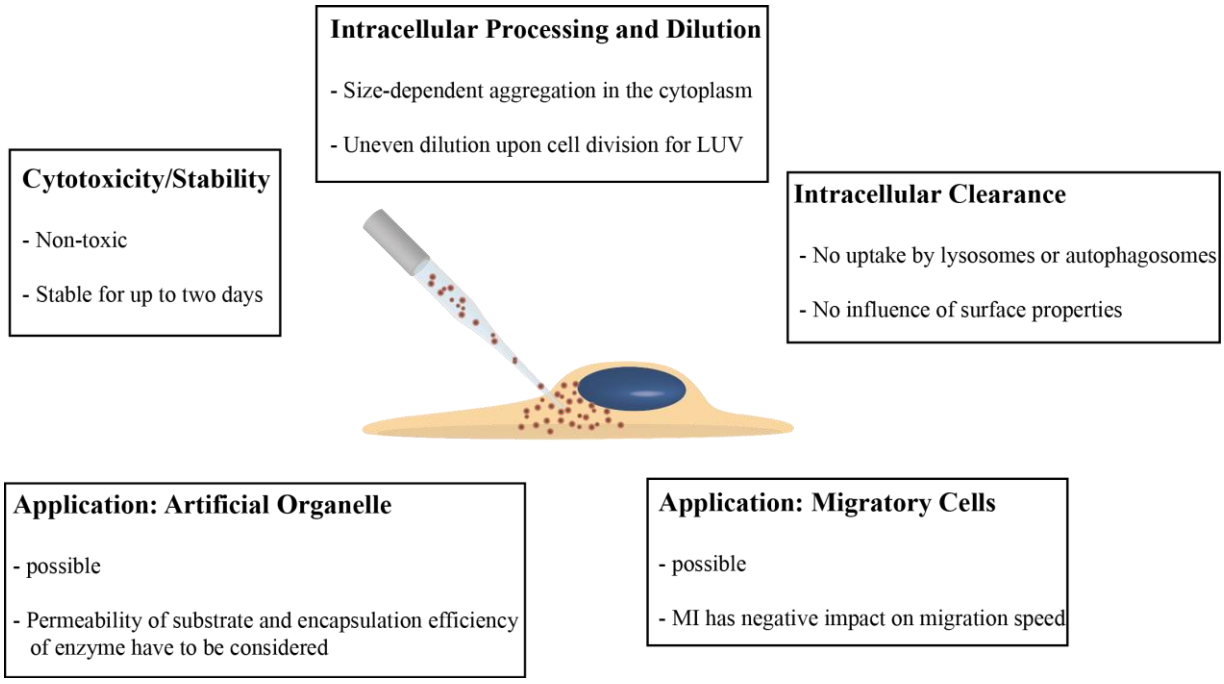

Figure 5.1 Main findings of this thesis.

These initial experiments showed that it was possible to introduce artificial vesicles in live cells *via* MI and that they could remain intact inside the cells for at least two days during which different aspects could be studied by fluorescence microscopy. Investigations on the intracellular processing of the injected liposomes were therefore carried out, revealing that over this period of two days the vesicles were not trapped inside of autophagosomes or lysosomes. This is a desirable outcome from a drug delivery perspective and a finding that differs from what has been reported for microinjected proteins and other NP like poly(styrene) beads [50, 53]. While interesting, it remains to be clarified why the liposomes were not detected and taken up by the autophagosomes. Although the shielding effect of PEGylation may contribute to the liposomes "invisibility" for the autophagic response [51], there were no differences in terms of colocalisation with autophagosomal or liposomal markers between the PEGylated and non-PEGylated liposomes. This would suggest that the reason for their stealth properties could be given by their lipid composition, which in resembling that of natural cell membranes, might have gone unnoticed by the cell's own machinery. Further investigations are needed to fully understand the underlying reasons for this positive outcome, which would be important in order to extend it to other drug delivery systems in the future.

Besides evading their capture by subcellular vesicles, the injected colloids were found to agglomerate in the cytosol following different patterns that appeared to correlate with some physicochemical properties. Whereas PEGylation did not seem to play a role, particle size was the main factor determining the differences in intracellular agglomeration. LUV agglomerated visibly after 8 hours of MI displaying a polarized distribution, while SUV did not segregate and instead remained more uniformly distributed in the cytosol. This could be connected to the architecture of the cytoplasm, which has been modelled as a "molecular sieve" of cytoskeletal components, as pointed out in Chapter 2, that form a meshwork through which molecules and nano-sized objects have to make their way [32]. In line

with the molecular sieve model, the larger particles would face more obstacles in their movement through the cytosol, accumulating in regions of lower sheer stress and ultimately adopting a polarized distribution. Interestingly, the agglomeration was reversible as the aggregates quickly redispersed in the cytosol upon injection of buffer, confirming that the liposomes did not coalesce. The colloids' size was found to affect not only their intracellular distribution in the cytosol but also their dilution pattern upon cell division. The dilution of material internalized by endocytosis had been previously studied in the context of cell division [174]. Our work revealed that SUV and QD were on average distributed evenly between the nascent daughter cells, whereas LUV were inherited unevenly by the cells of the new generation. This finding could have far-reaching implications for cell-based therapies. Although larger vesicles encapsulate larger amounts of cargo, they might entail difficulties when ensuring that the injected cells carry similar loads of material after their expansion for cell-based therapies. Further studies should pursue the size cut-off at which the dilution pattern upon cell division might become uneven.

In a second part of our study, we explored possible applications of liposomes delivered intracellularly by MI. We produced enzyme-encapsulating liposomes and showed that these exhibited catalytic activity inside the cells upon injection. Although a model enzyme was used for this proof-of-concept experiments, the study may be viewed as a first step towards the introduction of artificial organelles into cell by MI instead of co-incubation [68]. During the development of this system, we identified several crucial points that have to be addressed, like the low encapsulation efficiency of the enzyme in the liposomes, and the need for cell-permeable substrates that can be used to report on the catalytic activity of the enzyme after MI. Follow-up studies should address these points either by inserting channels into the liposomes membranes [68] or by changing the encapsulation method to for instance reverse phase evaporation [233].

Regarding the potential application of the developed liposomes for cell-based therapies, we found that the injected vesicles had inhibitory effects on the migratory properties of DC. In fact, the injection procedure itself inhibited cell migration, since similar results were obtained with injections of buffer. It is unclear if and to what extent these findings could affect potential *in vivo* experiments where the injected cells would be used as Trojan horses to deliver their cargo to the site of inflammation. The impact of MI on migration speed will need to be addressed in future studies to determine for instance if there is an injection volume that would not hamper cell migration. Alternatively, different approaches to manipulate the cells will need to be explored, such as injecting them with magnetic particles and actively directing their movement towards chosen sites [234]. This has been shown for natural killer cells (NK), which were labelled with Ab-bound magnetic beads and directed with an external magnet to tumor cells *in vitro*.

The introduction of a functional artificial organelle in migratory cells could open up new possibilities in drug delivery. For instance, enzyme-directed prodrug therapy could be implemented. In this concept, enzymes are either bound to polymers [235] or liposomes [236] to enhance half-life and accumulation in the tumor, or expressed by cells of the tumor tissue or migratory cells [237, 238]. Afterwards, non-toxic prodrugs, which are distributed within the whole body, get cleaved preferentially at the tumor site, where the corresponding enzymes are present. With the MI platform, it would be possible to harness the properties of migratory cells (or magnetically labeled cells) and combine them with liposome-encapsulated prodrug-converting enzymes (Fig. 5.2). These cells could be directed to the inflammation or tumor sites, activating the prodrug on site. Still, certain obstacles which we described in this thesis have to be overcome. The prodrug has to be carefully chosen in terms of cell and liposome permeability, and the low throughput of MI has to be taken into account.

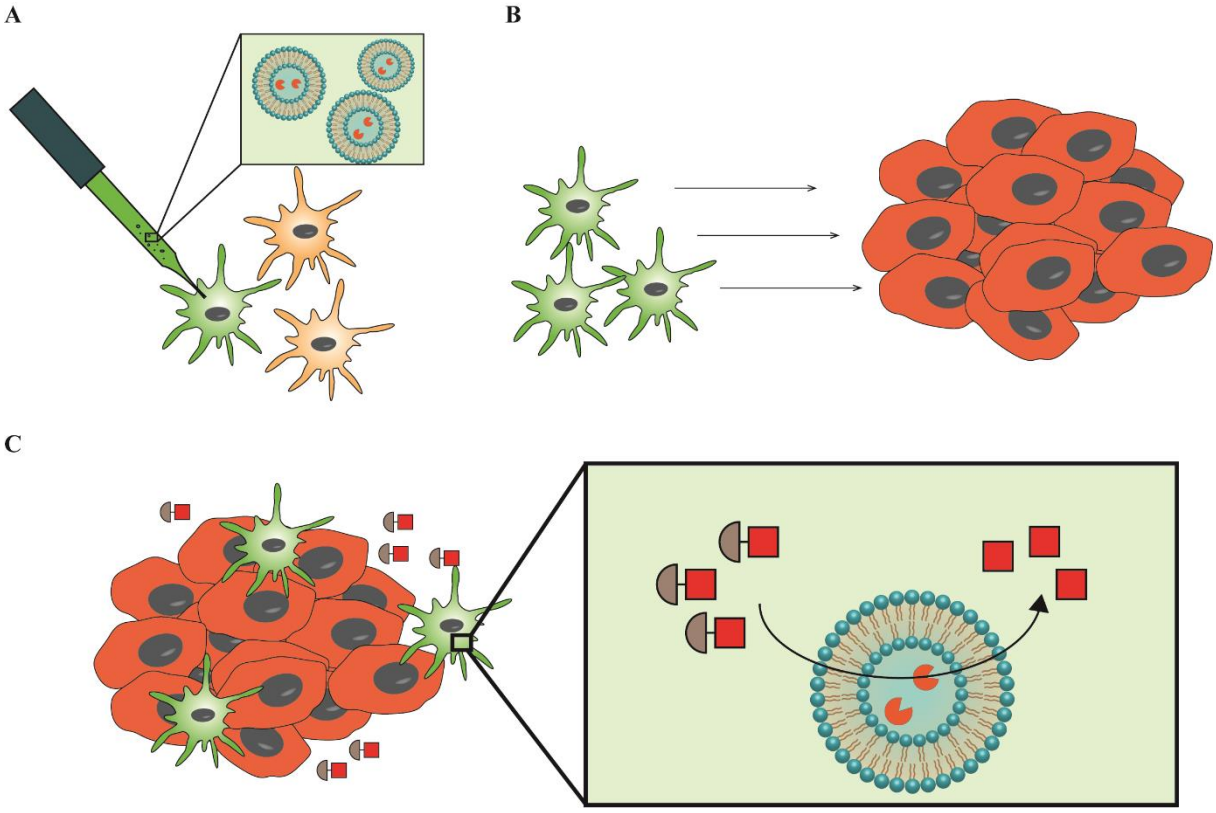

Figure 5.2 Possible application of MI of liposomes. A, Migratory cells (mesenchymal stem cells, T cells, DC (serving as example in this cartoon)) are injected with liposomes encapsulating a prodrug-converting enzyme. B, injected cells migrating towards tumor-sites due to chemotactic attraction. C, migratory cells invading the tumor and converting the non-toxic prodrug into its active form (red squares).

Furthermore, we attempted to use thermosensitive liposomes as an example of controlled release system that could be introduced in cells by MI and triggered externally by temperature increase. In this system, liposomes encapsulating ABC buffer would produce CO_2 bubbles upon heating, releasing their cargo due to transient cavitation. Although it was not possible to reproduce the system following the published protocols -which were cited in numerous follow-up publications by the same group- the successive attempts led us to identify the reasons for the system's irreproducibility. Several flaws were identified in the protocol and were confirmed experimentally, both in our facilities and in the laboratory where the system was originally developed. While our work with these allegedly thermosensitive liposomes did not lead to the interesting application of our fundamental findings that we envisaged, the conclusions published in the resulting communication to the corresponding journal will hopefully raise the attention about the limitations of this thermoresponsive system. For future studies, other better-established stimuli-responsive systems like those based on lysolipids or thermosensitive polymers should be employed.

In summary, we have established a new platform for modifying cells with artificial organelle-like vesicles that can be loaded with catalytically active enzymes and exhibit biological activity inside the cell. Given the presented versatility of our approach, we believe it will find widespread use in the scientific community in the coming years.

Appendix

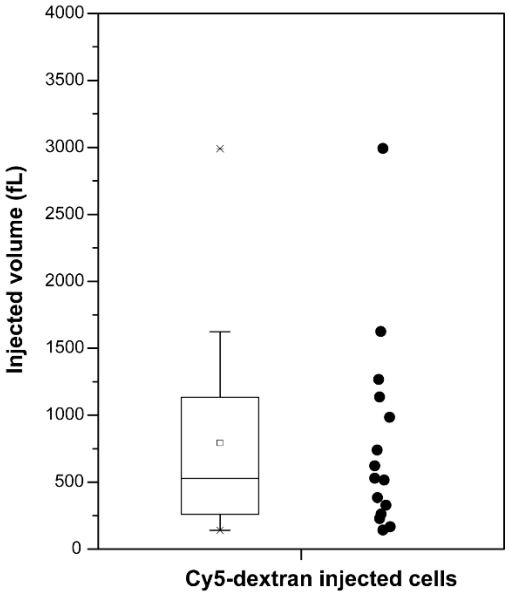

Figure A3.1 Quantification of the injected volume per cell. Box plot shows standard deviation (mean = 793 fL) and 25 and 75 percentiles of the volume of Cy5-dextran injected into HeLa cells. Dot plot shows individual measurements (n = 11). The injection volume was determined based on previously described methods [23].

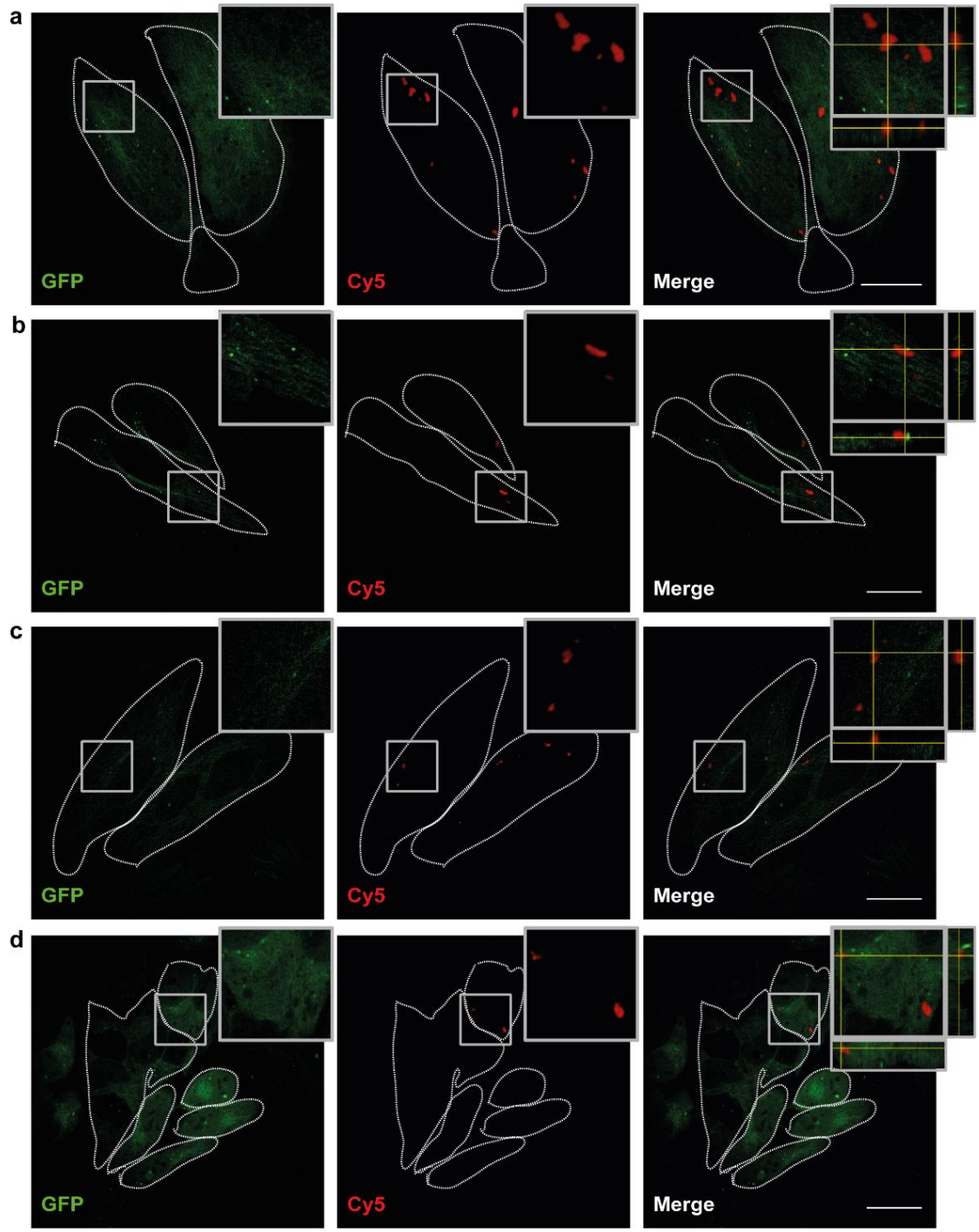

Figure A3.2 Absence of colocalization between the autophagosomes and LUV regardless of PEGylation state. (a-b) DPPC LUV (Cy5) 24 and 48 h after injection, respectively. (c-d) DPPC-PEG LUV 24 and 48 h after injection. Scale bar 25 µm. Autophagosomes were stained with LC3-GFP. White dotted lines indicate the perimeter of individual cells. Representative images of 18-23 images obtained during 3 independent experiments are shown.

Figure A3.3 Absence of colocalization between the lysosomes and LUV regardless of PEGylation state. (a-b) DPPC LUV (Cy5) 24 and 48 h after injection, respectively. (c-d) DPPC-PEG LUV 24 and 48 h after injection. Scale bar 25 μm. Lysosomes were stained with LAMP1-GFP. White dotted lines indicate the perimeter of individual cells. Representative images from 16-23 images obtained during 3 independent experiments are shown.

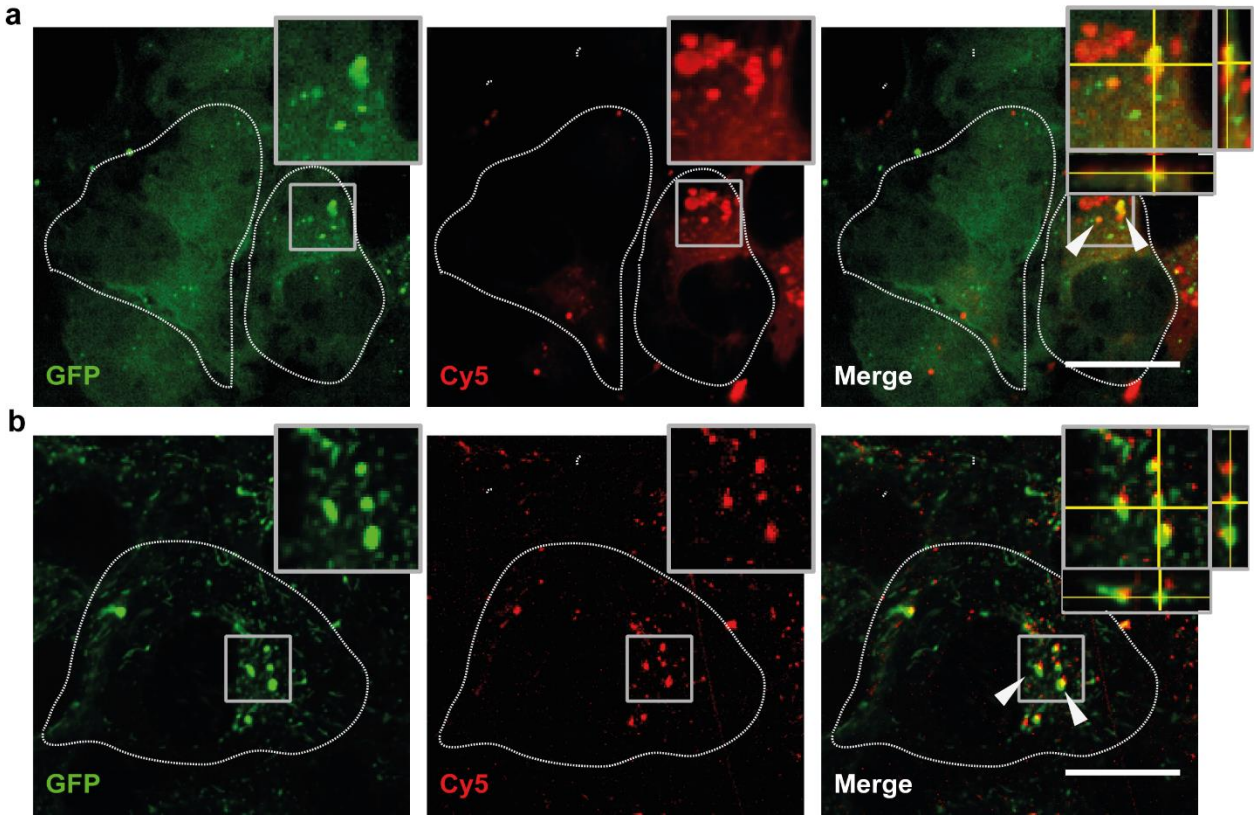

Figure A3.4 Positive controls for colocalization with autophagosomes and lysosomes. (a) DOTAP liposomes (Cy5) incubated for 2 h and internalized by HeLa-LC3 cells overexpressing the autophagosomes marker LC3-GFP. Scale bar 20 µm. White dotted lines indicate the perimeter of individual cells. White arrowheads indicate colocalization between the Cy5-labelled DOTAP liposomes and LC3-GFP. Representative images of 23 images obtained during 3 independent experiments are shown. (b) DPPC LUV internalized by HeLa cells upon 4 h incubation and imaged 24 h later. Scale bar 20 µm. Lysosomes were stained with the lysosomal marker LAMP1-GFP. White dotted lines indicate the perimeter of individual cells. White arrowheads indicate colocalization between the DPPC LUV and LAMP1-GFP. Representative images from 41 images obtained during 3 independent experiments are shown.

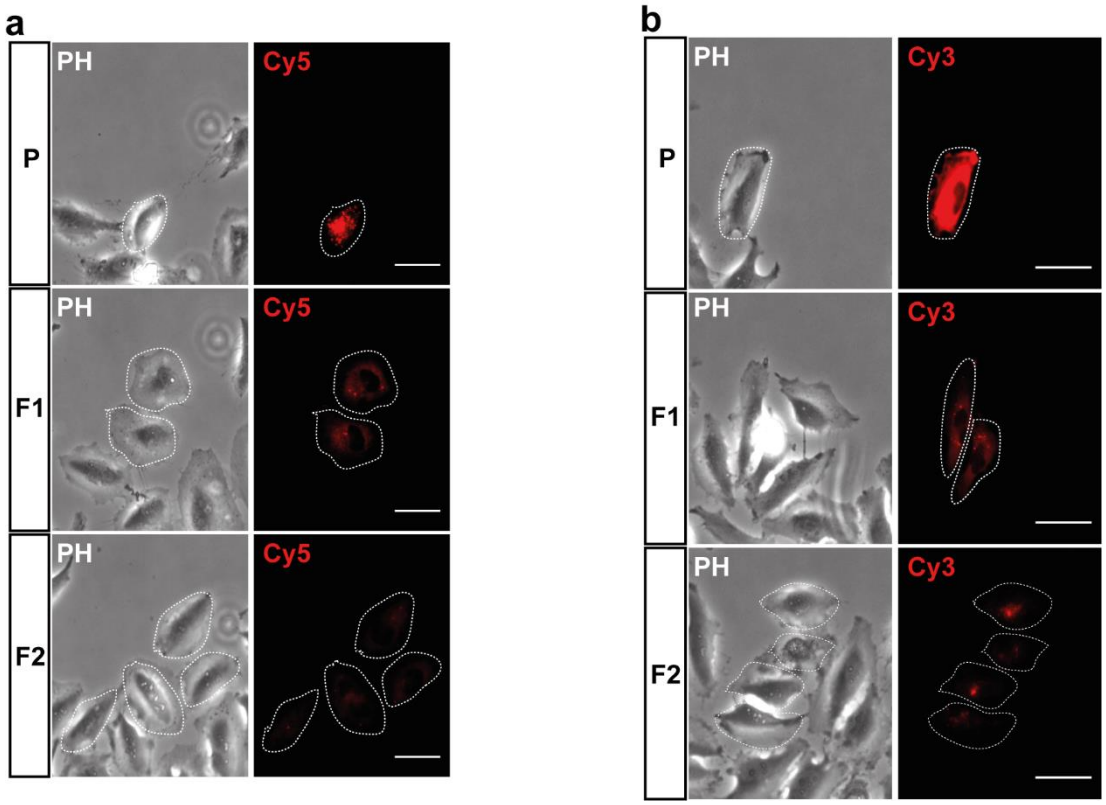

Figure A3.5 Dilution of injected SUV and QD during cell cycle progression. (a) Microscopy images of P, F1 and F2 generations of cells injected with SUV (Cy5). Scale bar 50 µm. White dotted lines indicate the perimeter of individual cells. A representative image from 24 images obtained during 3 independent experiments is shown. (b) Microscopy images of P, F1 and F2 generations of cells injected with QD (Cy3). Scale bar 50 µm. White dotted lines indicate the perimeter of individual cells. A representative image from 24 images obtained during 3 independent experiments is shown.

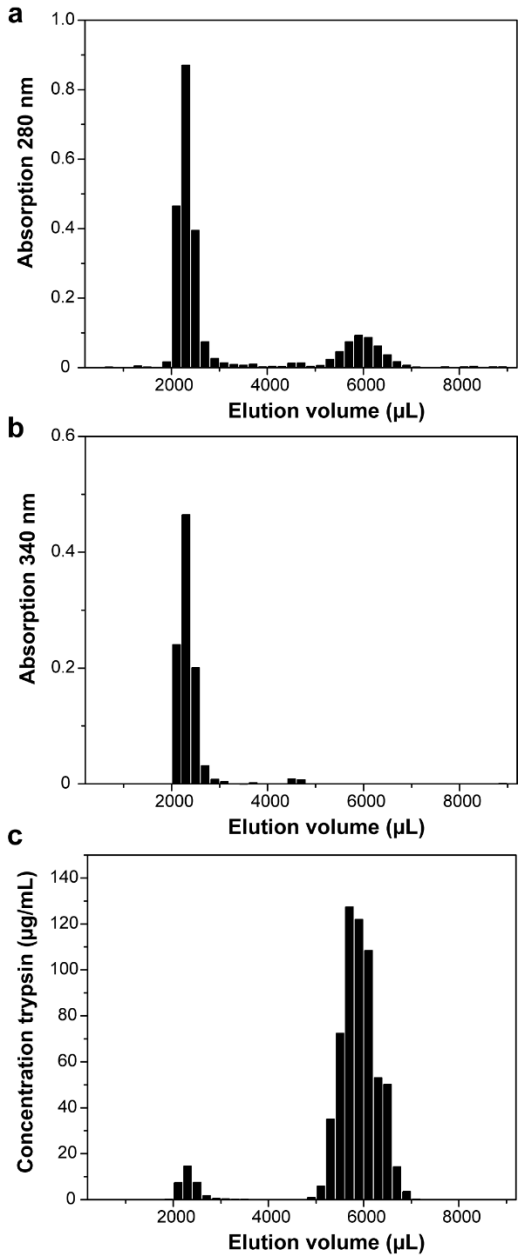

Figure A3.6 Purification of trypsin-encapsulating LUV. (a-b) UV absorption at 280 nm (a) and 340 nm (b) of the eluted fractions obtained during the purification of the trypsin-encapsulating LUV. (c) Fractions' enzyme content, calculated based on enzymatic activity measurements.

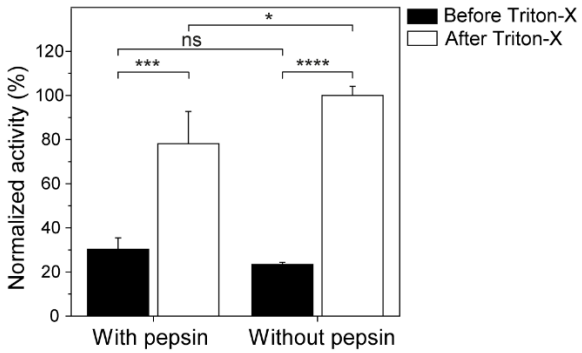

Figure A3.7 Absence of residual surface-bound trypsin enzyme in trypsin-encapsulating LUV. Enzymatic activity measurements performed on trypsin-encapsulating LUV incubated with or without pepsin to digest potential surface-bound trypsin, and before or after treatment with Triton X-100 to induce cargo release. Mean ± SD (n = 3). *p = 0.042, ***p < 0.001, ****p < 0.0001, ns = not significant.

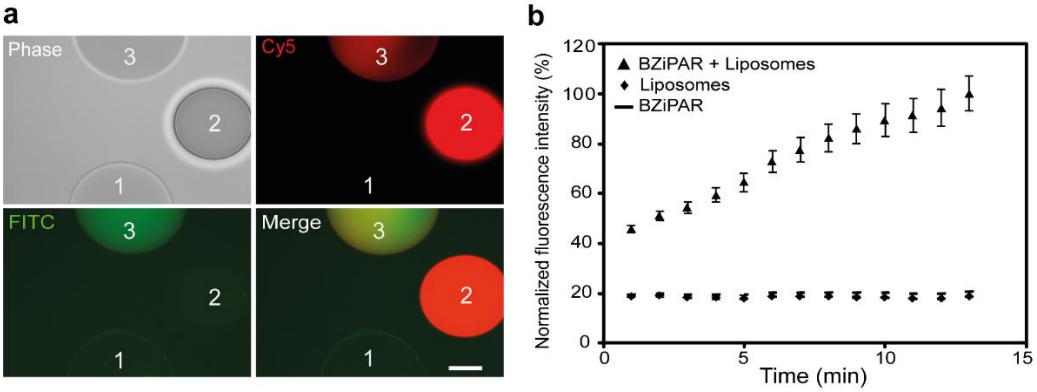

Figure A3.8 Validation of the enzymatic activity assay used to evaluate liposome-encapsulated trypsin. (a) Epifluorescence microscopy images of high viscosity silicon oil injected with droplets of BZiPAR substrate alone (1), DiD-labelled trypsin-encapsulating LUV (2) or a combination of the two (3). Scale bar 50 µm. A representative image from 6 images acquired during 3 independent experiments is shown. (b) Fluorescence intensity quantification of the droplets shown in a. Mean ± SD (n = 3).

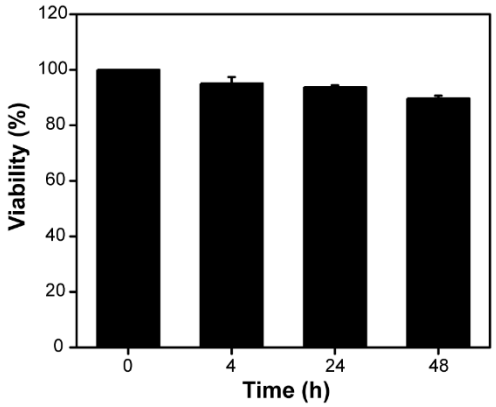

Figure A3.9 Cell viability upon injection of LUV encapsulating acidic buffer. Values were normalized for total injected cells at time 0 (mean + SD, n = 302 in 3 independent experiments).

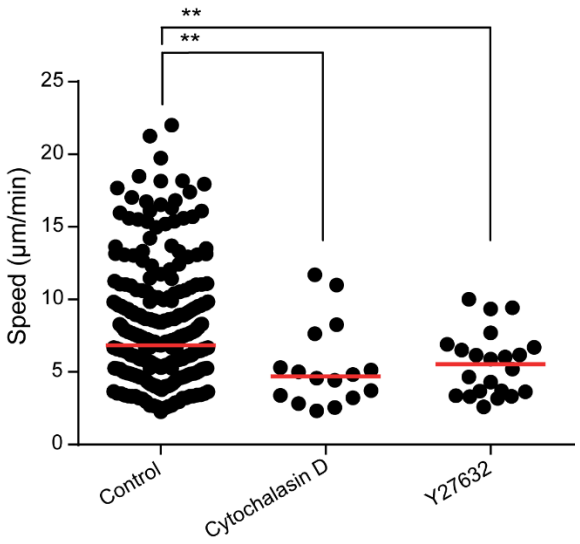

Figure A3.10 Positive controls for migration speed impairment. Analysis of the migratory speed of DC treated with the actin inhibitor cytochalasin D or the ROCK inhibitor Y27632, compared to untreated DC (Control). Red lines indicate the median values. Pooled data from 3 independent experiments are shown. A Mann-Whitney-U test was applied, n = 16 – 22 for treated cells (**p-value < 0.01).

Table A3.1 Sizes of liposomes after extrusion measured by DLS. For each sample, at least three independent batches were prepared and analyzed. SD represents the standard deviation among the three batches. Diameter and polydispersity index (PDI) are shown.

Sample name	Liposome formulation (mol%)	Diameter (nm)	PDI (±SD)
DPPC-PEG LUV	DPPC:CHOL:DSPE-PEG (50:45:5)	124 ± 6	0.08 ± 0.03
DPPC LUV	DPPC:CHOL (55:45)	135 ± 9	0.07 ± 0.02
DOPC-PEG LUV	DOPC:CHOL:DSPE-PEG (50:45:5)	120 ± 5	0.10 ± 0.06
DOPC LUV	DOPC:CHOL (55:45)	137 ± 18	0.12± 0.08
SA LUV	DPPC:CHOL:SA (40:50:10)	129 ± 5	0.08 ± 0.02
Trypsin-loaded LUV	Trypsin-loaded DOPC:CHOL (90:10)	130 ± 0.4	0.07 ± 0.01
DPPC-PEG SUV	DPPC:CHOL:DSPE-PEG (50:45:5)	78 ± 2	0.12 ± 0.01
DPPC SUV	DPPC:CHOL (55:45)	75 ± 1	0.05 ± 0.01

Table A3.2 Encapsulation efficiency of trypsin in liposomes. The encapsulation efficiency percentage of the trypsin-containing liposomes was calculated dividing the encapsulated amount in ng (determined *via* enzymatic activity measurements with the BZiPAR assay) over the amount of trypsin used during the encapsulation procedure (300 µg).

	Encapsulated trypsin (ng)	**Encapsulation efficiency (%)**
Batch 1	8115	2.71
Batch 2	10659	3.55
Batch 3	11914	3.97
Mean (±SD)		3.41 ± 0.53

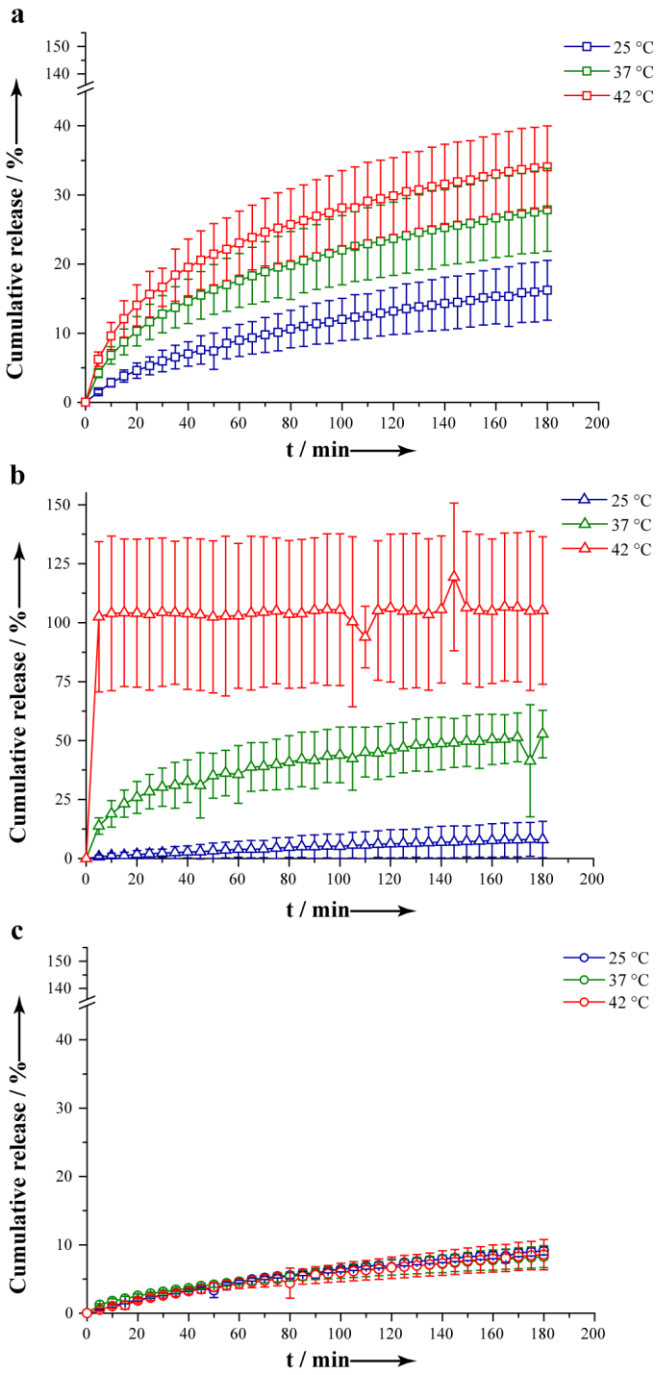

Figure A4.1 Cumulative release of encapsulated CF as a function of time. The release of CF from (a) ABC, (b) Positive control and (c) Negative control liposomes was measured at 25, 37 and 42 °C over a period of 180 min (mean ± SD, n = 3). CF was encapsulated at 40 mM according to the method described for calcein in the methods of Chapter 4.

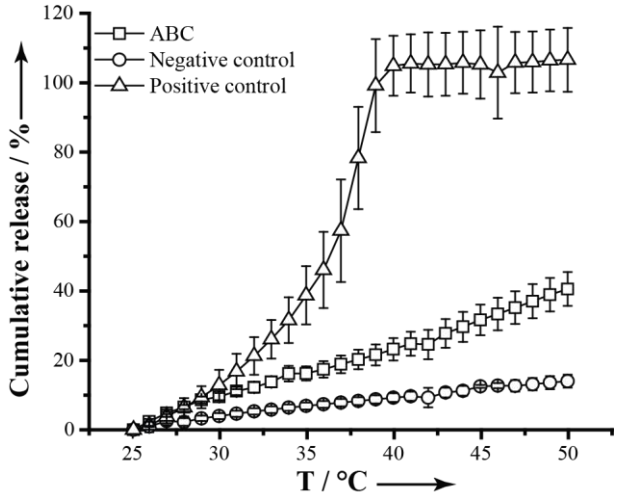

Figure A4.2 Cumulative release of encapsulated CF as a function of temperature. Fluorescence intensity was measured as temperature was increased 0.1 °C/min. Data were normalized to the fluorescence obtained after incubating the samples with Triton X–100, which was considered as 100% release (mean ± SD, n = 3).

List of Abbreviations

^{3}H-dTTP	^{3}H –(2'-deoxythymidine-5'-triphosphate)
Ab	Antibodies
ABC	Ammonium bicarbonate
AEBSF	4-(2-aminoethyl)benzenesulfonyl fluoride hydrochloride
AFM	Atomic force microscopy
ANOVA	Analysis of variance
ATP	Adenosine triphosphate
Au NP	Gold nanoparticles
BSA	Bovine serum albumin
BZiPar	Rhodamine 110, bis-(Cbz-L-isoleucyl-L-prolyl-L-arginin amide), dihydrochloride
CF	Carboxyfluorescein
CHOL	Cholesterol
COP	Vesicle associated coat protein
CRISPR/Cas9	Clustered regularly interspaced short palindromic repeats
DC	Dendritic cells
DiD	1,1'-dioctadecyl-3,3,3',3'-tetramethylindodicarbocyanine, 4-chlorobenzenesulfonate salt

DLS	Dynamic light scattering
DMEM	Dulbecco's modified eagle medium
DOPC	1,2-dioleoyl-*sn*-glycero-3-phosphocholine
DOTAP	1,2-dioleoyl-3-trimethylammonium-propane (chloride salt)
DOTMA	1,2-di-O-octadecenyl-3-trimethylammonium-propane (chloride salt)
DPPC	1,2-dipalmitoyl-*sn*-glycero-3-phosphocholine
DPX	p-xylene-*bis*-pyridinium bromide
DSPE-PEG_{2000}	1,2-distearoyl-*sn*-glycero-3-phosphoethanolamine-N-[methoxy(polyethylene glycol)-2000] (ammonium salt)
EBV	Epstein Barr virus
ESCRT	Endosomal sorting complexes required for transport
EsR	Estrogen receptor
FBS	Fetal bovine serum
FISH	Fluorescence *in situ* hybridisation
FRAP	Fluorescence recovery after photobleaching
FRET	Foerster Resonance Energy Transfer
GFP	Green fluorescent protein
GM-CSF	Granulocyte macrophage colony-stimulating factor
Hela	Human cervical cancer cells
HEPES	4-(2-hydroxyethyl)-1-piperazineethanesulfonic acid
HPTS	8-hydroxypyrene-1,3,6-trisulfonic acid (trisodium salt)
HRP	Horseradish peroxidase
Hrs	Hepatocyte growth factor regulated tyrosine kinase substrate
HSPC	Hydrogenated soybean phosphatidylcholine

imLECs	Immortalized mouse lymphatic endothelial cells
IVF	*In-vitro* fertilisation
LAMP-1	lysosomal associated membrane protein
LC3	microtubule-associated protein 1A/1B-light chain
LCF	Light chain ferritin
LCST	Lower critical solution temperature
LUV	Large unilamellar vesicles
MI	Microinjection
MLS	Mitchondrial localization sequence
MSPC	1-stearoyl-2-hydroxy-*sn*-glycero-3-phosphocholine
MW	Mass weight
NLS	Nuclear localization signal
NP	Nanoparticles
NPC	Nuclear pore complex
NSC	Neural stem cells
ON	Oligonucleotides
PBS	Phosphate buffered saline
PDI	Polydispersity index
PEG	Poly(ethylene) glycol
PEI	Poly(ethyleneimine)
PI	Propidium iodide
PLL	Poly(lysine)
Protac	Proteolysis of targeting chimeric molecule

QD	Quantum dots
ROCK	Rho-associated protein kinase
ROI	Region of interest
SA	Stearylamine
SUV	Small unilamellar vesicles
TRITC	Tetramethylrhodamineisothiocyanate
VSV-G	Vesicular stomatitis virus glycoprotein
YFP	Yellow fluorescent protein

Curriculum Vitae

Peter Gerhard Tiefenboeck

German citizen

born in Pegnitz on December 6th 1987

Schwamendingenstrasse 56

8050 Zürich

Education

03/2013 – 07/2017	**Graduate Studies** Swiss Federal Institute of Technology Zurich (ETH) Thesis Title: 'Microinjection of liposomal carriers into single cells' Supervisor: Prof. Jean-Christophe Leroux
Since 12/2012	**Approbation** as licensed pharmacist in Germany
12/2012	**3. Federal State Exam of Pharmaceutical Sciences** Regierung von Oberbayern
09/2009 – 10/2011	**2. Federal State Exam of Pharmaceutical Sciences** Friedrich-Alexander-University Erlangen Nuremberg (FAU) Department of Pharmaceutical Sciences
10/2007 – 08/2009	**1. Federal State Exam of Pharmaceutical Sciences** Friedrich-Alexander-University Erlangen Nuremberg (FAU) Department of Pharmaceutical Sciences

Research Activities and Work Experience

12/2012 – 02/2013	**Internship as Pharmacist** Stadtapotheke Pottenstein (Germany)
05/2012 – 10/2012	**Internship as pharmaceutical trainee** (Pharmazeut im Praktikum) Ohm Apotheke Erlangen
10/2011 – 04/2012	**Institute of Pharmaceutical Sciences, University of Iceland** Internship in research Title of project: 'Investigation of the marine bryozoan *Flustra foliacea*'

Awards and Scholarships

July 2016	Poster Prize 'Biointerfaces International Conference'
May 2016	Chemistry Travel Award
February 2012	Ludwig-Knorr-Price of the *Gustav-Adolf und Erika Dornhecker Stiftung*
October 2009	Price of the *Dr. August und Dr. Anni Lesmüller –Stiftung* for exceptional achievement in the studies
2007-2011	Scholar of the Max Weber-Program Bayern

Scientific Contributions

Publications

P. Tiefenboeck, J. A. Kim, F. Trunk, J.-C. Leroux, Comment on "A Liposomal System Capable of Generating CO_2 Bubbles to Induce Transient Cavitation, Lysosomal Rupturing and Cell Necrosis", Angew. Chem. Int. Ed., DOI: 10.1002/anie.201703740 and 10.1002/ange.201703740

P. Tiefenboeck, J. A. Kim, F. Trunk, T. Eicher, E. Russo, A. Teijeira, C. Halin, J.-C. Leroux, Microinjection for the *ex vivo* modification of cells with functional artificial organelles. *In revision.*

S. Pawar, R. Ungricht, **P. Tiefenboeck**, J.-C. Leroux, U. Kutay, Efficient protein targeting to the inner nuclear membrane requires Atlastin-dependent maintenance of ER topology. *In revision.*

Oral presentations

P. Tiefenboeck, J. A. Kim, F. Trunk, T. Eicher, J.-C. Leroux. Microinjection of liposomes: A new platform for cell modification with functional artificial organelles. Fudan University, Shanghai, China, March 2017.

P. Tiefenboeck, J. A. Kim, J.-C. Leroux. A novel cell engineering platform based on microinjection of enzyme-loaded liposomes. *Globalization of Pharmaceutics Education Network Conference*, Lawrence, KS, USA, November 2016.

P. Tiefenboeck, J. A. Kim, J.-C. Leroux. Microinjection of liposomal carriers into single cells. *Swiss Galenic Meeting*, Zurich, Switzerland, September 2016.

Poster presentations

P. Tiefenboeck, J. A. Kim, J.-C. Leroux. Modifying cells *via* microinjection of liposomes carrying biologically active cargo. *Swiss Pharma Science Day*, Bern, Switzerland, August 2016.

P. Tiefenboeck, J. A. Kim, J.-C. Leroux. Microinjection of liposomes – A novel way to modify cells. *Biointerfaces International Conference*, Zurich, Switzerland, August 2016.

P. Tiefenboeck, J. A. Kim, P. Luciani, J.-C. Leroux. Delivery of liposomes to cells *via* microinjection. *Swiss Pharma Science Day*, Bern, Switzerland, August 2015.

P. Tiefenboeck, J. A. Kim, P. Luciani, J.-C. Leroux. Microinjection of liposomes in living cells. *Materials and Processes Graduate Symposium*, Zurich, Switzerland, June 2015.

Acknowledgements

This work would not have been possible without the help of many people, who supported and motivated me throughout the last years.

My sincerest thanks go to my thesis supervisor, prof. Jean-Christophe Leroux. He gave me the opportunity to work on this exciting project and granted me the freedom to develop and fill the concept with my own ideas. Nevertheless, he was right behind me, when I or my data were challenged.

I would also like to thank prof. Cornelia Halin, not only for agreeing to be my coexaminer, yet also for the fruitful collaboration I had with her group and the deep discussions about our data.

I am indebted to all the former and current members of the Drug formulation and Delivery' group for creating an almost-everyday pleasant atmosphere.

Especially, I would like to thank Rea Deborah Signorell and Anna Pratsinis. You two were always open for discussions about scientific and many other issues and steadily kept a strong attitude about what proper science is. I am thankful for your friendship and constant support.

Big thanks also to Dr. Jong Ah Kim for helping me to order my sometimes woolly thoughts in organizing data and manuscripts as well as the English proofreading and editing of my work.

Thank you very much prof. Bruno Gander, for organizing every year a very nice and interesting Galenik Praktikum and for the trust in me, handling expensive tableting presses.

As well, I would like to thank all the former members of the group, with whom I was allowed to work. These are Drs. Arnaud Felber, Vincent Forster, Mattias Ivarsson, Kathrin Fuhrmann, Mi Liu, Lorine Brülisauer, Yuhui Gong, Jessica Schulz, Athanasia Dasargyri, Elena Moroz, Anna Polomska, Soo Hyeon Lee, Ander Estella, Saima Sadaf, Davide Brambilla, Valentina Agostoni, Giovanna Giacalone, Paola Luciani, Bastien Castagner, Tao Sun, Xiangang Huang, both of them I could visit in their home country, Maurizio Roveri and Diana Andina.

Many thanks go to the current members of the lab, Antonia Schantl, Aaron Schmidt, Anna Kletzmayr, Michael Burger, Sofia Bisso, Britta Hettich, Dr. Kun Liang, Dr. Irene Pereira des Sousa, Dr. Yinyin Bao, Dr. Sarah Kindgen and of course Simon Matoori, for not only being very kind lab and/or office members but also for the joyful time we spent outside of ETH, be it at the opera or in foreign countries.

To finish with my lab, I would like to thank all the administrative people I got to highly appreciate during my stay, especially Virginie Rusca and Nadine Häni-Doelly for always being helpful with all kinds of bureaucratical stuff and of course I am thanking Monica Langfritz for keeping my computer alive during all these years and sustaining my jokes.

Furthermore, big thanks to all my project and master students, Tamara Eicher, Ferdinand Trunk and Jasmin Cadalbert. You were always motivated in your work and helped me a lot in establishing crucial parts of my research. I appreciated also the time spending with you outside of the lab together with Carmen Egger, Jiawen Xiao, Simone Carmone and Stefanie Zürcher.

Besides the people of my lab, I would also like to thank my collaborators with whom I had the privilege to work with in the last years. Special thanks go to David Vukovic, with whom I spent many evenings at the microinjector discussing about fundamentals and nonsense, as well as Sumit Pawar for giving me an insight into very sophisticated molecular biology research. Many thanks for the dendritic cell studies go to Erica Russo and Alvaro Teijeira for having patience with me as a non-immunologist. Also, I would like to thank Anastasia Spyrogianni for the cool nanophosphor project and Ryan Dragoman. Besides, I thank the microscopy facility of ETH (ScopeM) for the constant support.

Finally, I am deeply indebted to my family and friends, who always supported me during good and tough times. My warmest thanks go to my parents, Anne and Peter, as well as my brother, Stefan, who frequently managed to bring me back from the ivory tower of science and let me enjoy the ‚real' life.

References

[1] M.P. Stewart, A. Sharei, X. Ding, G. Sahay, R. Langer, K.F. Jensen, In vitro and ex vivo strategies for intracellular delivery, Nature, 538 (2016) 183-192.

[2] J. Huotari, A. Helenius, Endosome maturation, EMBO Journal, 30 (2011) 3481-3500.

[3] R. Tang, C.S. Kim, D.J. Solfiell, S. Rana, R. Mout, E.M. Velazquez-Delgado, A. Chompoosor, Y. Jeong, B. Yan, Z.J. Zhu, C. Kim, J.A. Hardy, V.M. Rotello, Direct delivery of functional proteins and enzymes to the cytosol using nanoparticle-stabilized nanocapsules, ACS Nano, 7 (2013) 6667-6673.

[4] D.P. Morales, G.B. Braun, A. Pallaoro, R. Chen, X. Huang, J.A. Zasadzinski, N.O. Reich, Targeted intracellular delivery of proteins with spatial and temporal control, Mol. Pharm., 12 (2015) 600-609.

[5] E. Neumann, M. Schaefer-Ridder, Y. Wang, P.H. Hofschneider, Gene transfer into mouse lyoma cells by electroporation in high electric fields, EMBO J., 1 (1982) 841-845.

[6] A. Sharei, J. Zoldan, A. Adamo, W.Y. Sim, N. Cho, E. Jackson, S. Mao, S. Schneider, M.J. Han, A. Lytton-Jean, P.A. Basto, S. Jhunjhunwala, J. Lee, D.A. Heller, J.W. Kang, G.C. Hartoularos, K.S. Kim, D.G. Anderson, R. Langer, K.F. Jensen, A vector-free microfluidic platform for intracellular delivery, Proc. Natl. Acad. Sci. U. S. A., 110 (2013) 2082-2087.

[7] Y. Zhang, Single-cell microinjection technologies, Methods Mol. Biol., 853 (2012) 169-176.

[8] S. Van Meirvenne, L. Straetman, C. Heirman, M. Dullaers, C. De Greef, V. Van Tendeloo, K. Thielemans, Efficient genetic modification of murine dendritic cells by electroporation with mRNA, Cancer Gene Ther., 9 (2002) 787-797.

[9] A. Bolhassani, A. Khavari, Z. Orafa, Electroporation – Advantages and Drawbacks for Delivery of Drug, Gene and Vaccine, in: A.D. Sezer (Ed.) Application of Nanotechnology in Drug Delivery, InTech, Rijeka, 2014, pp. 369-398.

[10] P.E. Boukany, A. Morss, W.C. Liao, B. Henslee, H. Jung, X. Zhang, B. Yu, X. Wang, Y. Wu, L. Li, K. Gao, X. Hu, X. Zhao, O. Hemminger, W. Lu, G.P. Lafyatis, L.J. Lee, Nanochannel electroporation delivers precise amounts of biomolecules into living cells, Nat. Nanotechnol., 6 (2011) 747-754.

[11] J. Lee, A. Sharei, W.Y. Sim, A. Adamo, R. Langer, K.F. Jensen, M.G. Bawendi, Nonendocytic delivery of functional engineered nanoparticles into the cytoplasm of live cells using a novel, high-throughput microfluidic device, Nano Lett., 12 (2012) 6322-6327.

[12] M.A. Barber, A Technic for the Inoculation of Bacteria and Other Substances into Living Cells, J. Infect. Dis., 8 (1911) 348-360.

[13] E.G. Diacumakos, S. Holland, P. Pecora, A microsurgical methodology for human cells in vitro: evolution and applications, Proc. Natl. Acad. Sci. U. S. A., 65 (1970) 911-918.

[14] A. Graessmann, M. Graessmann, Über die Bildung von Melanin in Muskelzellen nach der direkten Übertragung von RNA aus HARDING-PASSEY-Melanomzellen, Hoppe Seylers Z. Physiol. Chem., 352 (1971) 527-532.

[15] W. Ansorge, Improved system for capillary microinjection into living cells, Exp. Cell Res., 140 (1982) 31-37.

[16] Y. Zhang, L.C. Yu, Microinjection as a tool of mechanical delivery, Curr. Opin. Biotechnol., 19 (2008) 506-510.

[17] Y. Zhang, A.C. LeBlanc, Microinjections to Study the Specific Role of Proapoptotic Proteins in Neurons, in: A.C. LeBlanc (Ed.) Apoptosis Techniques and Protocols, Springer New York, Totowa, NJ, 2002, pp. 83-106.

[18] B.R. Davis, J. Yannariello-Brown, N.L. Prokopishyn, Z. Luo, M.R. Smith, J. Wang, N.D. Victor Carsrud, D.B. Brown, Glass needle-mediated microinjection of macromolecules and transgenes into primary human blood stem/progenitor cells, Blood, 95 (2000) 437-444.

[19] A. Graessmann, H. Wolf, G.W. Bornkamm, Expression of Epstein-Barr virus genes in different cell types after microinjection of viral DNA, Proc. Natl. Acad. Sci. U. S. A., 77 (1980) 433-436.

[20] C. Ross, Intracytoplasmic sperm injection (ICSI), in: K. Coward, D. Wells (Eds.) Textbook of Clinical Embryology, Cambridge University Press, Cambridge, 2013, pp. 262-274.

[21] R.E. Hammer, V.G. Pursel, C.E. Rexroad, R.J. Wall, D.J. Bolt, K.M. Ebert, R.D. Palmiter, R.L. Brinster, Production of transgenic rabbits, sheep and pigs by microinjection, Nature, 315 (1985) 680-683.

[22] R.N. Cottle, C.M. Lee, D. Archer, G. Bao, Controlled delivery of beta-globin-targeting TALENs and CRISPR/Cas9 into mammalian cells for genome editing using microinjection, Sci. Rep., 5 (2015) 16031.

[23] G. Minaschek, J. Bereiterhahn, G. Bertholdt, Quantitation of the volume of liquid injected into cells by means of pressure, Exp. Cell Res., 183 (1989) 434-442.

[24] G.M. Lee, Measurement of volume injected into individual cells by quantitative fluorescence microscopy, J. Cell Sci., 94 (Pt 3) (1989) 443-447.

[25] M. Pagano, R. Pepperkok, F. Verde, W. Ansorge, G. Draetta, Cyclin A is required at two points in the human cell cycle, EMBO J., 11 (1992) 961-971.

[26] N.J.C. Lamb, A. Fernandez, Microinjection of antibodies into mammalian cells, in: Methods Enzymol., 1997, pp. 72-83.

[27] B. Honer, S. Citi, J. Kendrick-Jones, B.M. Jockush, Modulation of cellular morphology and locomotory activity by antibodies against myosin, J. Cell Biol., 107 (1988) 2181-2189.

[28] R. Pepperkok, J. Scheel, H. Horstmann, H.P. Hauri, G. Griffiths, T.E. Kreis, Beta-COP is essential for biosynthetic membrane transport from the endoplasmic reticulum to the Golgi complex in vivo, Cell, 74 (1993) 71-82.

[29] H.F. Paterson, A.J. Self, M.D. Garrett, I. Just, K. Aktories, A. Hall, Microinjection of recombinant p21rho induces rapid changes in cell morphology, J. Cell Biol., 111 (1990) 1001-1007.

[30] M.R. Capecchi, High efficiency transformation by direct microinjection of DNA into cultured mammalian cells, Cell, 22 (1980) 479-488.

[31] J.P. Clarenc, B. Lebleu, J.P. Leonetti, Characterization of the nuclear binding sites of oligodeoxyribonucleotides and their analogs, J. Biol. Chem., 268 (1993) 5600-5604.

[32] K. Luby-Phelps, Cytoarchitecture and physical properties of cytoplasm: volume, viscosity, diffusion, intracellular surface area, Int. Rev. Cytol., 192 (2000) 189-221.

[33] D. Lechardeur, A.S. Verkman, G.L. Lukacs, Intracellular routing of plasmid DNA during non-viral gene transfer, Adv. Drug Del. Rev., 57 (2005) 755-767.

[34] M.E. Dowty, P. Williams, G.F. Zhang, J.E. Hagstrom, J.A. Wolff, Plasmid DNA Entry into Postmitotic Nuclei of Primary Rat Myotubes, Proc. Natl. Acad. Sci. U. S. A., 92 (1995) 4572-4576.

[35] A. Meister, M. Gabi, P. Behr, P. Studer, J. Vörös, P. Niedermann, J. Bitterli, J. Polesel-Maris, M. Liley, H. Heinzelmann, T. Zambelli, FluidFM: Combining Atomic Force Microscopy and Nanofluidics in a Universal Liquid Delivery System for Single Cell Applications and Beyond, Nano Lett., 9 (2009) 2501-2507.

[36] O. Guillaume-Gentil, E. Potthoff, D. Ossola, P. Dörig, T. Zambelli, J.A. Vorholt, Force-Controlled Fluidic Injection into Single Cell Nuclei, Small, 9 (2013) 1904-1907.

[37] E. Taverna, C. Haffner, R. Pepperkok, W.B. Huttner, A new approach to manipulate the fate of single neural stem cells in tissue, Nat. Neurosci., 15 (2012) 329-337.

[38] G. Becattini, L.S. Mattos, D.G. Caldwell, A fully automated system for adherent cells microinjection, IEEE J. Biomed. Health Inform., 18 (2014) 83-93.

[39] W. Wang, Y. Sun, M. Zhang, R. Anderson, L. Langille, W. Chan, A system for high-speed microinjection of adherent cells, Rev. Sci. Instrum., 79 (2008) 104302.

[40] A. Adamo, K.F. Jensen, Microfluidic based single cell microinjection, Lab Chip, 8 (2008) 1258-1261.

[41] Y.T. Chow, S. Chen, C. Liu, C. Liu, L. Li, C.W.M. Kong, S.H. Cheng, R.A. Li, D. Sun, A High-Throughput Automated Microinjection System for Human Cells With Small Size, IEEE/ASME Trans. Mechatronics, 21 (2016) 838-850.

[42] K. Meller, Axoplasmic transport of horseradish peroxidase in single neurons of the dorsal root ganglion studied in vitro by microinjection, Cell Tissue Res., 270 (1992) 139-148.

[43] J.J.-C. Lin, J.R. Feramisco, Disruption of the in vivo distribution of the intermediate filaments in fibroblasts through the microinjection of a specific monoclonal antibody, Cell, 24 (1981) 185-193.

[44] L. Damalakiene, V. Karabanovas, S. Bagdonas, M. Valius, R. Rotomskis, Intracellular distribution of nontargeted quantum dots after natural uptake and microinjection, Int. J. Nanomedicine, 8 (2013) 555-568.

[45] S. Oliveira, I. van Rooy, O. Kranenburg, G. Storm, R.M. Schiffelers, Fusogenic peptides enhance endosomal escape improving siRNA-induced silencing of oncogenes, Int. J. Pharm., 331 (2007) 211-214.

[46] I. Richard, M. Thibault, G. De Crescenzo, M.D. Buschmann, M. Lavertu, Ionization behavior of chitosan and chitosan-DNA polyplexes indicate that chitosan has a similar capability to induce a proton-sponge effect as PEI, Biomacromolecules, 14 (2013) 1732-1740.

[47] D. Walczyk, F.B. Bombelli, M.P. Monopoli, I. Lynch, K.A. Dawson, What the Cell "Sees" in Bionanoscience, J. Am. Chem. Soc., 132 (2010) 5761-5768.

[48] A. Salvati, A.S. Pitek, M.P. Monopoli, K. Prapainop, F.B. Bombelli, D.R. Hristov, P.M. Kelly, C. Aberg, E. Mahon, K.A. Dawson, Transferrin-functionalized nanoparticles lose their targeting capabilities when a biomolecule corona adsorbs on the surface, Nat. Nanotechnol., 8 (2013) 137-143.

[49] J. Suh, K.L. Choy, S.K. Lai, J.S. Suk, B.C. Tang, S. Prabhu, J. Hanes, PEGylation of nanoparticles improves their cytoplasmic transport, Int. J. Nanomedicine, 2 (2007) 735-741.

[50] D.W. Stacey, V.G. Allfrey, Evidence for the autophagy of microinjected proteins in HeLA cells, J. Cell Biol., 75 (1977) 807-817.

[51] D. Lißе, C.P. Richter, C. Drees, O. Birkholz, C. You, E. Rampazzo, J. Piehler, Monofunctional Stealth Nanoparticle for Unbiased Single Molecule Tracking Inside Living Cells, Nano Lett., 14 (2014) 2189-2195.

[52] N. Symens, R. Walczak, J. Demeester, I. Mattaj, S.C. De Smedt, K. Remaut, Nuclear inclusion of nontargeted and chromatin-targeted polystyrene beads and plasmid DNA containing nanoparticles, Mol. Pharm., 8 (2011) 1757-1766.

[53] K. Remaut, V. Oorschot, K. Braeckmans, J. Klumperman, S.C. De Smedt, Lysosomal capturing of cytoplasmic injected nanoparticles by autophagy: an additional barrier to non viral gene delivery, J. Control. Release, 195 (2014) 29-36.

[54] N. Mizushima, Autophagy: process and function, Genes Dev., 21 (2007) 2861-2873.

[55] A. Akbarzadeh, R. Rezaei-Sadabady, S. Davaran, S.W. Joo, N. Zarghami, Y. Hanifehpour, M. Samiei, M. Kouhi, K. Nejati-Koshki, Liposome: classification, preparation, and applications, Nanoscale Res. Lett., 8 (2013) 102-102.

[56] O. Seksek, J. Biwersi, A.S. Verkman, Direct Measurement of trans-Golgi pH in Living Cells and Regulation by Second Messengers, J. Biol. Chem., 270 (1995) 4967-4970.

[57] A.K. Chen, Z. Cheng, M.A. Behlke, A. Tsourkas, Assessing the sensitivity of commercially available fluorophores to the intracellular environment, Anal. Chem., 80 (2008) 7437-7444.

[58] S. Ganta, H. Devalapally, A. Shahiwala, M. Amiji, A review of stimuli-responsive nanocarriers for drug and gene delivery, J. Control. Release, 126 (2008) 187-204.

[59] G.V. Orsinger, J.D. Williams, M. Romanowski, Intracellular light-induced release of signaling molecules from gold-coated liposomes, in: Progress in Biomedical Optics and Imaging - Proceedings of SPIE, 2014.

[60] P. Stano, P. Luigi Luisi, Reactions in Liposomes, in: U. Brinker, J.-L. Mieusset (Eds.) Molecular Encapsulation, John Wiley & Sons, Ltd, Chichester, UK, 2010, pp. 455-491.

[61] A. Kuchler, M. Yoshimoto, S. Luginbuhl, F. Mavelli, P. Walde, Enzymatic reactions in confined environments, Nat. Nanotechnol., 11 (2016) 409-420.

[62] A. Grochmal, L. Prout, R. Makin-Taylor, R. Prohens, S. Tomas, Modulation of reactivity in the cavity of liposomes promotes the formation of peptide bonds, J. Am. Chem. Soc., 137 (2015) 12269-12275.

[63] G. Clergeaud, R. Genc, M. Ortiz, C.K. O'Sullivan, Liposomal nanoreactors for the synthesis of monodisperse palladium nanoparticles using glycerol, Langmuir, 29 (2013) 15405-15413.

[64] R.J. Peters, M. Marguet, S. Marais, M.W. Fraaije, J.C. van Hest, S. Lecommandoux, Cascade reactions in multicompartmentalized polymersomes, Angew. Chem. Int. Ed. Engl., 53 (2014) 146-150.

[65] E. Sugawara, H. Nikaido, OmpA protein of Escherichia coli outer membrane occurs in open and closed channel forms, J. Biol. Chem., 269 (1994) 17981-17987.

[66] I. Petrikovics, K. Hong, G. Omburo, Q.Z. Hu, L. Pei, W.D. McGuinn, D. Sylvester, C. Tamulinas, D. Papahadjopoulos, J.C. Jaszberenyi, J.L. Way, Antagonism of Paraoxon Intoxication by Recombinant Phosphotriesterase Encapsulated within Sterically Stabilized Liposomes, Toxicol. Appl. Pharmacol., 156 (1999) 56-63.

[67] N. Ben-Haim, P. Broz, S. Marsch, W. Meier, P. Hunziker, Cell-specific integration of artificial organelles based on functionalized polymer vesicles, Nano Lett., 8 (2008) 1368-1373.

[68] P. Tanner, V. Balasubramanian, C.G. Palivan, Aiding nature's organelles: artificial peroxisomes play their role, Nano Lett., 13 (2013) 2875-2883.

[69] J.C. Roth, D.T. Curiel, L. Pereboeva, Cell vehicle targeting strategies, Gene Ther., 15 (2008) 716-729.

[70] E.V. Batrakova, H.E. Gendelman, A.V. Kabanov, Cell-mediated drug delivery, Expert Opin. Drug Deliv., 8 (2011) 415-433.

[71] M.A. Fischbach, J.A. Bluestone, W.A. Lim, Cell-based therapeutics: the next pillar of medicine, Sci. Transl. Med., 5 (2013) 179ps177.

[72] S.H. Thorne, R.S. Negrin, C.H. Contag, Synergistic antitumor effects of immune cell-viral biotherapy, Science, 311 (2006) 1780-1784.

[73] M.R. Choi, K.J. Stanton-Maxey, J.K. Stanley, C.S. Levin, R. Bardhan, D. Akin, S. Badve, J. Sturgis, J.P. Robinson, R. Bashir, N.J. Halas, S.E. Clare, A cellular Trojan Horse for delivery of therapeutic nanoparticles into tumors, Nano Lett., 7 (2007) 3759-3765.

[74] D. Alvarez, E.H. Vollmann, U.H. von Andrian, Mechanisms and Consequences of Dendritic Cell Migration, Immunity, 29 (2008) 325-342.

[75] Y. Cheng, R. Morshed, S.H. Cheng, A. Tobias, B. Auffinger, D.A. Wainwright, L. Zhang, C. Yunis, Y. Han, C.T. Chen, L.W. Lo, K.S. Aboody, A.U. Ahmed, M.S. Lesniak, Nanoparticle-programmed self-destructive neural stem cells for glioblastoma targeting and therapy, Small, 9 (2013) 4123-4129.

[76] M.R. Choi, R. Bardhan, K.J. Stanton-Maxey, S. Badve, H. Nakshatri, K.M. Stantz, N. Cao, N.J. Halas, S.E. Clare, Delivery of nanoparticles to brain metastases of breast cancer using a cellular Trojan horse, Cancer Nanotechnol., 3 (2012) 47-54.

[77] E.V. Batrakova, S. Li, A.D. Reynolds, R.L. Mosley, T.K. Bronich, A.V. Kabanov, H.E. Gendelman, A macrophage-nanozyme delivery system for Parkinson's disease, Bioconjug. Chem., 18 (2007) 1498-1506.

[78] A.R. Blaudszun, Q. Lian, M. Schnabel, B. Loretz, U. Steinfeld, H.H. Lee, G. Wenz, C.M. Lehr, M. Schneider, A. Philippi, Polyester-idarubicin nanoparticles and a polymer-photosensitizer complex as potential drug formulations for cell-mediated drug delivery, Int. J. Pharm., 474 (2014) 70-79.

[79] B. Huang, W.D. Abraham, Y. Zheng, S.C. Bustamante López, S.S. Luo, D.J. Irvine, Active targeting of chemotherapy to disseminated tumors using nanoparticle-carrying T cells, Sci. Transl. Med., 7 (2015) 291ra294.

[80] M.-F. Chung, K.-J. Chen, H.-F. Liang, Z.-X. Liao, W.-T. Chia, Y. Xia, H.-W. Sung, A liposomal system capable of generating CO_2 bubbles to induce transient cavitation, lysosomal rupturing, and cell necrosis, Angew. Chem. Int. Ed., 51 (2012) 10089-10093.

[81] A. Paillard, F. Hindré, C. Vignes-Colombeix, J.-P. Benoit, E. Garcion, The importance of endo-lysosomal escape with lipid nanocapsules for drug subcellular bioavailability, Biomaterials, 31 (2010) 7542-7554.

[82] A. Koshkaryev, A. Piroyan, V.P. Torchilin, Bleomycin in octaarginine-modified fusogenic liposomes results in improved tumor growth inhibition, Cancer Lett, 334 (2013) 293-301.

[83] C.-J. Chu, J. Dijkstra, M.-Z. Lai, K. Hong, F.C. Szoka, Efficiency of Cytoplasmic Delivery by pH-Sensitive Liposomes to Cells in Culture, Pharm. Res., 7 (1990) 824-834.

[84] W. Chen, W. Deng, E.M. Goldys, Light-Triggerable Liposomes for Enhanced Endolysosomal Escape and Gene Silencing in PC12 Cells, Mol. Ther. Nucleic Acids, 7 (2017) 366-377.

[85] B. Chatin, M. Mével, J. Devallière, L. Dallet, T. Haudebourg, P. Peuziat, T. Colombani, M. Berchel, O. Lambert, A. Edelman, B. Pitard, Liposome-based Formulation for Intracellular Delivery of Functional Proteins, Mol. Ther. Nucleic Acids, 4 (2015) e244.

[86] Y. Wang, Y. Yang, L. Yan, S.Y. Kwok, W. Li, Z. Wang, X. Zhu, G. Zhu, W. Zhang, X. Chen, P. Shi, Poking cells for efficient vector-free intracellular delivery, Nat. Comm., 5 (2014) 4466.

[87] M.D. Fridman, J. Liu, Y. Sun, R.M. Hamilton, Microinjection Technique for Assessment of Gap Junction Function, Methods Mol. Biol., 1437 (2016) 145-154.

[88] H. Pollard, G. Toumaniantz, J.L. Amos, H. Avet-Loiseau, G. Guihard, J.P. Behr, D. Escande, Ca2+-sensitive cytosolic nucleases prevent efficient delivery to the nucleus of injected plasmids, J. Gene Med., 3 (2001) 153-164.

[89] J.J. Ludtke, M.G. Sebestyen, J.A. Wolff, The effect of cell division on the cellular dynamics of microinjected DNA and dextran, Mol. Ther., 5 (2002) 579-588.

[90] T.V. Tsulaia, N.L. Prokopishyn, A. Yao, N.D.V. Carsrud, M.C. Carou, D.B. Brown, B.R. Davis, J. Yannariello-Brown, Glass Needle-Mediated Microinjection of Macromolecules and Transgenes into Primary Human Mesenchymal Stem Cells, J. Biomed. Sci., 10 (2003) 328-336.

[91] R. Wick, P.L. Luisi, Enzyme-containing liposomes can endogenously produce membrane-constituting lipids, Chem. Biol., 3 (1996) 277-285.

[92] R. Wick, M.I. Angelova, P. Walde, P.L. Luisi, Microinjection into giant vesicles and light microscopy investigation of enzyme-mediated vesicle transformations, Chem. Biol., 3 (1996) 105-111.

[93] D. Hevia, A. Rodriguez-Garcia, M. Alonso-Gervós, I. Quirós-González, H.M. Cimadevilla, C. Gómez-Cordovés, R.M. Sainz, J.C. Mayo, Cell volume and geometric parameters determination in living cells using confocal microscopy and 3D reconstruction, Protocol Exchange, (2011).

[94] M. Graessmann, A. Graessmann, Microinjection of tissue culture cells, Methods Enzymol., 101 (1983) 482-492.

[95] A.P. Tartia, N. Rudraraju, T. Richards, M.A. Hammer, P. Talbot, J.M. Baltz, Cell volume regulation is initiated in mouse oocytes after ovulation, Development, 136 (2009) 2247-2254.

[96] Y. Jin, C. Maosheng, S. Mingzhu, Z. Xin, Quantitative microinjection on the picoliter scale based on the gas-liquid interface positioning control, in: 2015 34th Chinese Control Conference (CCC), 2015, pp. 5977-5982.

[97] Y. Zhang, Microinjection technique and protocol to single cells, Protocol Exchange, (2007).

[98] Y.T. Chow, S. Chen, R. Wang, C. Liu, C.W. Kong, R.A. Li, S.H. Cheng, D. Sun, Single Cell Transfection through Precise Microinjection with Quantitatively Controlled Injection Volumes, Sci. Rep., 6 (2016) 24127.

[99] J. Yu, H. Kwon, H.-s. Park, S. Hong, Y. Choi, Femtoliter scale quantitative injection control by experimental and theoretical modeling, Biomed. Eng. Lett., 6 (2016) 250-255.

[100] K. Kojima, Y. Amano, K. Yoshino, N. Tanaka, K. Sugamura, T. Takeshita, ESCRT-0 Protein Hrs Is Targeted to Endosomes Independent of STAM and the Complex Formation with STAM Promotes Its Endosomal Dissociation, J. Biol. Chem., 289 (2014) 33296–33310.

[101] M. Pruschy, Y. Ju, L. Spitz, E. Carafoli, D.S. Goldfarb, Facilitated nuclear transport of calmodulin in tissue culture cells, J. Cell Biol., 127 (1994) 1527-1536.

[102] W.D. Richardson, A.D. Mills, S.M. Dilworth, R.A. Laskey, C. Dingwall, Nuclear protein migration involves two steps: Rapid binding at the nuclear envelope followed by slower translocation through nuclear pores, Cell, 52 (1988) 655-664.

[103] M. Breeuwer, D.S. Goldfarb, Facilitated nuclear transport of histone H1 and other small nucleophilic proteins, Cell, 60 (1990) 999-1008.

[104] K. Krah, K. Meller, Axonal and dendritic transport in Purkinje cells of cerebellar slice cultures studied by microinjection of horseradish peroxidase, Cell Tissue Res., 295 (1999) 55-64.

[105] Y.L. Wang, F. Lanni, P.L. McNeil, B.R. Ware, D.L. Taylor, Mobility of cytoplasmic and membrane-associated actin in living cells, Proc. Natl. Acad. Sci. U. S. A., 79 (1982) 4660-4664.

[106] T.E. Kreis, B. Geiger, J. Schlessinger, Mobility of microinjected rhodamine actin within living chicken gizzard cells determined by fluorescence photobleaching recovery, Cell, 29 (1982) 835-845.

[107] P. Watson, R. Forster, K.J. Palmer, R. Pepperkok, D.J. Stephens, Coupling of ER exit to microtubules through direct interaction of COPII with dynactin, Nat. Cell Biol., 7 (2005) 48-55.

[108] I.B. Alieva, T. Berezinskaya, G.G. Borisy, I.A. Vorobjev, Centrosome nucleates numerous ephemeral microtubules and only few of them participate in the radial array, Cell Biol. Int., 39 (2015) 1203-1216.

[109] A.J. Ridley, A. Hall, The small GTP-binding protein rho regulates the assembly of focal adhesions and actin stress fibers in response to growth factors, Cell, 70 (1992) 389-399.

[110] Y. Zhang, C. Goodyer, A. LeBlanc, Selective and protracted apoptosis in human primary neurons microinjected with active caspase-3, -6, -7, and -8, J. Neurosci., 20 (2000) 8384-8389.

[111] B. Zhivotovsky, S. Orrenius, O.T. Brustugun, S.O. Doskeland, Injected cytochrome c induces apoptosis, Nature, 391 (1998) 449-450.

[112] O.T. Brustugun, K.E. Fladmark, S.O. Doskeland, S. Orrenius, B. Zhivotovsky, Apoptosis induced by microinjection of cytochrome c is caspase-dependent and is inhibited by Bcl-2, Cell Death Differ., 5 (1998) 660-668.

[113] F. Li, A. Srinivasan, Y. Wang, R.C. Armstrong, K.J. Tomaselli, L.C. Fritz, Cell-specific induction of apoptosis by microinjection of cytochrome c. Bcl-x(L) has activity independent of cytochrome c release, J. Biol. Chem., 272 (1997) 30299-30305.

[114] K. Roberg, K. Kågedal, K. Öllinger, Microinjection of Cathepsin D Induces Caspase-Dependent Apoptosis in Fibroblasts, Am. J. Pathol., 161 (2002) 89-96.

[115] S.H. Chang, P.C. Phelps, I.K. Berezesky, M.L. Ebersberger, B.F. Trump, Studies on the Mechanisms and Kinetics of Apoptosis Induced by Microinjection of Cytochrome c in Rat Kidney Tubule Epithelial Cells (NRK-52E), Am. J. Pathol., 156 (2000) 637-649.

[116] K.M. Sakamoto, K.B. Kim, R. Verma, A. Ransick, B. Stein, C.M. Crews, R.J. Deshaies, Development of Protacs to target cancer-promoting proteins for ubiquitination and degradation, Mol. Cell. Proteomics, 2 (2003) 1350-1358.

[117] S. Burns, A.J. Thrasher, M.P. Blundell, L. Machesky, G.E. Jones, Configuration of human dendritic cell cytoskeleton by Rho GTPases, the WAS protein, and differentiation, Blood, 98 (2001) 1142-1149.

[118] W.E. Allen, G.E. Jones, J.W. Pollard, A.J. Ridley, Rho, Rac and Cdc42 regulate actin organization and cell adhesion in macrophages, J. Cell Sci., 110 (Pt 6) (1997) 707-720.

[119] L.S. Mulcahy, M.R. Smith, D.W. Stacey, Requirement for ras proto-oncogene function during serum-stimulated growth of NIH 3T3 cells, Nature, 313 (1985) 241-243.

[120] C.R. Dixon, M. Platani, A.A. Makarov, E.C. Schirmer, Microinjection of Antibodies Targeting the Lamin A/C Histone-Binding Site Blocks Mitotic Entry and Reveals Separate Chromatin Interactions with HP1, CenpB and PML, Cells, 6 (2017).

[121] V.I. Rodionov, F.K. Gyoeva, V.I. Gelfand, Kinesin is responsible for centrifugal movement of pigment granules in melanophores, Proc. Natl. Acad. Sci. U. S. A., 88 (1991) 4956-4960.

[122] F.K. Gyoeva, V.I. Gelfand, Coalignment of vimentin intermediate filaments with microtubules depends on kinesin, Nature, 353 (1991) 445-448.

[123] V.I. Rodionov, F.K. Gyoeva, E. Tanaka, A.D. Bershadsky, J.M. Vasiliev, V.I. Gelfand, Microtubule-dependent control of cell shape and pseudopodial activity is inhibited by the antibody to kinesin motor domain, J. Cell Biol., 123 (1993) 1811-1820.

[124] T.E. Kreis, Microinjected antibodies against the cytoplasmic domain of vesicular stomatitis virus glycoprotein block its transport to the cell surface, EMBO J., 5 (1986) 931-941.

[125] R. Hartig, R.L. Shoeman, A. Janetzko, S. Grüb, P. Traub, Active nuclear import of single-stranded oligonucleotides and their complexes with non-karyophilic macromolecules, Biol. Cell, 90 (1998) 407-426.

[126] D.A. Dean, Import of plasmid DNA into the nucleus is sequence specific, Exp. Cell Res., 230 (1997) 293-302.

[127] P.L. Felgner, T.R. Gadek, M. Holm, R. Roman, H.W. Chan, M. Wenz, J.P. Northrop, G.M. Ringold, M. Danielsen, Lipofection: a highly efficient, lipid-mediated DNA-transfection procedure, Proc. Natl. Acad. Sci. U. S. A., 84 (1987) 7413-7417.

[128] F.L. Graham, A.J. van der Eb, A new technique for the assay of infectivity of human adenovirus 5 DNA, Virology, 52 (1973) 456-467.

[129] R.C. Mulligan, B.H. Howard, P. Berg, Synthesis of rabbit [beta]-globin in cultured monkey kidney cells following infection with a SV40 [beta]-globin recombinant genome, Nature, 277 (1979) 108-114.

[130] A. Farina, M. Cirone, M. York, S. Lenna, C. Padilla, S. McLaughlin, A. Faggioni, R. Lafyatis, M. Trojanowska, G.A. Farina, Epstein–Barr Virus Infection Induces Aberrant TLR Activation Pathway and Fibroblast–Myofibroblast Conversion in Scleroderma, J. Invest. Dermatol., 134 (2014) 954-964.

[131] L. Herrfurth, V. Theis, V. Matschke, C. May, K. Marcus, C. Theiss, Morphological Plasticity of Emerging Purkinje Cells in Response to Exogenous VEGF, Front. Mol. Neurosci., 10 (2017) 2.

[132] F.K. Wong, C. Haffner, W.B. Huttner, E. Taverna, Microinjection of membrane-impermeable molecules into single neural stem cells in brain tissue, Nat. Protoc., 9 (2014) 1170.

[133] C. Lappe-Siefke, C. Maas, M. Kneussel, Microinjection into cultured hippocampal neurons: a straightforward approach for controlled cellular delivery of nucleic acids, peptides and antibodies, J. Neurosci. Methods, 175 (2008) 88-95.

[134] S. Sixou, J.F.C. Szoka, G.A. Green, B. Giusti, G. Zon, D.J. Chin, Intracellular oligonucleotide hybridization detected by fluorescence resonance energy transfer (FRET), Nucleic Acids Res., 22 (1994) 662-668.

[135] D. Lechardeur, K.J. Sohn, M. Haardt, P.B. Joshi, M. Monck, R.W. Graham, B. Beatty, J. Squire, H. O'Brodovich, G.L. Lukacs, Metabolic instability of plasmid DNA in the cytosol: a potential barrier to gene transfer, Gene Ther., 6 (1999) 482-497.

[136] H. Pollard, J.S. Remy, G. Loussouarn, S. Demolombe, J.P. Behr, D. Escande, Polyethylenimine but not cationic lipids promotes transgene delivery to the nucleus in mammalian cells, J. Biol. Chem., 273 (1998) 7507-7511.

[137] G. Liu, D. Li, M.K. Pasumarthy, T.H. Kowalczyk, C.R. Gedeon, S.L. Hyatt, J.M. Payne, T.J. Miller, P. Brunovskis, T.L. Fink, O. Muhammad, R.C. Moen, R.W. Hanson, M.J. Cooper, Nanoparticles of compacted DNA transfect postmitotic cells, J. Biol. Chem., 278 (2003) 32578-32586.

[138] W. Zauner, S. Brunner, M. Buschle, M. Ogris, E. Wagner, Differential behaviour of lipid based and polycation based gene transfer systems in transfecting primary human fibroblasts: a potential role of polylysine in nuclear transport, Biochim. Biophys. Acta, 1428 (1999) 57-67.

[139] T. Hashimoto, T. Kawazu, T. Nagasaki, A. Murakami, T. Yamaoka, Quantitative comparison between poly(L-arginine) and poly(L-lysine) at each step of polyplex-based gene transfection using a microinjection technique, Sci. Technol. Adv. Mater., 13 (2012) 015009.

[140] H. Akita, D. Kurihara, M. Schmeer, M. Schleef, H. Harashima, Effect of the Compaction and the Size of DNA on the Nuclear Transfer Efficiency after Microinjection in Synchronized Cells, Pharmaceutics, 7 (2015) 64-73.

[141] J. Zabner, A.J. Fasbender, T. Moninger, K.A. Poellinger, M.J. Welsh, Cellular and Molecular Barriers to Gene-Transfer by a Cationic Lipid, J. Biol. Chem., 270 (1995) 18997-19007.

[142] A. Wittrup, A. Ai, X. Liu, P. Hamar, R. Trifonova, K. Charisse, M. Manoharan, T. Kirchhausen, J. Lieberman, Visualizing lipid-formulated siRNA release from endosomes and target gene knockdown, Nat. Biotechnol., 33 (2015) 870-876.

[143] P. Verderio, S. Avvakumova, G. Alessio, M. Bellini, M. Colombo, E. Galbiati, S. Mazzucchelli, J.P. Avila, B. Santini, D. Prosperi, Delivering colloidal nanoparticles to mammalian cells: a nano-bio interface perspective, Adv. Healthcare Mater., 3 (2014) 957-976.

[144] M.E. Grady, E. Parrish, M.A. Caporizzo, S.C. Seeger, R.J. Composto, D.M. Eckmann, Intracellular nanoparticle dynamics affected by cytoskeletal integrity, Soft Matter, 13 (2017) 1873-1880.

[145] B. Dubertret, P. Skourides, D.J. Norris, V. Noireaux, A.H. Brivanlou, A. Libchaber, In vivo imaging of quantum dots encapsulated in phospholipid micelles, Science, 298 (2002) 1759-1762.

[146] K. Boeneman, J.B. Delehanty, K. Susumu, M.H. Stewart, I.L. Medintz, Intracellular bioconjugation of targeted proteins with semiconductor quantum dots, J. Am. Chem. Soc., 132 (2010) 5975-5977.

[147] E. Muro, A. Fragola, T. Pons, N. Lequeux, A. Ioannou, P. Skourides, B. Dubertret, Comparing intracellular stability and targeting of sulfobetaine quantum dots with other surface chemistries in live cells, Small, 8 (2012) 1029-1037.

[148] I.L. Medintz, T. Pons, J.B. Delehanty, K. Susumu, F.M. Brunel, P.E. Dawson, H. Mattoussi, Intracellular delivery of quantum dot-protein cargos mediated by cell penetrating peptides, Bioconjug. Chem., 19 (2008) 1785-1795.

[149] A.M. Derfus, W.C.W. Chan, S.N. Bhatia, Intracellular Delivery of Quantum Dots for Live Cell Labeling and Organelle Tracking, Adv. Mater., 16 (2004) 961-966.

[150] E. Oh, J.B. Delehanty, L.D. Field, A.J. Mäkinen, R. Goswami, A.L. Huston, I.L. Medintz, Synthesis and Characterization of PEGylated Luminescent Gold Nanoclusters Doped with Silver and Other Metals, Chem. Mater., 28 (2016) 8676-8688.

[151] N. Pante, M. Kann, Nuclear pore complex is able to transport macromolecules with diameters of about 39 nm, Mol. Biol. Cell, 13 (2002) 425-434.

[152] P. Candeloro, L. Tirinato, N. Malara, A. Fregola, E. Casals, V. Puntes, G. Perozziello, F. Gentile, M.L. Coluccio, G. Das, C. Liberale, F. De Angelis, E. Di Fabrizio, Nanoparticle microinjection and Raman spectroscopy as tools for nanotoxicology studies, Analyst, 136 (2011) 4402-4408.

[153] P. Tiefenboeck, J.A. Kim, F. Trunk, T. Eicher, E. Russo, A. Teijeira, C. Halin, J.-C. Leroux, Microinjection for the ex Vivo Modification of Cells with Artificial Organelles, ACS Nano, 11 (2017) 7758-7769.

[154] B. Lucas, K. Remaut, N.N. Sanders, K. Braeckmans, S.C. De Smedt, J. Demeester, Towards a better understanding of the dissociation behavior of liposome-oligonucleotide complexes in the cytosol of cells, J. Control. Release, 103 (2005) 435-450.

[155] Y. Tseng, T.P. Kole, D. Wirtz, Micromechanical mapping of live cells by multiple-particle-tracking microrheology, Biophys. J., 83 (2002) 3162-3176.

[156] M. Guo, A.J. Ehrlicher, M.H. Jensen, M. Renz, J.R. Moore, R.D. Goldman, J. Lippincott-Schwartz, F.C. Mackintosh, D.A. Weitz, Probing the stochastic, motor-driven properties of the cytoplasm using force spectrum microscopy, Cell, 158 (2014) 822-832.

[157] M. Ehrenberg, J.L. McGrath, Binding between particles and proteins in extracts: implications for microrheology and toxicity, Acta Biomater., 1 (2005) 305-315.

[158] K. Luby-Phelps, P.E. Castle, D.L. Taylor, F. Lanni, Hindered diffusion of inert tracer particles in the cytoplasm of mouse 3T3 cells, Proc. Natl. Acad. Sci. U. S. A., 84 (1987) 4910-4913.

[159] U. Resch-Genger, M. Grabolle, S. Cavaliere-Jaricot, R. Nitschke, T. Nann, Quantum dots versus organic dyes as fluorescent labels, Nat. Methods, 5 (2008) 763-775.

[160] Y. Su, Y. He, H. Lu, L. Sai, Q. Li, W. Li, L. Wang, P. Shen, Q. Huang, C. Fan, The cytotoxicity of cadmium based, aqueous phase – Synthesized, quantum dots and its modulation by surface coating, Biomaterials, 30 (2009) 19-25.

[161] S. Saurabh, L.E. Beck, S. Maji, C.J. Baty, Y. Wang, Q. Yan, S.C. Watkins, M.P. Bruchez, Multiplexed modular genetic targeting of quantum dots, ACS Nano, 8 (2014) 11138-11146.

[162] K. Luby-Phelps, D.L. Taylor, F. Lanni, Probing the structure of cytoplasm, J. Cell Biol., 102 (1986) 2015-2022.

[163] D.W. Provance, Jr., A. McDowall, M. Marko, K. Luby-Phelps, Cytoarchitecture of size-excluding compartments in living cells, J. Cell Sci., 106 (Pt 2) (1993) 565-577.

[164] K. Luby-Phelps, S. Mujumdar, R.B. Mujumdar, L.A. Ernst, W. Galbraith, A.S. Waggoner, A novel fluorescence ratiometric method confirms the low solvent viscosity of the cytoplasm, Biophys. J., 65 (1993) 236-242.

[165] K. Luby-Phelps, Physical properties of cytoplasm, Curr. Opin. Cell Biol., 6 (1994) 3-9.

[166] L.W. Janson, K. Ragsdale, K. Luby-Phelps, Mechanism and size cutoff for steric exclusion from actin-rich cytoplasmic domains, Biophys. J., 71 (1996) 1228-1234.

[167] G.L. Lukacs, P. Haggie, O. Seksek, D. Lechardeur, N. Freedman, A.S. Verkman, Size-dependent DNA mobility in cytoplasm and nucleus, J. Biol. Chem., 275 (2000) 1625-1629.

[168] J.P. Leonetti, N. Mechti, G. Degols, C. Gagnor, B. Lebleu, Intracellular distribution of microinjected antisense oligonucleotides, Proc. Natl. Acad. Sci. U. S. A., 88 (1991) 2702-2706.

[169] E.E. Vaughan, D.A. Dean, Intracellular trafficking of plasmids during transfection is mediated by microtubules, Mol. Ther., 13 (2006) 422-428.

[170] E.E. Vaughan, R.C. Geiger, A.M. Miller, P.L. Loh-Marley, T. Suzuki, N. Miyata, D.A. Dean, Microtubule acetylation through HDAC6 inhibition results in increased transfection efficiency, Mol. Ther., 16 (2008) 1841-1847.

[171] J.V. Jokerst, T. Lobovkina, R.N. Zare, S.S. Gambhir, Nanoparticle PEGylation for imaging and therapy, Nanomedicine, 6 (2011) 715-728.

[172] B.J.C. Quah, H.S. Warren, C.R. Parish, Monitoring lymphocyte proliferation in vitro and in vivo with the intracellular fluorescent dye carboxyfluorescein diacetate succinimidyl ester, Nat. Protoc., 2 (2007) 2049-2056.

[173] J.A. Kim, C. Aberg, A. Salvati, K.A. Dawson, Role of cell cycle on the cellular uptake and dilution of nanoparticles in a cell population, Nat. Nanotechnol., 7 (2012) 62-68.

[174] H.D. Summers, P. Rees, M.D. Holton, M. Rowan Brown, S.C. Chappell, P.J. Smith, R.J. Errington, Statistical analysis of nanoparticle dosing in a dynamic cellular system, Nat. Nanotechnol., 6 (2011) 170-174.

[175] H.D. Summers, M.R. Brown, M.D. Holton, J.A. Tonkin, N. Hondow, A.P. Brown, R. Brydson, P. Rees, Quantification of nanoparticle dose and vesicular inheritance in proliferating cells, ACS Nano, 7 (2013) 6129-6137.

[176] R.D. Leek, C.E. Lewis, R. Whitehouse, M. Greenall, J. Clarke, A.L. Harris, Association of macrophage infiltration with angiogenesis and prognosis in invasive breast carcinoma, Cancer Res., 56 (1996) 4625-4629.

[177] S. Taherkhani, M. Mohammadi, J. Daoud, S. Martel, M. Tabrizian, Covalent binding of nanoliposomes to the surface of magnetotactic bacteria for the synthesis of self-propelled therapeutic agents, ACS Nano, 8 (2014) 5049-5060.

[178] C.H. Jones, M. Chen, A. Gollakota, A. Ravikrishnan, G. Zhang, S. Lin, M. Tan, C. Cheng, H. Lin, B.A. Pfeifer, Structure–function assessment of mannosylated poly(β-amino esters) upon targeted antigen presenting cell gene delivery, Biomacromolecules, 16 (2015) 1534-1541.

[179] U. Steinfeld, C. Pauli, N. Kaltz, C. Bergemann, H.-H. Lee, T lymphocytes as potential therapeutic drug carrier for cancer treatment, Int. J. Pharm., 311 (2006) 229-236.

[180] J. Choi, H.-Y. Kim, E.J. Ju, J. Jung, J. Park, H.-K. Chung, J.S. Lee, J.S. Lee, H.J. Park, S.Y. Song, S.-Y. Jeong, E.K. Choi, Use of macrophages to deliver therapeutic and imaging contrast agents to tumors, Biomaterials, 33 (2012) 4195-4203.

[181] H. Dou, C.J. Destache, J.R. Morehead, R.L. Mosley, M.D. Boska, J. Kingsley, S. Gorantla, L. Poluektova, J.A. Nelson, M. Chaubal, J. Werling, J. Kipp, B.E. Rabinow, H.E. Gendelman, Development of a macrophage-based nanoparticle platform for antiretroviral drug delivery, Blood, 108 (2006) 2827-2835.

[182] A.M. Brynskikh, Y. Zhao, R.L. Mosley, S. Li, M.D. Boska, N.L. Klyachko, A.V. Kabanov, H.E. Gendelman, E.V. Batrakova, Macrophage delivery of therapeutic nanozymes in a murine model of Parkinson's disease, Nanomedicine, 5 (2010) 379-396.

[183] B. Zarabi, A. Nan, J. Zhuo, R. Gullapalli, H. Ghandehari, Macrophage targeted N-(2-hydroxypropyl)methacrylamide conjugates for magnetic resonance imaging, Mol. Pharm., 3 (2006) 550-557.

[184] P.J. Tacken, I.J.M. de Vries, R. Torensma, C.G. Figdor, Dendritic-cell immunotherapy: from ex vivo loading to in vivo targeting, Nature Reviews Immunology, 7 (2007) 790-802.

[185] S. Hamdy, A. Haddadi, R.W. Hung, A. Lavasanifar, Targeting dendritic cells with nano-particulate PLGA cancer vaccine formulations, Adv. Drug Del. Rev., 63 (2011) 943-955.

[186] O. Felfoul, M. Mohammadi, S. Taherkhani, D. de Lanauze, Y. Zhong Xu, D. Loghin, S. Essa, S. Jancik, D. Houle, M. Lafleur, L. Gaboury, M. Tabrizian, N. Kaou, M. Atkin, T. Vuong, G. Batist, N. Beauchemin, D. Radzioch, S. Martel, Magneto-aerotactic bacteria deliver drug-containing nanoliposomes to tumour hypoxic regions, Nat. Nanotechnol., 11 (2016) 941-947.

[187] S.H. Thorne, R.S. Negrin, C.H. Contag, Synergistic antitumor effects of immune cell-viral biotherapy, Science, 311 (2006) 1780-1784.

[188] H. Hillaireau, P. Couvreur, Nanocarriers' entry into the cell: Relevance to drug delivery, Cell. Mol. Life Sci., 66 (2009) 2873-2896.

[189] J.S. Lee, T. Groothuis, C. Cusan, D. Mink, J. Feijen, Lysosomally cleavable peptide-containing polymersomes modified with anti-EGFR antibody for systemic cancer chemotherapy, Biomaterials, 32 (2011) 9144-9153.

[190] R. Shrestha, M. Elsabahy, S. Florez-Malaver, S. Samarajeewa, K.L. Wooley, Endosomal escape and siRNA delivery with cationic shell crosslinked knedel-like nanoparticles with tunable buffering capacities, Biomaterials, 33 (2012) 8557-8568.

[191] O.M. Merkel, T. Kissel, Quo vadis polyplex?, J. Controlled Release, 190 (2014) 415-423.

[192] Y. Zhang, L.C. Yu, Single-cell microinjection technology in cell biology, Bioessays, 30 (2008) 606-610.

[193] J.M. Dubach, M.K. Balaconis, H.A. Clark, Fluorescent nanoparticles for the measurement of ion concentration in biological systems, Journal of Visualized Experiments, (2011) 2896.

[194] M.J. Haney, Y. Zhao, S. Li, S.M. Higginbotham, S.L. Booth, H.-Y. Han, J.A. Vetro, R.L. Mosley, A.V. Kabanov, H.E. Gendelman, E.V. Batrakova, Cell-mediated transfer of catalase nanoparticles from macrophages to brain endothelial, glial and neuronal cells, Nanomedicine, 6 (2011) 1215-1230.

[195] P. Tanner, P. Baumann, R. Enea, O. Onaca, C. Palivan, W. Meier, Polymeric vesicles: From drug carriers to nanoreactors and artificial organelles, Acc. Chem. Res., 44 (2011) 1039-1049.

[196] H.-J. Choi, C.D. Montemagno, Artificial organelle: ATP synthesis from cellular mimetic polymersomes, Nano Lett., 5 (2005) 2538-2542.

[197] M.J. Hope, M.B. Bally, G. Webb, P.R. Cullis, Production of large unilamellar vesicles by a rapid extrusion procedure - characterization of size distribution, trapped volume and ability to maintain a membrane-potential, Biochim. Biophys. Acta, 812 (1985) 55-65.

[198] Z.V. Leonenko, E. Finot, H. Ma, T.E.S. Dahms, D.T. Cramb, Investigation of temperature-induced phase transitions in DOPC and DPPC phospholipid bilayers using temperature-controlled scanning force microscopy, Biophys. J., 86 (2004) 3783-3793.

[199] N. Kučerka, J.F. Nagle, J.N. Sachs, S.E. Feller, J. Pencer, A. Jackson, J. Katsaras, Lipid bilayer structure determined by the simultaneous analysis of neutron and X-ray scattering data, Biophys. J., 95 (2008) 2356-2367.

[200] J.J. Pan, S. Tristram-Nagle, J.F. Nagle, Effect of cholesterol on structural and mechanical properties of membranes depends on lipid chain saturation, Physical Review E, 80 (2009) 021931.

[201] Y. Tahara, Y. Fujiyoshi, A new method to measure bilayer thickness: Cryo-electron microscopy of frozen hydrated liposomes and image simulation, Micron, 25 (1994) 141-149.

[202] T.L.M. Thurston, M.P. Wandel, N. von Muhlinen, A. Foeglein, F. Randow, Galectin 8 targets damaged vesicles for autophagy to defend cells against bacterial invasion, Nature, 482 (2012) 414-418.

[203] R. Roberts, W.T. Al-Jamal, M. Whelband, P. Thomas, M. Jefferson, J. van den Bossche, P.P. Powell, K. Kostarelos, T. Wileman, Autophagy and formation of tubulovesicular autophagosomes provide a barrier against nonviral gene delivery, Autophagy, 9 (2013) 667-682.

[204] V. Forster, R.D. Signorell, M. Roveri, J.-C. Leroux, Liposome-supported peritoneal dialysis for detoxification of drugs and endogenous metabolites, Sci. Transl. Med., 6 (2014) 258ra141.

[205] J. Schindelin, I. Arganda-Carreras, E. Frise, V. Kaynig, M. Longair, T. Pietzsch, S. Preibisch, C. Rueden, S. Saalfeld, B. Schmid, J.-Y. Tinevez, D.J. White, V. Hartenstein, K. Eliceiri, P. Tomancak, A. Cardona, Fiji: an open-source platform for biological-image analysis, Nat. Methods, 9 (2012) 676-682.

[206] E. Russo, A. Teijeira, K. Vaahtomeri, A.-H. Willrodt, Joël S. Bloch, M. Nitschké, L. Santambrogio, D. Kerjaschki, M. Sixt, C. Halin, Intralymphatic CCL21 promotes tissue egress of dendritic cells through afferent lymphatic vessels, Cell Reports, 14 (2016) 1723-1734.

[207] T. Zal, A. Volkmann, B. Stockinger, Mechanisms of tolerance induction in major histocompatibility complex class II-restricted T cells specific for a blood-borne self-antigen, J. Exp. Med., 180 (1994) 2089-2099.

[208] L. Larsson, E. Timms, K. Blight, D.E. Restall, P.S. Jat, A.G. Fisher, Characterization of murine thymic stromal-cell lines immortalized by temperature-sensitive simian virus 40 large T or adenovirus 5 E1a, Dev. Immunol., 1 (1991) 279-293.

[209] M.M. Al-Alwan, G. Rowden, T.D.G. Lee, K.A. West, Cutting edge: the dendritic cell cytoskeleton is critical for the formation of the immunological synapse, J. Immunol., 166 (2001) 1452-1456.

[210] M. Nitschké, D. Aebischer, M. Abadier, S. Haener, M. Lucic, B. Vigl, H. Luche, H.J. Fehling, O. Biehlmaier, R. Lyck, C. Halin, Differential requirement for ROCK in dendritic cell migration within lymphatic capillaries in steady-state and inflammation, Blood, 120 (2012) 2249-2258.

[211] J. Kurniawan, N.-N. Yin, G.-y. Liu, T.L. Kuhl, Interaction forces between ternary lipid bilayers containing cholesterol, Langmuir, 30 (2014) 4997-5004.

[212] Y. Obata, S. Saito, N. Takeda, S. Takeoka, Plasmid DNA-encapsulating liposomes: Effect of a spacer between the cationic head group and hydrophobic moieties of the lipids on gene expression efficiency, Biochim. Biophys. Acta, 1788 (2009) 1148-1158.

[213] L. Dézsi, T. Fülöp, T. Mészáros, G. Szénási, R. Urbanics, C. Vázsonyi, E. Őrfi, L. Rosivall, R. Nemes, R.J. Kok, J.M. Metselaar, G. Storm, J. Szebeni, Features of complement activation-related pseudoallergy to liposomes with different surface charge and PEGylation: Comparison of the porcine and rat responses, J. Controlled Release, 195 (2014) 2-10.

[214] E. Mayhew, M. Ito, R. Lazo, Toxicity of non-drug-containing liposomes for cultured human cells, Exp. Cell Res., 171 (1987) 195-202.

[215] Y. Kabeya, N. Mizushima, T. Ueno, A. Yamamoto, T. Kirisako, T. Noda, E. Kominami, Y. Ohsumi, T. Yoshimori, LC3, a mammalian homologue of yeast Apg8p, is localized in autophagosome membranes after processing, The EMBO Journal, 19 (2000) 5720-5728.

[216] W. Hunziker, H.J. Geuze, Intracellular trafficking of lysosomal membrane proteins, Bioessays, 18 (1996) 379-389.

[217] E. Moeendarbary, L. Valon, M. Fritzsche, A.R. Harris, D.A. Moulding, A.J. Thrasher, E. Stride, L. Mahadevan, G.T. Charras, The cytoplasm of living cells behaves as a poroelastic material, Nat. Mater., 12 (2013) 253-261.

[218] M.M. Pakulska, I.E. Donaghue, J.M. Obermeyer, A. Tuladhar, C.K. McLaughlin, T.N. Shendruk, M.S. Shoichet, Encapsulation-free controlled release: Electrostatic adsorption eliminates the need for protein encapsulation in PLGA nanoparticles, Sci. Adv., 2 (2016) e1600519.

[219] J.-P. Colletier, B. Chaize, M. Winterhalter, D. Fournier, Protein encapsulation in liposomes: efficiency depends on interactions between protein and phospholipid bilayer, BMC Biotechnol., 2 (2002) 9.

[220] J. Banchereau, R.M. Steinman, Dendritic cells and the control of immunity, Nature, 392 (1998) 245-252.

[221] Y.-C. Wang, X.-B. Hu, F. He, F. Feng, L. Wang, W. Li, P. Zhang, D. Li, Z.-S. Jia, Y.-M. Liang, H. Han, Lipopolysaccharide-induced maturation of bone marrow-derived dendritic cells is regulated by notch signaling through the up-regulation of CXCR4, J. Biol. Chem., 284 (2009) 15993-16003.

[222] J.W. Walker, S.H. Gilbert, R.M. Drummond, M. Yamada, R. Sreekumar, R.E. Carraway, M. Ikebe, F.S. Fay, Signaling pathways underlying eosinophil cell motility revealed by using caged peptides, Proc. Natl. Acad. Sci. U. S. A., 95 (1998) 1568-1573.

[223] J.R. Casey, S. Grinstein, J. Orlowski, Sensors and regulators of intracellular pH, Nat. Rev. Mol. Cell Biol., 11 (2010) 50-61.

[224] T. Ta, T.M. Porter, Thermosensitive liposomes for localized delivery and triggered release of chemotherapy, J. Control. Release, 169 (2013) 112-125.

[225] B. Banno, L.M. Ickenstein, G.N. Chiu, M.B. Bally, J. Thewalt, E. Brief, E.K. Wasan, The functional roles of poly(ethylene glycol)-lipid and lysolipid in the drug retention and release from lysolipid-containing thermosensitive liposomes in vitro and in vivo, J. Pharm. Sci., 99 (2010) 2295-2308.

[226] M.C. Sandstrom, L.M. Ickenstein, L.D. Mayer, K. Edwards, Effects of lipid segregation and lysolipid dissociation on drug release from thermosensitive liposomes, J. Control. Release, 107 (2005) 131-142.

[227] K.-J. Chen, H.-F. Liang, H.-L. Chen, Y. Wang, P.-Y. Cheng, H.-L. Liu, Y. Xia, H.-W. Sung, A Thermoresponsive Bubble-Generating Liposomal System for Triggering Localized Extracellular Drug Delivery, ACS Nano, 7 (2013) 438-446.

[228] K.-J. Chen, E.-Y. Chaung, S.-P. Wey, K.-J. Lin, F. Cheng, C.-C. Lin, H.-L. Liu, H.-W. Tseng, C.-P. Liu, M.-C. Wei, C.-M. Liu, H.-W. Sung, Hyperthermia-Mediated Local Drug Delivery by a Bubble-Generating Liposomal System for Tumor-Specific Chemotherapy, ACS Nano, 8 (2014) 5105-5115.

[229] Z.-X. Liao, E.-Y. Chuang, C.-C. Lin, Y.-C. Ho, K.-J. Lin, P.-Y. Cheng, K.-J. Chen, H.-J. Wei, H.-W. Sung, An AS1411 aptamer-conjugated liposomal system containing a bubble-generating agent for tumor-specific chemotherapy that overcomes multidrug resistance, J. Control. Release, 208 (2015) 42-51.

[230] E.-Y. Chuang, C.-C. Lin, K.-J. Chen, D.-H. Wan, K.-J. Lin, Y.-C. Ho, P.-Y. Lin, H.-W. Sung, A FRET-guided, NIR-responsive bubble-generating liposomal system for in vivo targeted therapy with spatially and temporally precise controlled release, Biomaterials, 93 (2016) 48-59.

[231] D. Needham, G. Anyarambhatla, G. Kong, M.W. Dewhirst, A new temperature-sensitive liposome for use with mild hyperthermia: characterization and testing in a human tumor xenograft model, Cancer Res., 60 (2000) 1197-1201.

[232] Y. Barenholz, G. Haran, Method of amphiphatic drug loading in liposomes by ammonium ion gradient, in: Y.R.D.C.o.t.H.U.o. Jerusalem (Ed.), Google Patents, 1994.

[233] K.J. Hill, M. Kaszuba, J.E. Creeth, M.N. Jones, Reactive liposomes encapsulating a glucose oxidase-peroxidase system with antibacterial activity, Biochim. Biophys. Acta, 1326 (1997) 37-46.

[234] Y. Nakashima, M. Deie, S. Yanada, P. Sharman, M. Ochi, Magnetically labeled human natural killer cells, accumulated in vitro by an external magnetic force, are effective against HOS osteosarcoma cells, Int. J. Oncol., 27 (2005) 965-971.

[235] R. Duncan, S. Gac-Breton, R. Keane, R. Musila, Y.N. Sat, R. Satchi, F. Searle, Polymer-drug conjugates, PDEPT and PELT: basic principles for design and transfer from the laboratory to clinic, J. Control. Release, 74 (2001) 135-146.

[236] M.H. Vingerhoeds, H.J. Haisma, S.O. Belliot, R.H.P. Smit, D.J.A. Crommelin, G. Storm, Immunoliposomes as Enzyme-Carriers (Immuno-Enzymosomes) for Antibody-Directed Enzyme Prodrug Therapy (ADEPT): Optimization of Prodrug Activating Capacity, Pharm. Res., 13 (1996) 604-610.

[237] M. Chaszczewska-Markowska, K. Stebelska, A. Sikorski, J. Madej, A. Opolski, M. Ugorski, Liposomal formulation of 5-fluorocytosine in suicide gene therapy with cytosine deaminase--for colorectal cancer, Cancer Lett., 262 (2008) 164-172.

[238] I.T. Cavarretta, V. Altanerova, M. Matuskova, L. Kucerova, Z. Culig, C. Altaner, Adipose tissue-derived mesenchymal stem cells expressing prodrug-converting enzyme inhibit human prostate tumor growth, Mol. Ther., 18 (2010) 223-231.